Active methods with focus on time information

-LIDAR Light detection and ranging

-RADAR Radio detection and ranging

-SODAR Sound detection and ranging

Basic components

Emitted signal (pulsed)

Radio waves, light, sound

Reflection (scattering) at different distances

Scattering, Fluorescence

Detection of signal strength as function of time

Scattering processes:

Rayleigh-scattering ($r << \lambda$)

Raman-scattering ($r << \lambda$, inelastic)

Particle-scattering (e.g. Mie-scattering)

Bragg-scattering (turbulence elements)

Rayleigh-scattering ($r \ll \lambda$)

The incident light induces a periodically varying dipole at the place of the scattering particle.

This dipole then itself becomes an emitter of radiation.

The angular dependence of the scattering probability is referred to as ‚phase function‘

Incident light

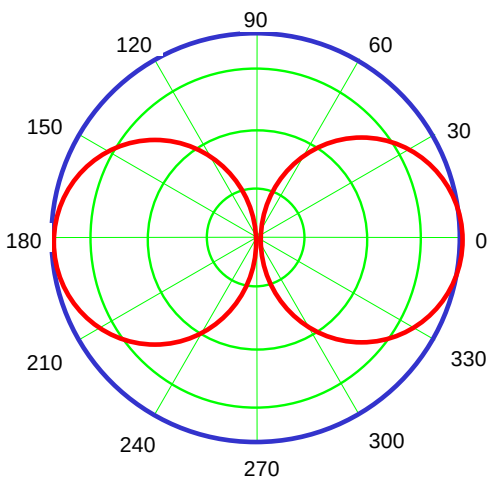

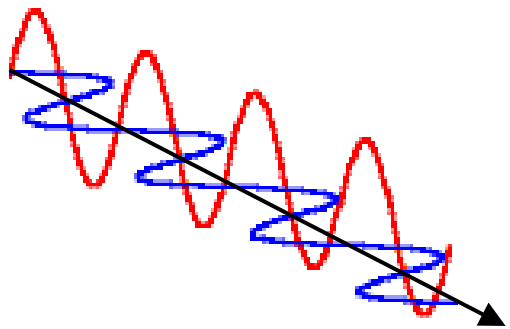

red: p-polarisation, blue: s-polarisation

Influence of inelastic scattering

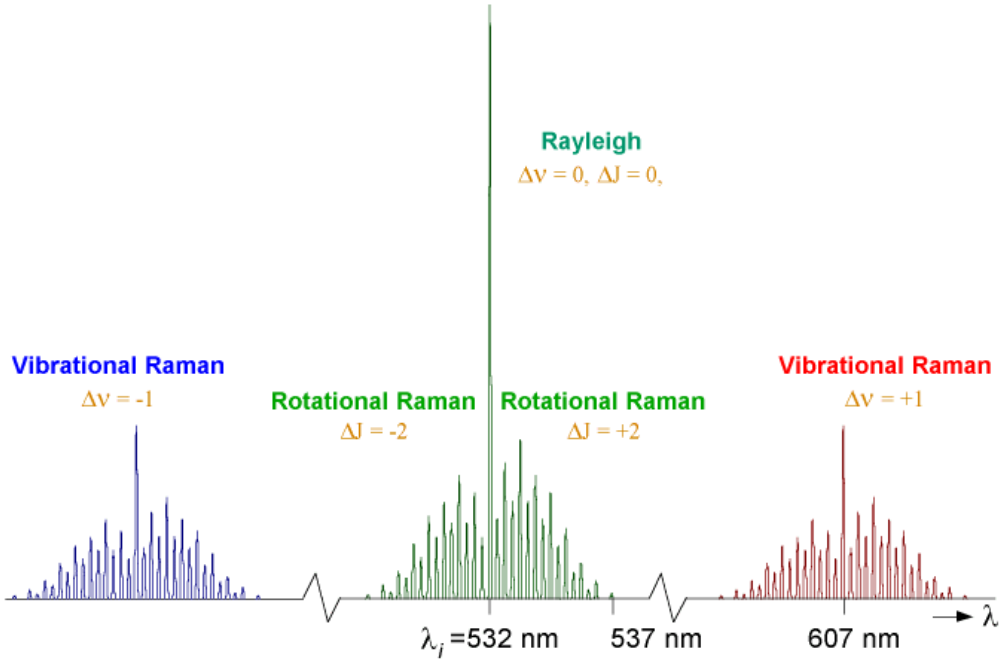

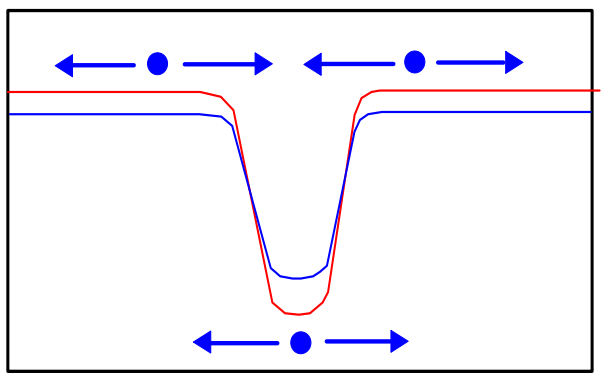

‚Filling-in' of spectral structures: Ring effect

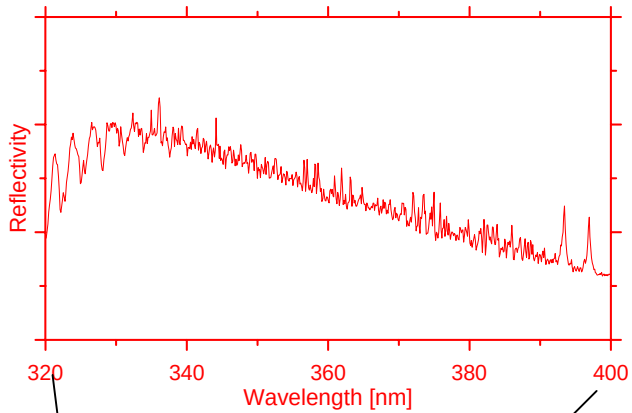

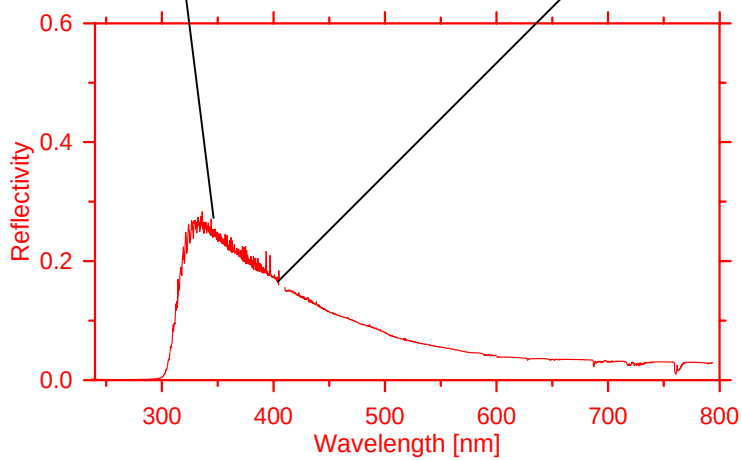

If the extension of a particle is larger than the wavelength, interference effects become important

The scattering particle can be thought of as build up of many individual emitting dipoles

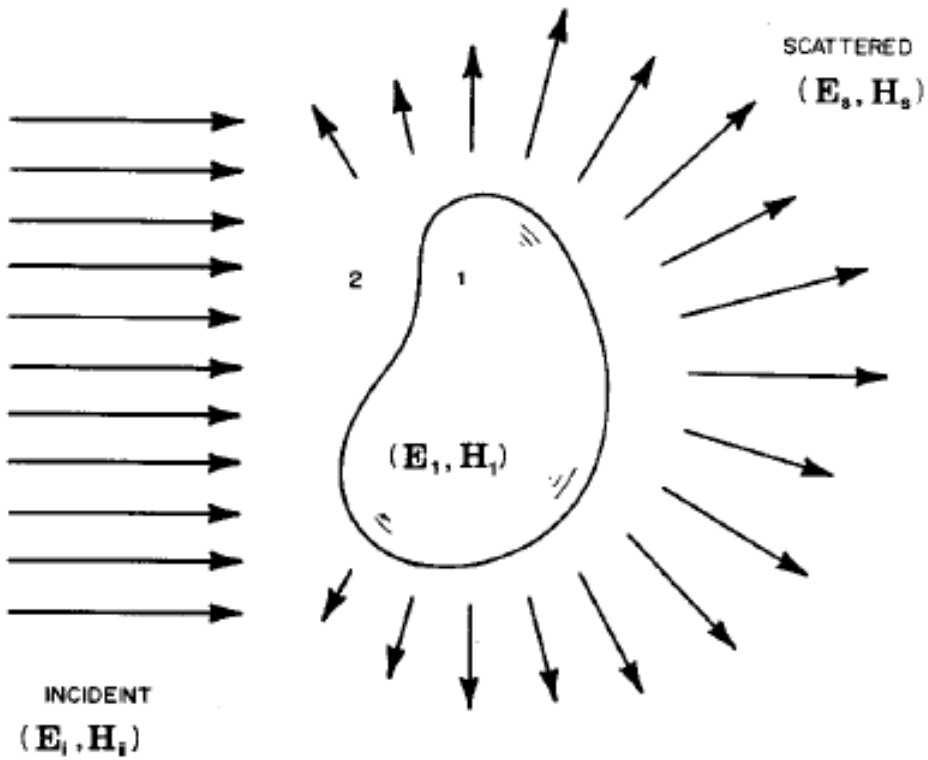

Figure 2.1: The incident field $(\mathbf{E}_i, \mathbf{H}_i)$ gives rise to a field $(\mathbf{E}_1, \mathbf{H}_1)$ inside the particle and a scattered field $(\mathbf{E}_s, \mathbf{H}_s)$ in the medium surrounding the particle (from Bohren and Huffman, 1998).

Wavelength dependence of scattering processes

Mie extinction cross section (r: 500 nm, refractive index: 1.5)

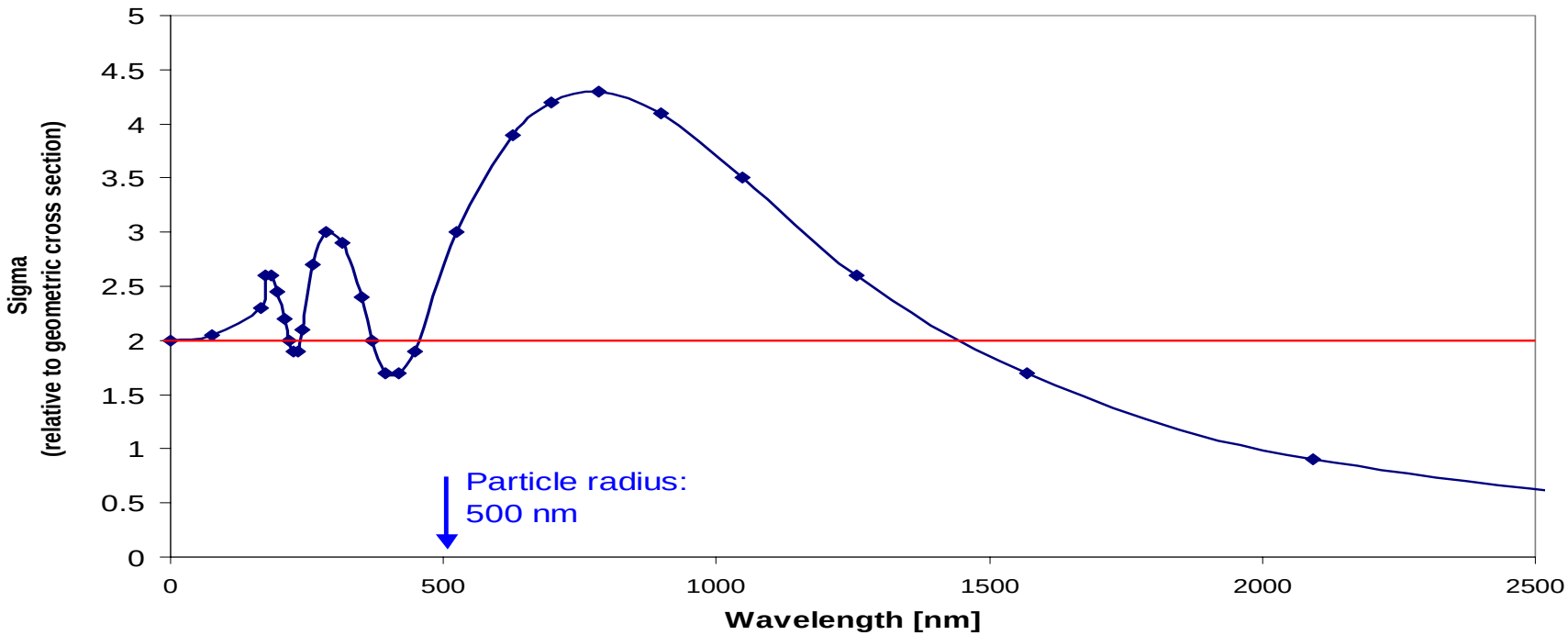

$\lambda >> r \Rightarrow \quad \sigma \sim \lambda^{-4}$ (Rayleigh scattering)

$\lambda << r \Rightarrow \quad \sigma \sim \lambda^{-0}$ (Clouds)

for typical aerosol size distributions: $\sigma \sim \lambda^{-1}$ to $\lambda^{-1.5}$

Angular and polarisation dependence of scattering processes

$\lambda >> r$

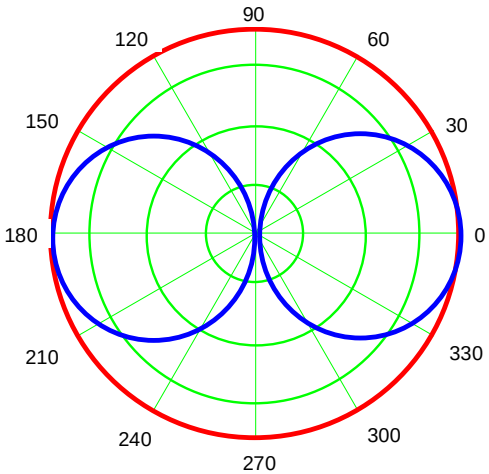

$\lambda \sim r$

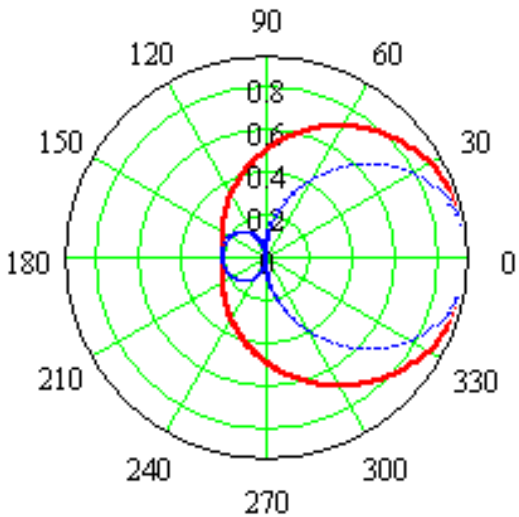

$\lambda < r$

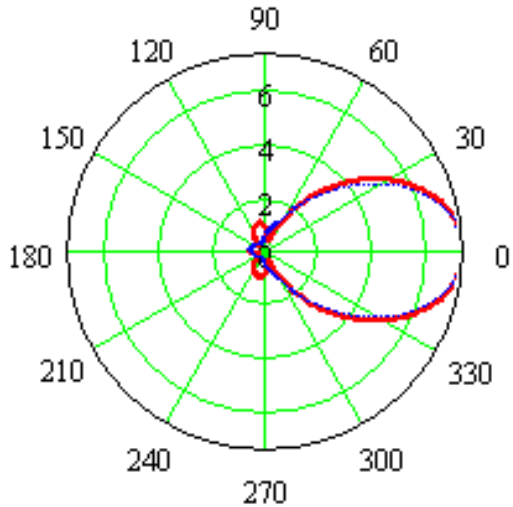

red: s-polarisation, blue: p-polarisation

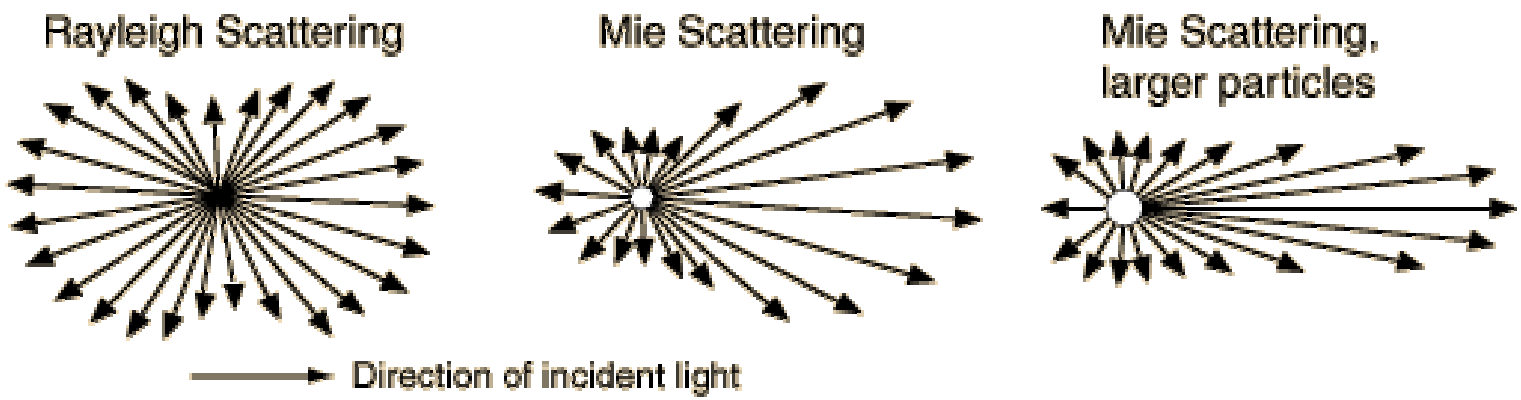

Comprehensive theory for spherical particles: Mie scattering

$$I(\Theta, R) = \frac{I_0 \lambda^2 (i_1 + i_2)}{8\pi^2 R^2}$$

Mie intensity parameters i_1 and i_2 (for perpendicular polarised light) are complex functions of the refractive index of the scatterer, the size parameter and scattering angle

Size parameter:

$$\alpha = \frac{2\pi r}{\lambda}$$

The (complex) refractive index describes the scattering and absorption properties:

$n = n_r (1 – ai)$

With

n_r : real refractive index

a: constant proportional to the absorption coefficient

Species	Refractive index
Vacuum	1
Water vapor	1.00025
Air	1.00029
Water (liquid)	1.333
Ice	1.309
Rock salt	1.544
Sodium chloride in aqueous solution	1.342 – 1.378
Sulfuric acid in aqueous solution	1.339 – 1.437
Benzene	1.5011
Alpha pinene	1.465
Delta Limonene	1.471
Nitrobenzene	1.55
Dioctylphtalate	1.49
Oleic acid	1.46
Polystyrene latex	1.6
Carbon	1.59-0.66i
Iron	1.51-1.63i
Magentite	2.58-0.58i
Copper	0.62-2.63i

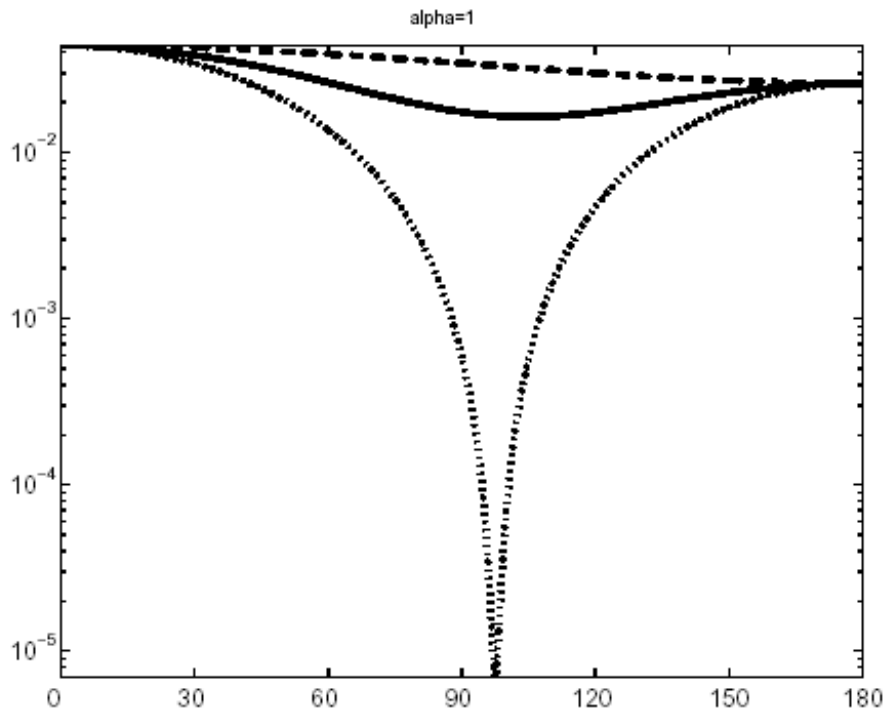

(a) Scattering diagram for x=1. The dotted and the broken lines represent the two orthogonal polarization states, whereas the solid line represents unpolarized light.

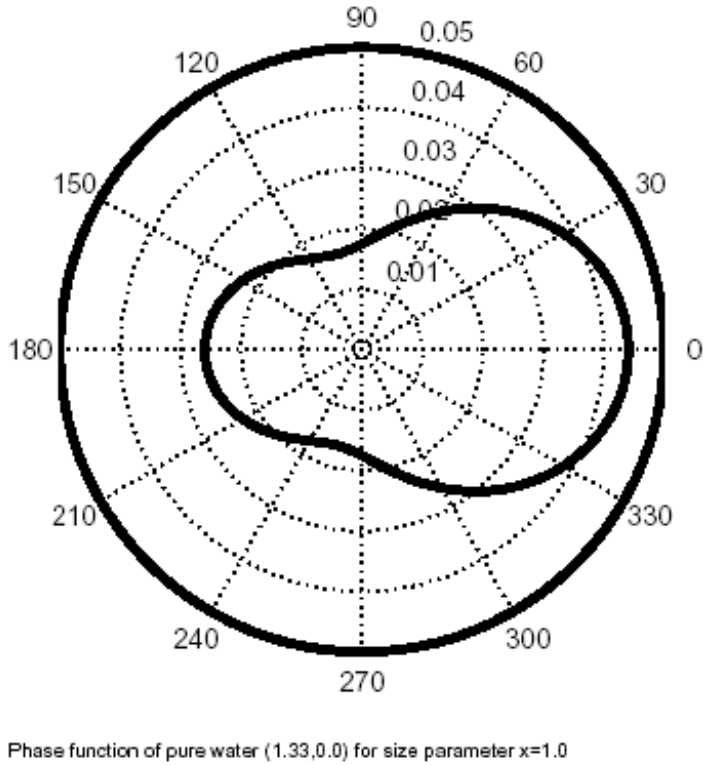

(b) A polar plot of the scattering profile of a water droplet of size parameter x =1.

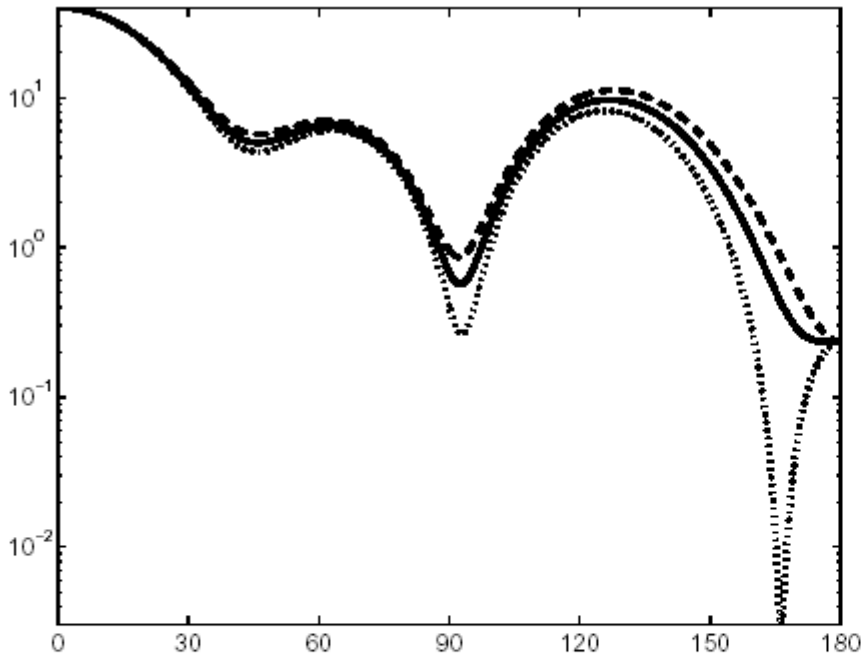

(a) Scattering diagram for x=3. The dotted and the broken lines represent the two orthogonal polarization states, whereas the solid line represents unpolarized light.

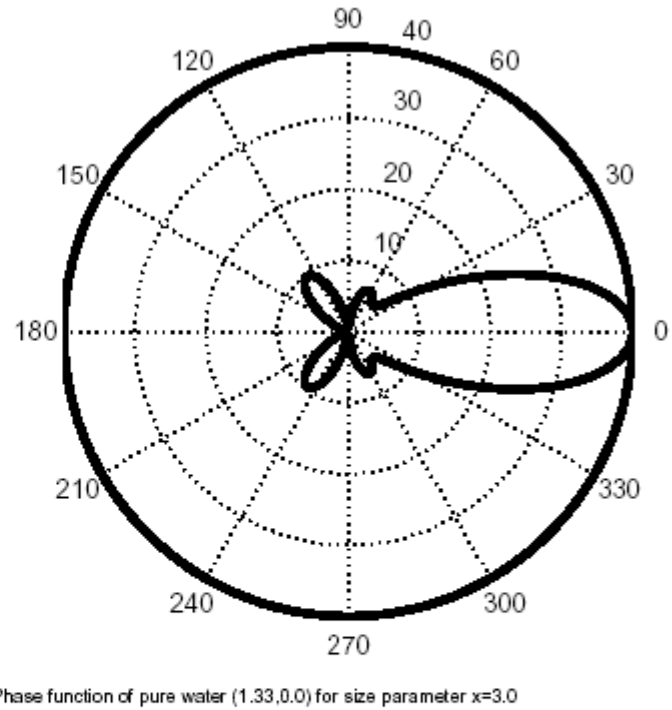

(b) A polar plot of the scattering profile of a water droplet of size parameter x =3.

Figure 2.16: Phase functions of a water droplet with x=3

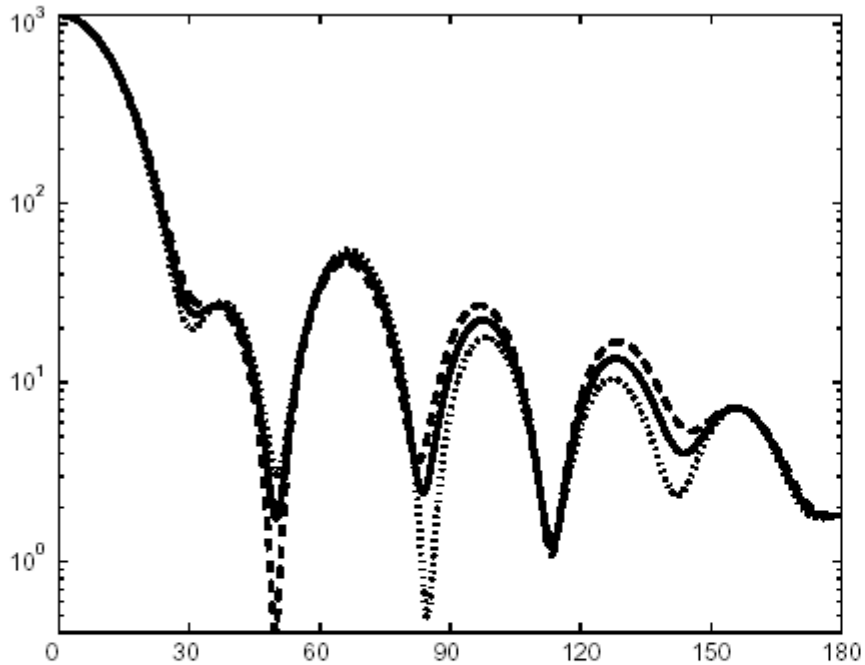

(a) Scattering diagram for x=5. The dotted and the broken lines represent the two orthogonal polarization states, whereas the solid line represents unpolarized light.

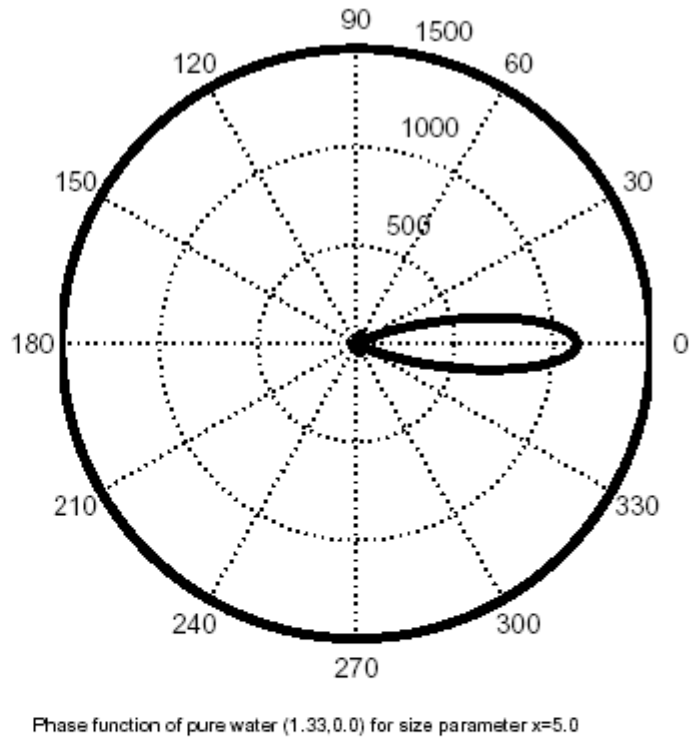

(b) A polar plot of the scattering profile of a water droplet of size parameter x =5.

Figure 2.17: Phase functions of a water droplet with x=5

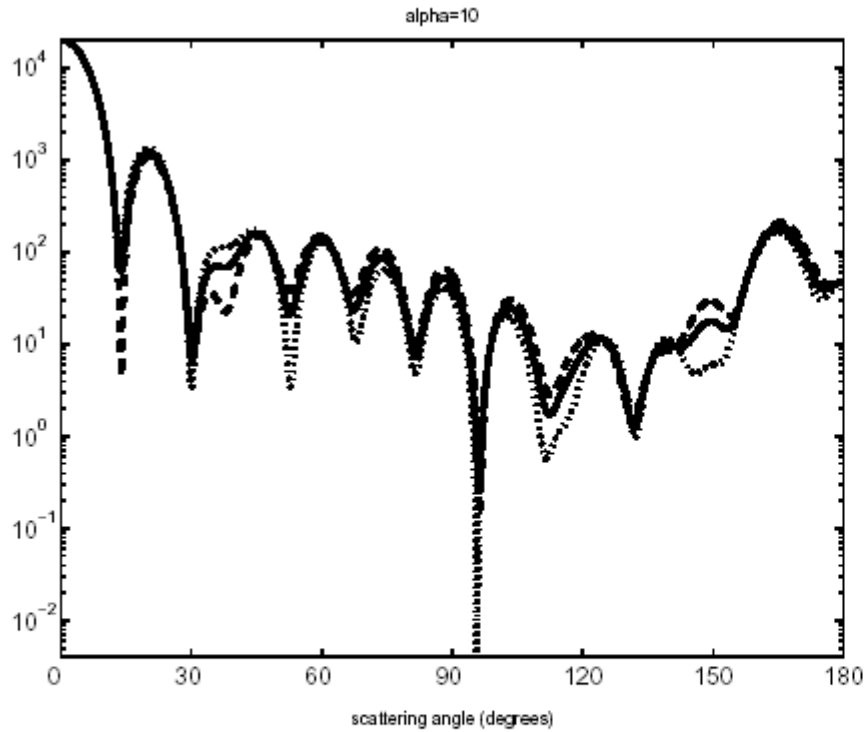

(a) Scattering diagram for x=10. The dotted and the broken lines represent the two orthogonal polarization states, whereas the solid line represents unpolarized light.

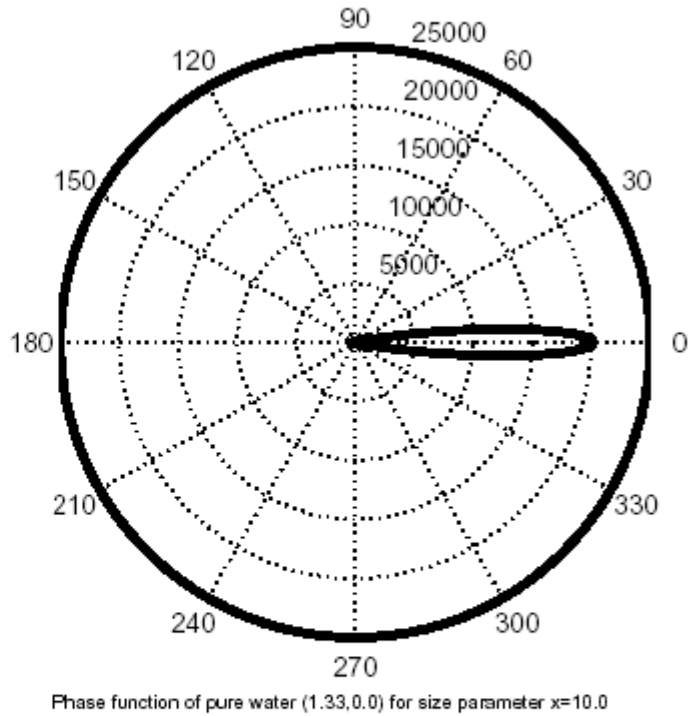

(b) A polar plot of the scattering profile of a water droplet of size parameter x =10.

In reality atmospheric aerosols contain a mixture of different radii. Thus the interference patterns smear-out due to the overlap of the scattering dependencies of many particles

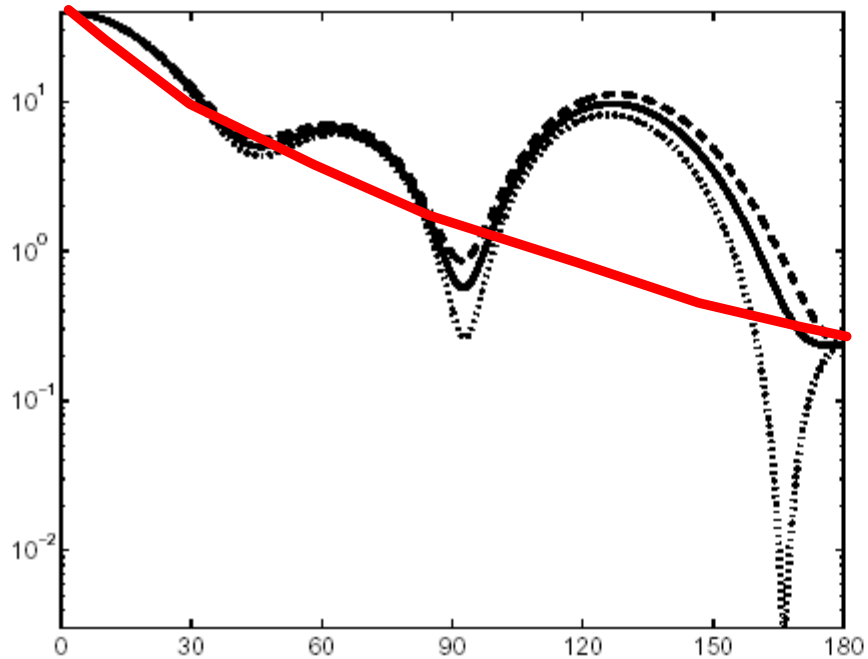

(a) Scattering diagram for x=3. The dotted and the broken lines represent the two orthogonal polarization states, whereas the solid line represents unpolarized light.

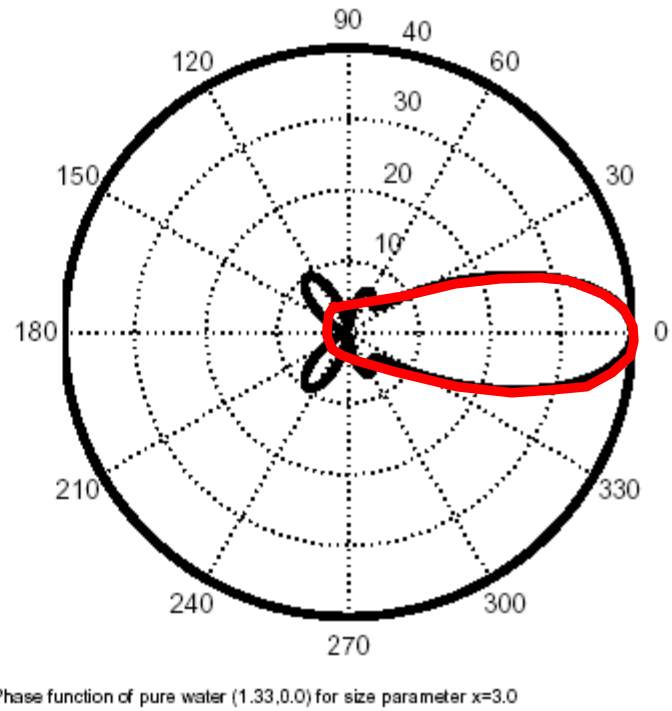

(b) A polar plot of the scattering profile of a water droplet of size parameter x =3.

Figure 2.16: Phase functions of a water droplet with x=3

Information on distance from time delay:

$\Delta t = (2*d)/c$

$c_{EM} = 3*10^{8} m/s$

$c_{sound} = 3*10^{2} m/s$

Dependence of the speed of sound on temperature

Effect of temperature			
Temperature	Speed of sound	Density of air	Acoustic impedance
ϑ in °C	c in $m \cdot s^{-1}$	ρ in $kg \cdot m^{-3}$	Z in $N \cdot s \cdot m^{-3}$
−25	315.8	1.423	449.4
−20	318.9	1.395	444.9
−15	322.1	1.368	440.6
−10	325.2	1.342	436.1
−5	328.3	1.317	432.0
0	331.3	1.292	428.4
+5	334.3	1.269	424.3
+10	337.3	1.247	420.6
+15	340.3	1.225	416.8
+20	343.2	1.204	413.2
+25	346.1	1.184	409.8
+30	349.0	1.164	406.2
+35	351.9	1.146	403.3

Active methods with focus on time information

-LIDAR **Light detection and ranging**

-RADAR Radio detection and ranging

-SODAR Sound detection and ranging

LIght Detection And Ranging: LIDAR

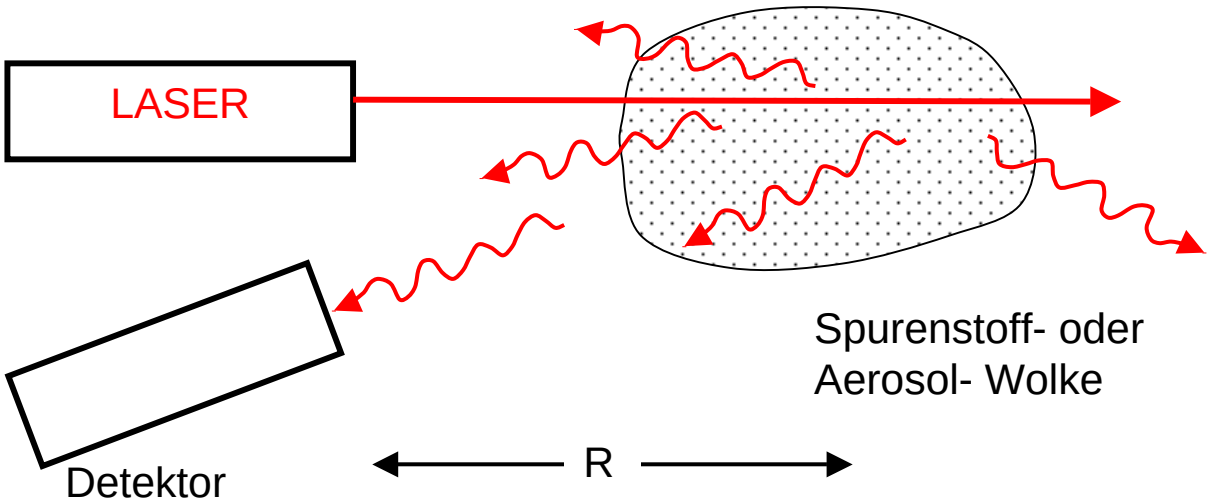

Prinzip:

Kurze Strahlungsimpulse einer starken, gebündelten Lichtquelle (üblicherweise eines LASERs) werden in die Atmosphäre ausgestrahlt.

Laufzeit ergibt Höhe (Echo), Intensität ergibt Streustärke (Konzentration)

→ räumliche Verteilung von Aerosol bzw. Spurengasen

in der Richtung des ausgesandten Strahles

Laufzeit der Signale

$t = 2 R / c$

R = Abstand aus der die (betrachtete) Strahlungsintensität zurückgestreut wird.

c = Lichtgeschwindigkeit

t = Zeit (nach Aussenden des Laser-pulses) zu der das Signal den Detektor erreicht

Für Pulslänge dt ergibt sich die Auflösung

$dR = dt\ c/2$

(1 µs Laserpuls gibt Höhenauflösung von 150 m)

Frequenz 10-100 Hz

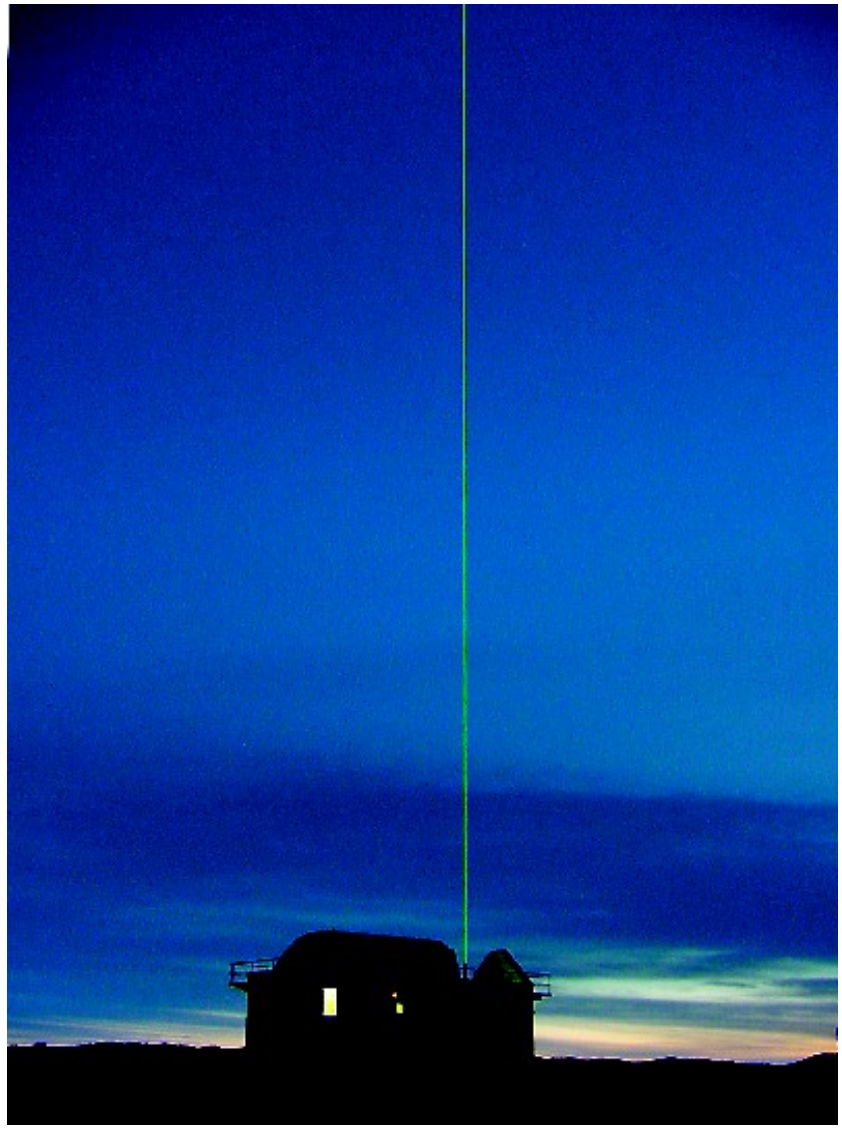

http://www.aad.gov.au/asset/information/photos_2/lidar.jpg

kleines Sendeteleskop,
großes (0.3-1.5 m)
Empfängerteleskop

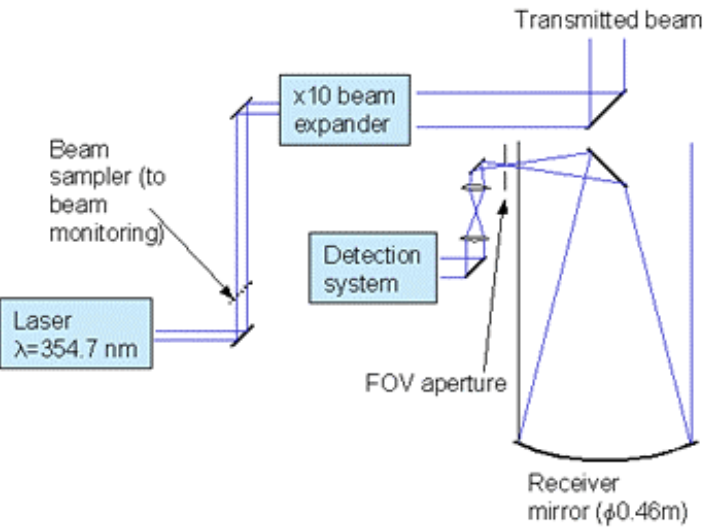

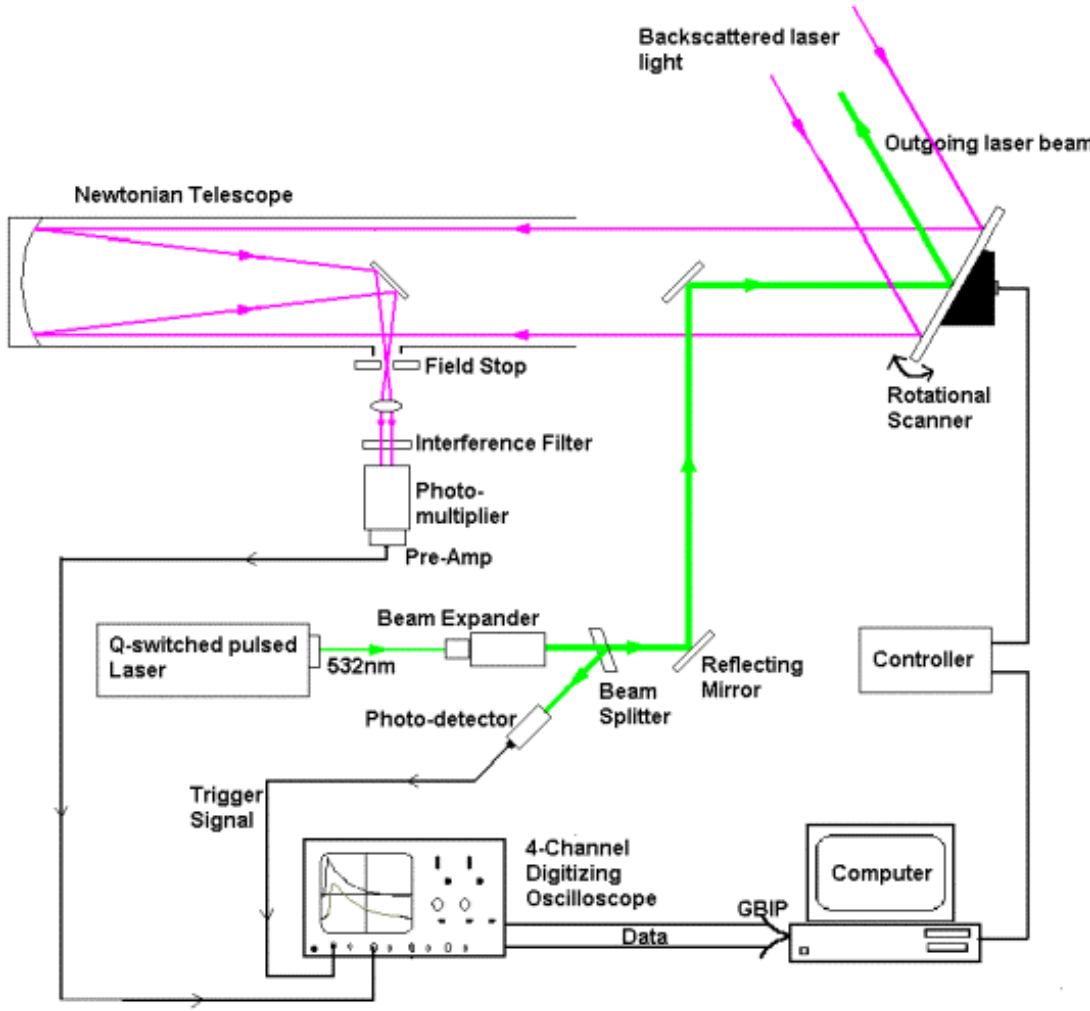

http://aposf02.cityu.edu.hk/~mcg/remote_sensing/Lidar/images/Lidar_profiling.gif

Aerosolmessungen mit Mie-LIDAR

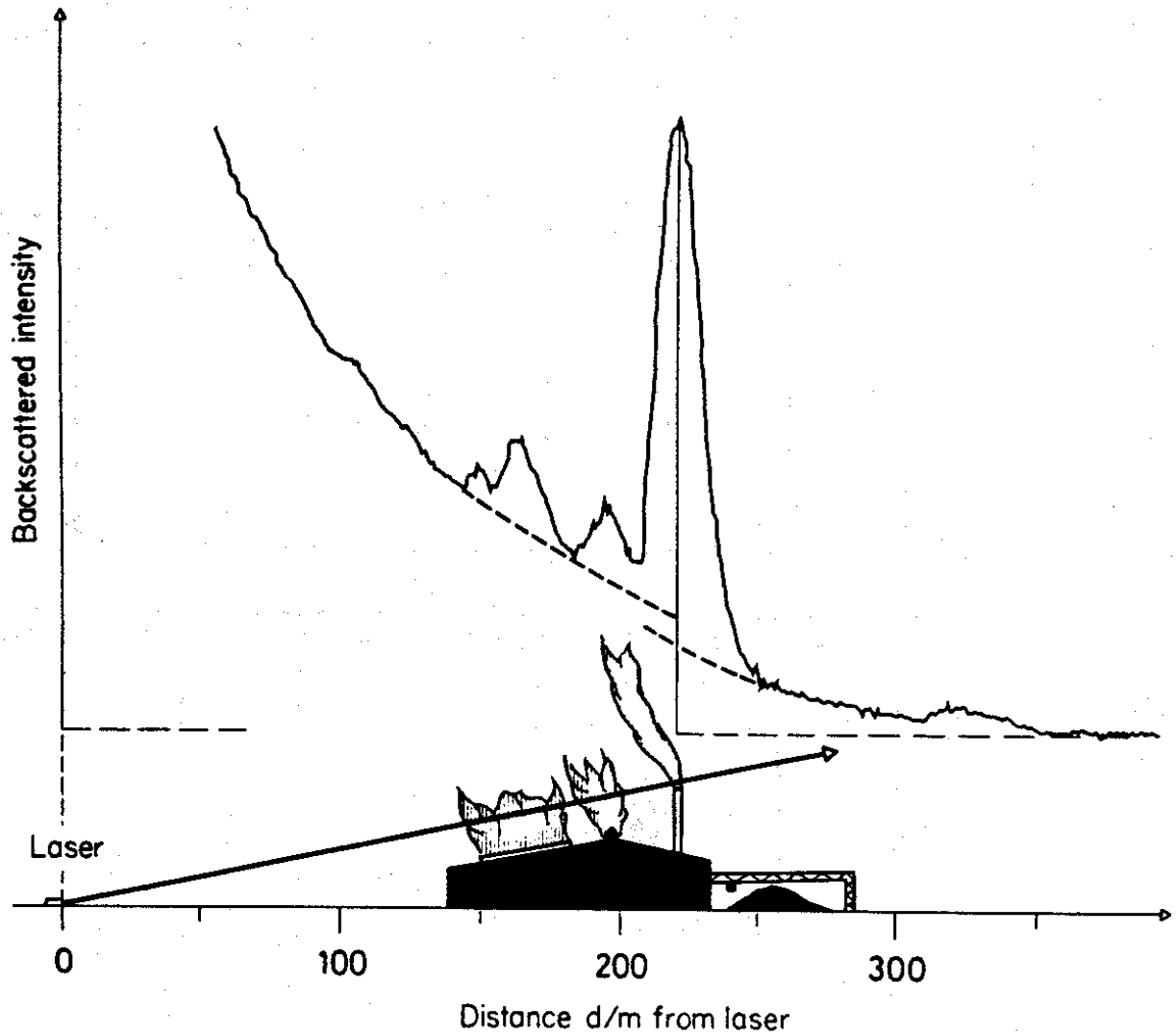

Figure 3.9. Mie scattering lidar particle monitoring at an iron-alloy plant. From Fredriksson et al. (1976).

PSCs over Kiruna © C.-F. Enell

Different LIDAR signals of PSCs

Amplitude
=> Particle amount

Ratio of intensity at diferent wavelengths
=> Particle size

Ratio of intensity at diferent polarisation
=> Thermodynamical state

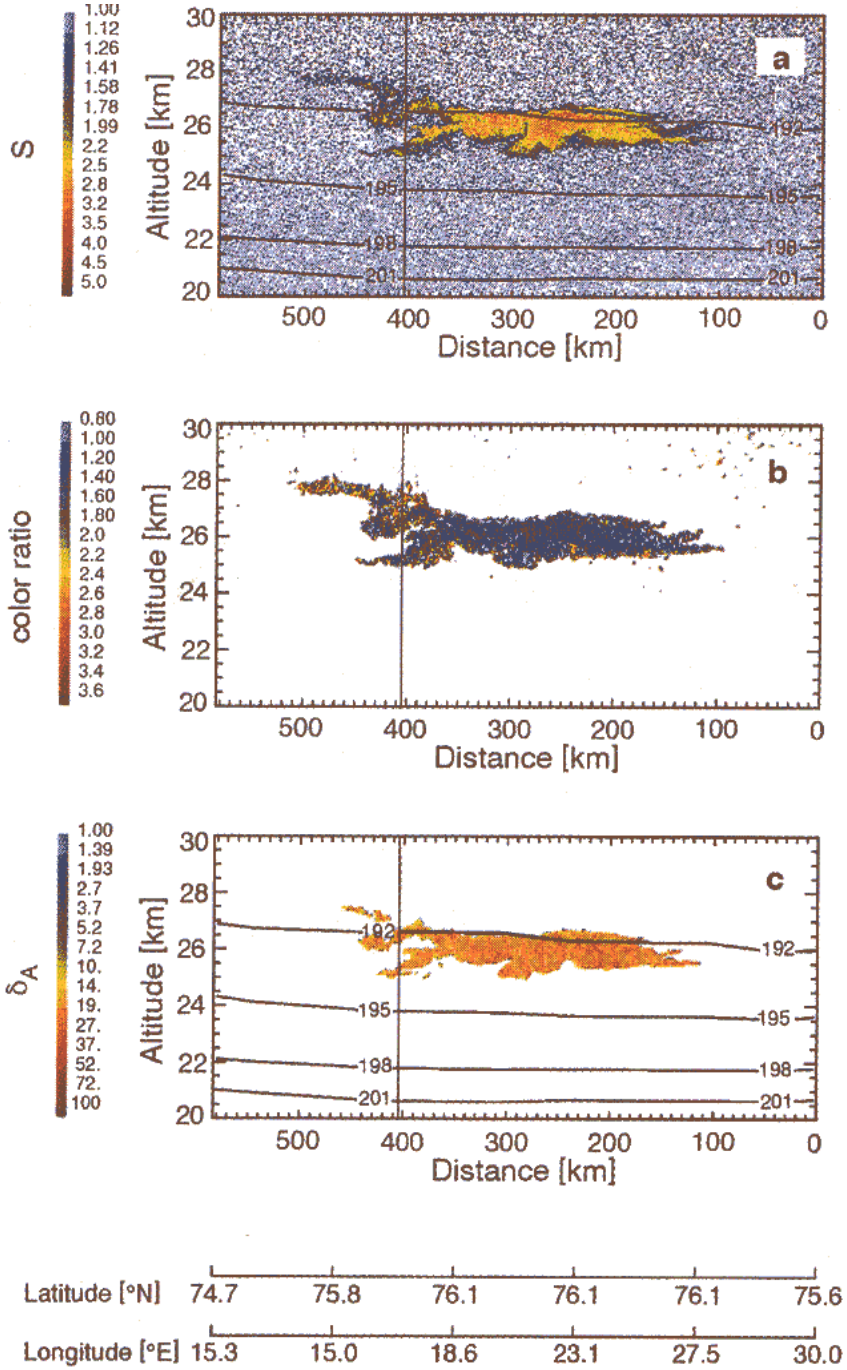

Aerosolschicht nach Ausbruch des Pinatubo 1991

Scattering ratio = Mie-scattering / Rayleigh scattering

3. August 1991 – 28. Feb.1992

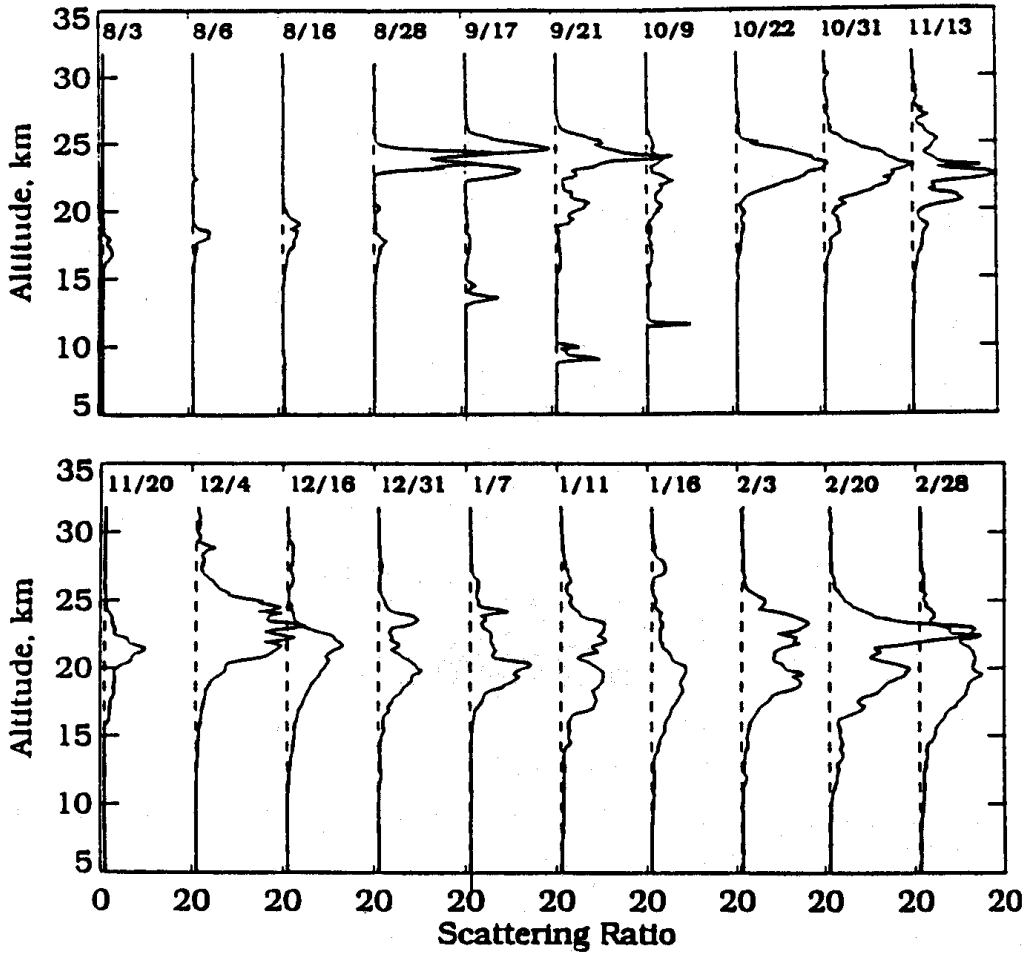

Figure 3.10. Lidar recordings of stratospheric dust due to the Mt. Pinatubo volcanic eruption. The Mie scattered intensity divided by the expected Rayleigh scattering intensity from a particle-free atmosphere has been plotted. Recordings taken at Hampton, Virginia, covering the period, Aug. 3, 1991, to Feb. 28, 1992. From Osborn et al. (1992).

The eruption of Pinatubo in the Philippines, 12 June 1991, the largest volcanic eruption since 1912.

Aerosolschicht nach Ausbruch des Pinatubo 1991

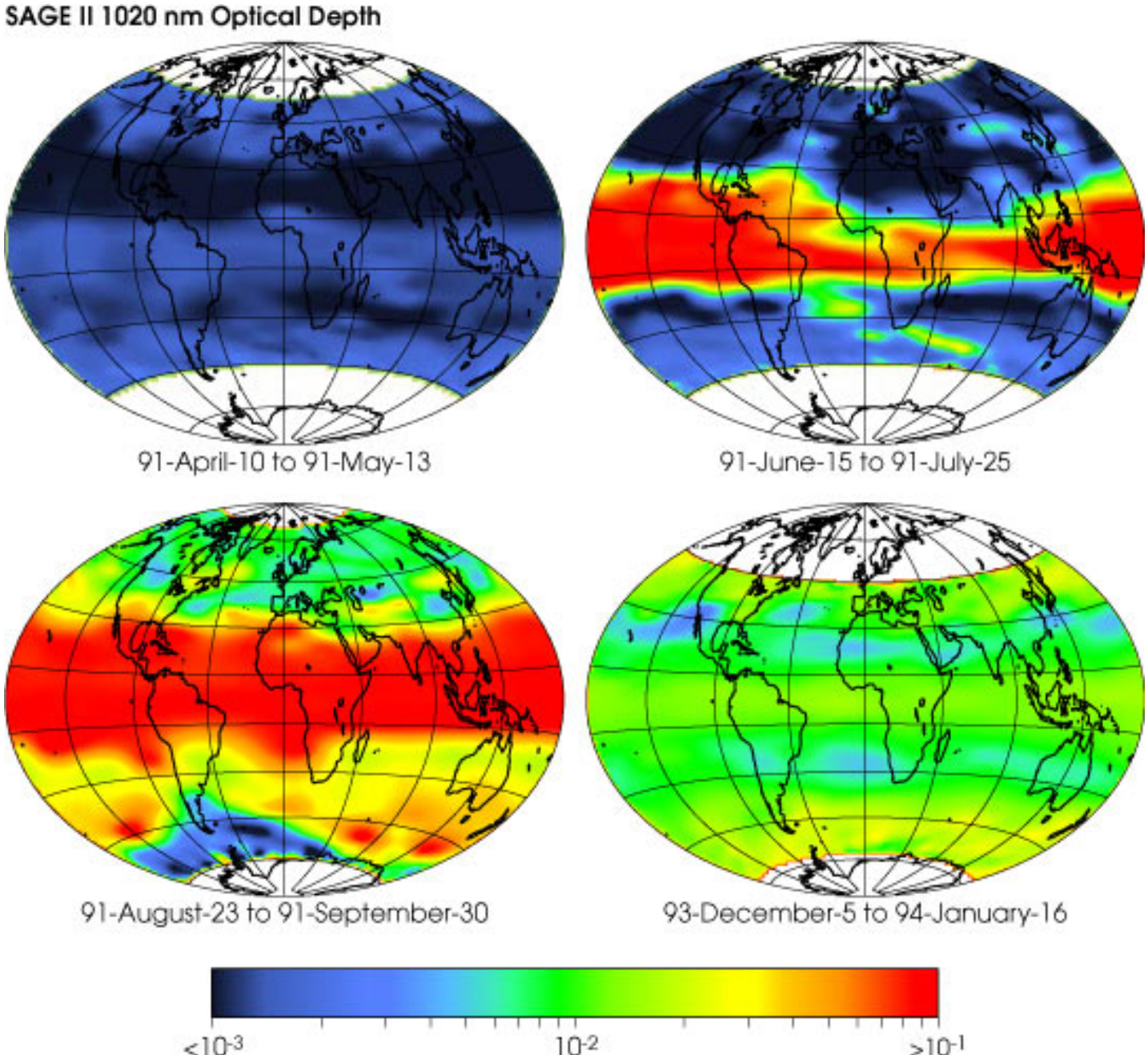

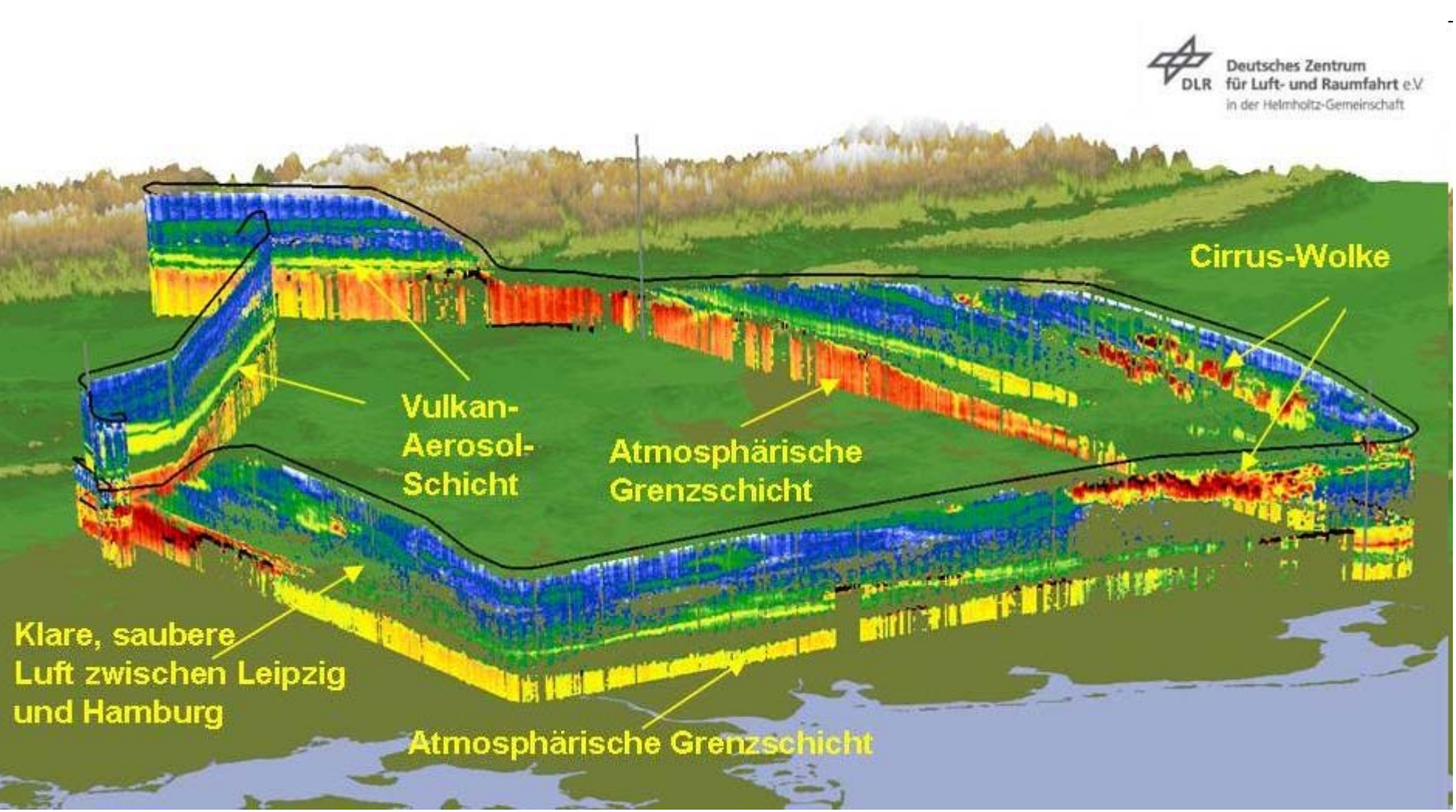

Lidar-Messung der Signal-Stärke entlang des Flugweges der Falcon am 19. April 2010; die schwarze Linie zeigt den Flugweg und die Flughöhe an; rote-schwarze Farben zeigen hohe Signale von Wolken (niedrige Wolken in 2-3 km und hohe Cirrus-Wolken) und Aerosol in der bodennahen atmosphärischen Grenzschicht; Vulkan-Aerosolschichten sind im südlichen Bereich von München bis Leipzig zu erkennen, wohingegen zwischen Leipzig und Hamburg keine Schichten oberhalb von 3 km zu erkennen sind.

http://www.dlr.de/pa/DesktopDefault.aspx/tabid-2342/6725_read-23886/

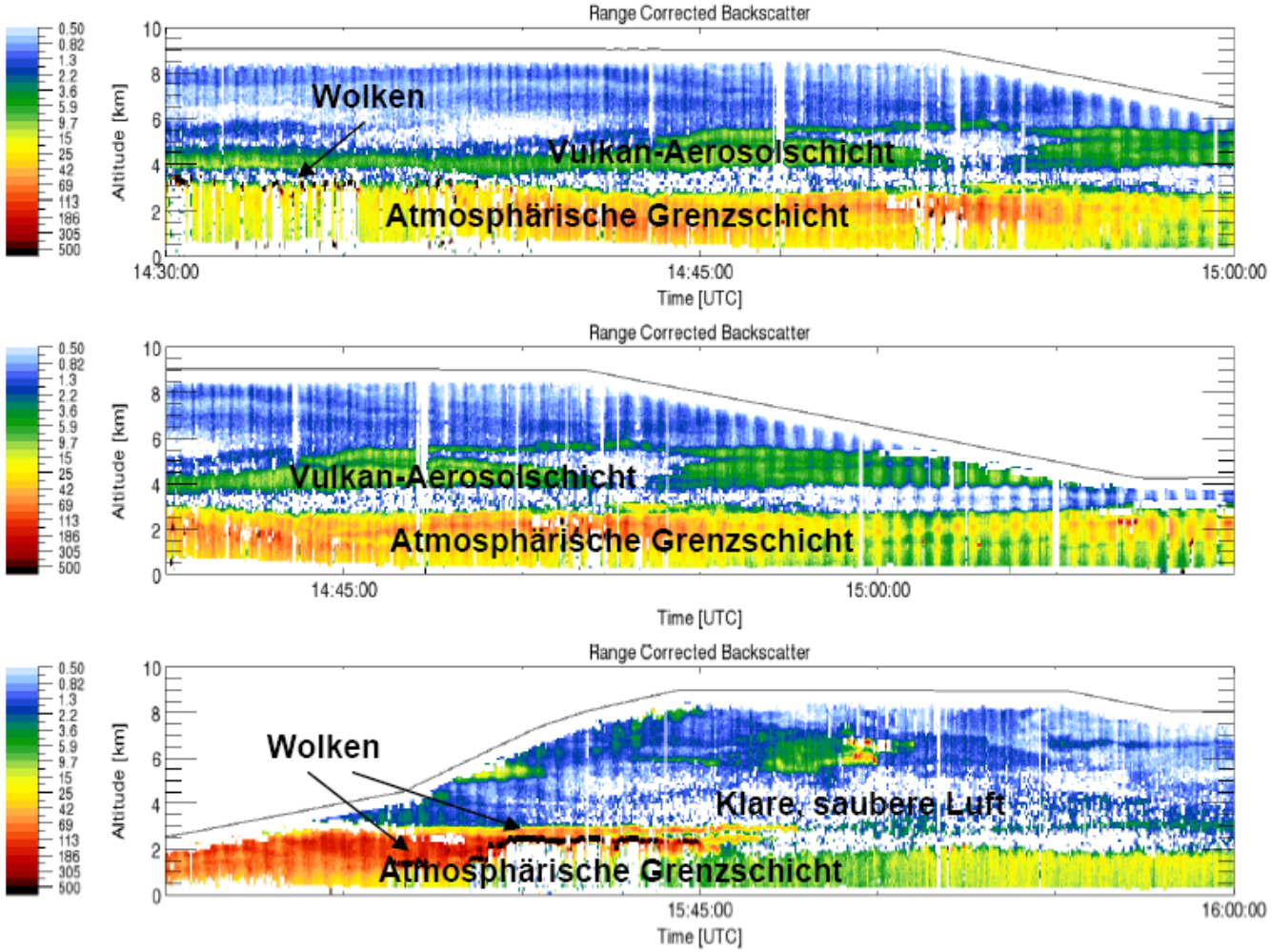

Lidar-Messung der Signal-Stärke entlang des Flugweges der Falcon am 19. April 2010; die schwarze Linie zeigt den Flugweg und die Flughöhe an; rote-schwarze Farben zeigen hohe Signale von Wolken (niedrige Wolken in 2-3 km und hohe Cirrus-Wolken) und Aerosol in der bodennahen atmosphärischen Grenzschicht; Vulkan-Aerosolschichten sind im südlichen Bereich von München bis Leipzig zu erkennen, wohingegen zwischen Leipzig und Hamburg keine Schichten oberhalb von 3 km zu erkennen sind.

http://www.dlr.de/pa/DesktopDefault.aspx/tabid-2342/6725_read-23886/

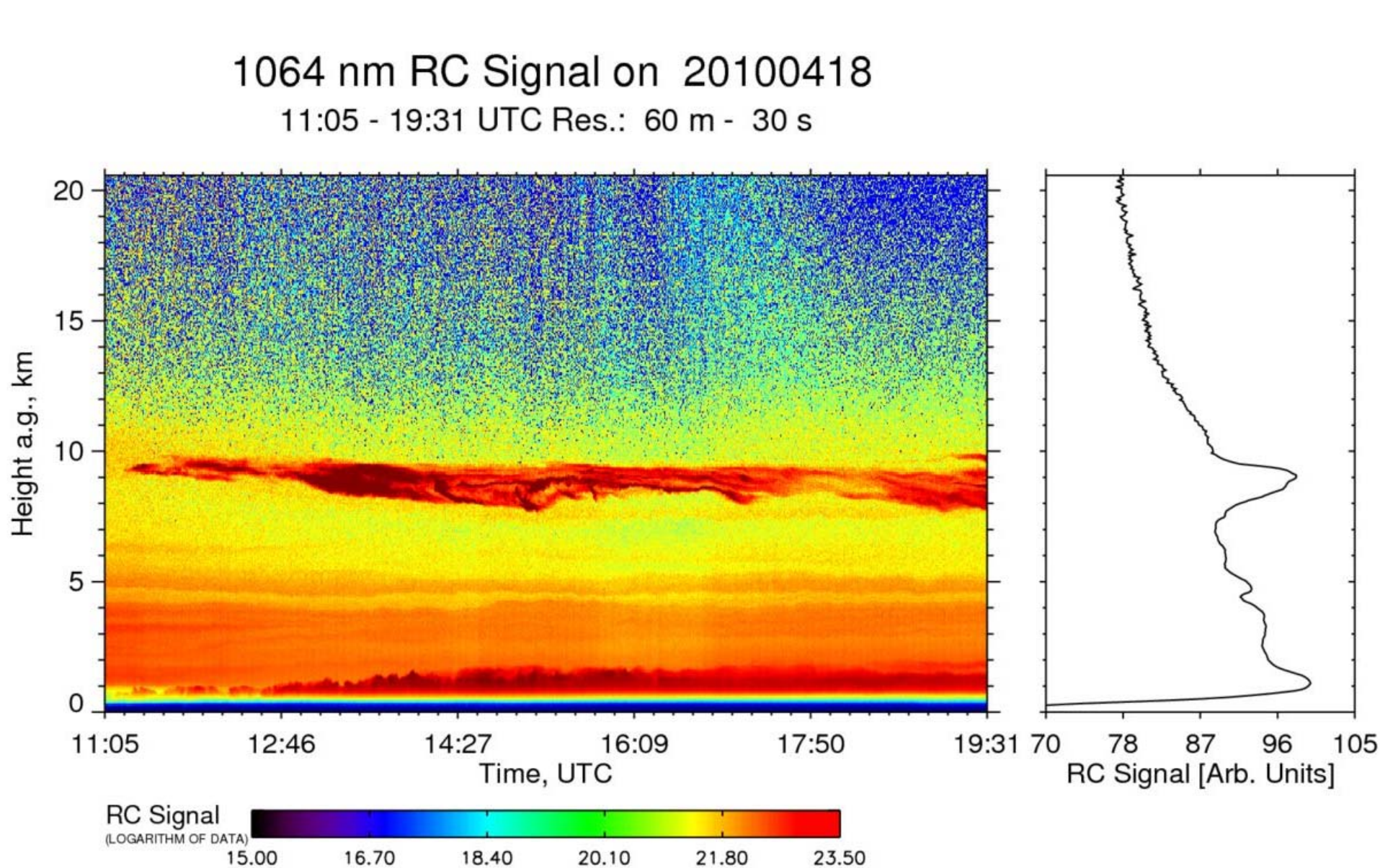

http://polly.tropos.de/martha/

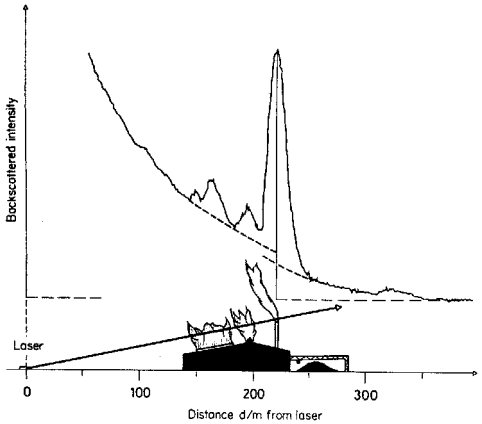

Figure 3.9. Mie scattering lidar particle monitoring at an iron-alloy plant. From Fredriksson et al. (1976).

- Lidar equation is the fundamental equation in laser remote sensing field to relate the received photon counts (or light power) with the transmitted laser photon counts (or laser power), light propagation in background atmosphere, physical interaction between light and objects, and lidar system efficiency and geometry, etc.

$$N_S(\lambda,R) = N_L(\lambda_L)\cdot\left[\beta(\lambda,\lambda_L,\theta,R)\Delta R\right]\cdot\frac{A}{R^2}\cdot\left[T(\lambda_L,R)T(\lambda,R)\right]\cdot\left[\eta(\lambda,\lambda_L)G(R)\right]+N_B$$

N_S (R) - expected received photon number from a distance R
N_L - number of transmitted laser photons,
β(R) - volume scatter coefficient at distance R for angle θ,
ΔR - thickness of the range bin
A - area of receiver,
T(R) - one way transmission of the light from laser source to distance R or from distance R to the receiver,
η - system optical efficiency,
G(R) - geometrical factor of the system,
N_B - background photon counts.

$$N_S(\lambda,R) = N_L(\lambda_L)\cdot\left[\beta(\lambda,\lambda_L,\theta,R)\Delta R\right]\cdot\frac{A}{R^2}\cdot\left[T(\lambda_L,R)T(\lambda,R)\right]\cdot\left[\eta(\lambda,\lambda_L)G(R)\right]+N_B$$

Volume backscatter coefficient β is the probability per unit distance travel that a photon is scattered into wavelength λ in unit solid angle at angle $\theta = \pi$.

Volume backscatter coefficient β is equal to

$$\beta(\lambda,\lambda_L,z) = \sum_i\left[\frac{d\sigma_i(\lambda_L)}{d\Omega}n_i(z)\,p_i(\lambda)\right]$$

$\frac{d\sigma_i(\lambda_L)}{d\Omega}$ Is the differential backscatter cross-section of single particle

$n_i(z)$ Is the number density of scatter species i

$p_i(\lambda)$ Is the probability of the scattered photons falling into the wavelength λ.

$$N_S(\lambda,R) = N_L(\lambda_L)\cdot\left[\beta(\lambda,\lambda_L,\theta,R)\Delta R\right]\cdot\frac{A}{R^2}\left[T(\lambda_L,R)T(\lambda,R)\right]\cdot\left[\eta(\lambda,\lambda_L)G(R)\right]+N_B$$

The probability that a scatter photon is collected by the receiving telescope, i.e., the solid angle subtended by the receiver aperture to the scatterer (perception angle)

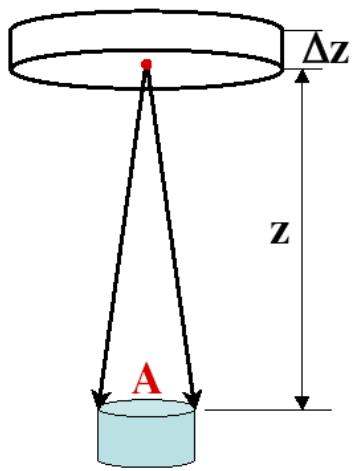

$$N_S(\lambda,R) = N_L(\lambda_L)\cdot\left[\beta(\lambda,\lambda_L,\theta,R)\Delta R\right]\cdot\frac{A}{R^2}\cdot\left[T(\lambda_L,R)T(\lambda,R)\right]\left[\eta(\lambda,\lambda_L)G(R)\right]+N_B$$

$T(\lambda_L,z)T(\lambda,z)$ is the atmospheric transmittance at outgoing wavelength λ_L and return wavelength λ

$$T(\lambda_L,R) = \exp\left[-\int_0^R \alpha(\lambda_L,r)dr\right] \qquad T(\lambda,R) = \exp\left[-\int_0^R \alpha(\lambda,r)dr\right]$$

$$T(\lambda_L,R)T(\lambda,R) = \exp\left[-\left(\int_0^R \alpha(\lambda_L,r)dr + \int_0^R \alpha(\lambda,r)dr\right)\right]$$

when $\lambda = \lambda_L$ $= \exp\left[-2\int_0^R \alpha(\lambda,r)dr\right]$

$\alpha(\lambda,R)$ is the extinction coefficient

$$\alpha(\lambda,R) = \sum_i\left[\sigma_{i,ext}(\lambda)n_i(R)\right]$$

$$\sigma_{ext} = \sigma_{scattering} + \sigma_{absorption}$$

$\sigma_{ext}(\lambda)$ is the integral extinction cross-section, since scattering into all directions contributes to light extinction, which is different than the case for backscatter coefficient definition.

$$N_S(\lambda,R) = N_L(\lambda_L)\cdot\left[\beta(\lambda,\lambda_L,\theta,R)\Delta R\right]\cdot\frac{A}{R^2}\cdot\left[T(\lambda_L,R)T(\lambda,R)\right]\left[\eta(\lambda,\lambda_L)G(R)\right]+N_B$$

$\eta(\lambda,\lambda_L)=\eta_T(\lambda_L)\cdot\eta_R(\lambda)$ is the lidar hardware optical efficiency

e.g., mirrors, lens, filters, detectors, etc

$G(z)$ is the geometrical form factor, mainly concerning the overlap of the area of laser irradiation with the field of view of the receiver optics

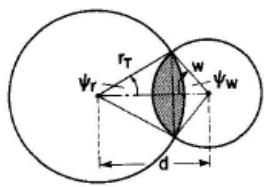

(b)

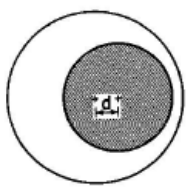

(c)

$$N_S(\lambda,R) = N_L(\lambda_L)\cdot\left[\beta(\lambda,\lambda_L,\theta,R)\Delta R\right]\cdot\frac{A}{R^2}\cdot\left[T(\lambda_L,R)T(\lambda,R)\right]\cdot\left[\eta(\lambda,\lambda_L)G(R)\right]+N_B$$

N_B is the expected photon counts per range bin per unit time, due to background noise (e.g., solar scattering) and detector/circuit shot noise.

LIDAR equation for β and α

$$N_S(\lambda,z) = \left[N_L(\lambda_L) \right] \left[\beta(\lambda,\lambda_L,z)\Delta z \right] \left(\frac{A}{z^2} \right) \exp\left[-2\int_0^z \alpha(\lambda,z')dz' \right] \left[\eta(\lambda,\lambda_L)G(z) \right] + N_B \Delta t$$

General problem:

-Two unknown quantities (β and α) should be determined from one observation

-in particular, no absolute value of aerosol extinction can be derived

Simple solution: assume (constant) extinction-to-backscatter ratio (lidar ratio)

-high values indicate low probability for back-scattering
-8.4 sr for Rayleigh-scattering
-30 sr is a common value for submicron aerosols

Extinction-to-backscatter ratio (lidar ratio) depends on

a) Single scattering albedo (1- ratio of absorption and extinction)

Single scattering albedo = 0
=> only absorption

Single scattering albedo = 1
=> only scattering

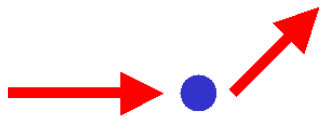

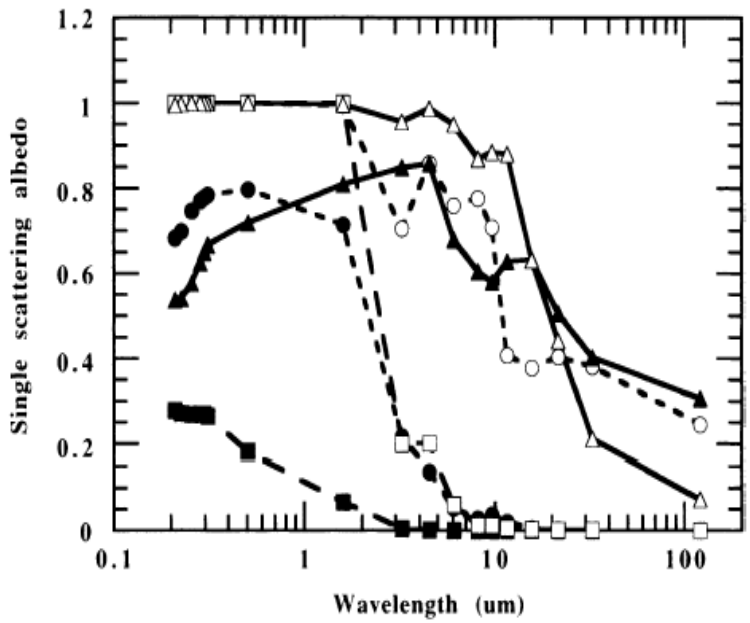

Single scattering albedo

for different aerosol types

(Takemura et al., J. of Climate, 2002)

Extinction-to-backscatter ratio (lidar ratio) depends on

a) Single scattering albedo (1- ratio of absorption and extinction)

Single scattering albedo = 0
=> only absorption

Single scattering albedo = 0
=> only scattering

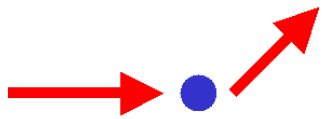

b) Phase function

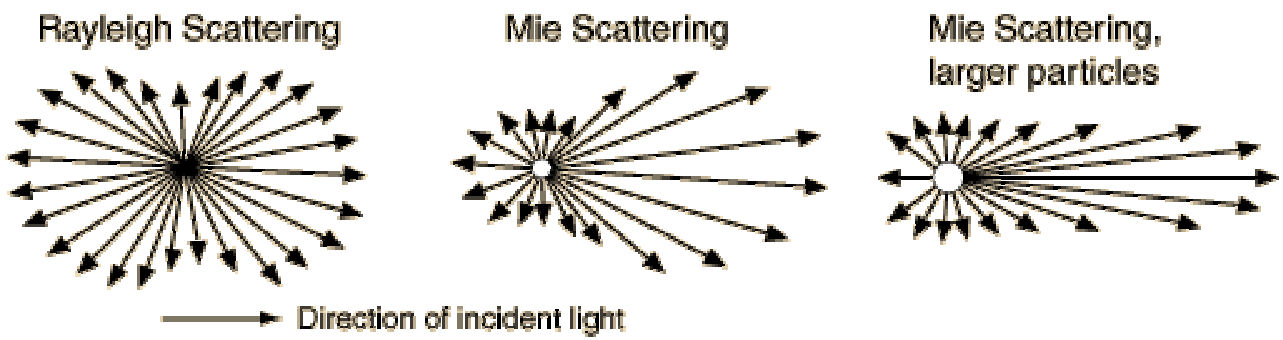

Extinction-to-backscatter ratio
-8.4 sr for Rayleigh-scattering
-30 sr is a common value for submicron aerosols

Sofisticated (instrumental) solutions

a)

Combined LIDAR and sun photometer observations:

-From the LIDAR, the high-resolved (relative) extinction profile is derived

-from the sun-photometer, the total optical depth of aerosol extinction is determined

=> From combination => the high-resolved absolute extinction profile

Sofisticated (instrumental) solutions

b)

RAMAN-LIDAR:

-Observe light at wavelength slightly shifted to emitted wavelength

=> the received light is RAMAN-scattered only by air molecules for which the total cross section and the LIDAR-ratio is known

-the attenuation term contains both the extinction due to molecules (known) and aerosols

=> From RAMAN-LIDAR the absolute optical depth of aerosol extinction can be determined

Problem: low signal to noise, operation often only during night

Sofisticated (instrumental) solutions

b)

RAMAN-LIDAR:

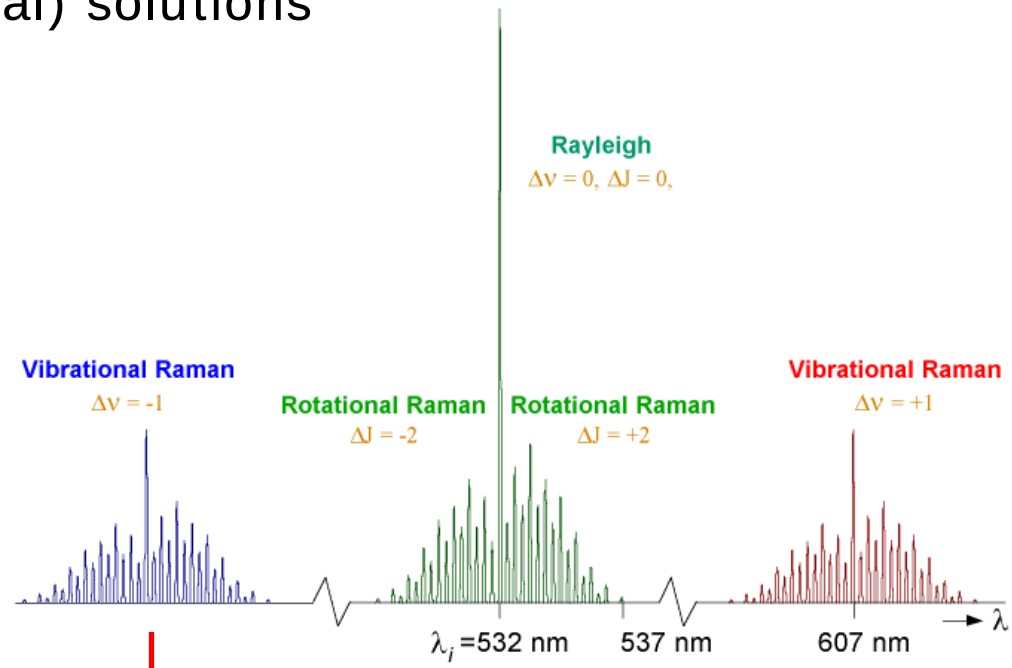

Wavelength at which the light is emitted in the atmosphere

Light observed at a ‚Raman wavelength' is only scattered from molecules

=> The effects of scattering and absorption are separated

Raman-LIDAR für N_2

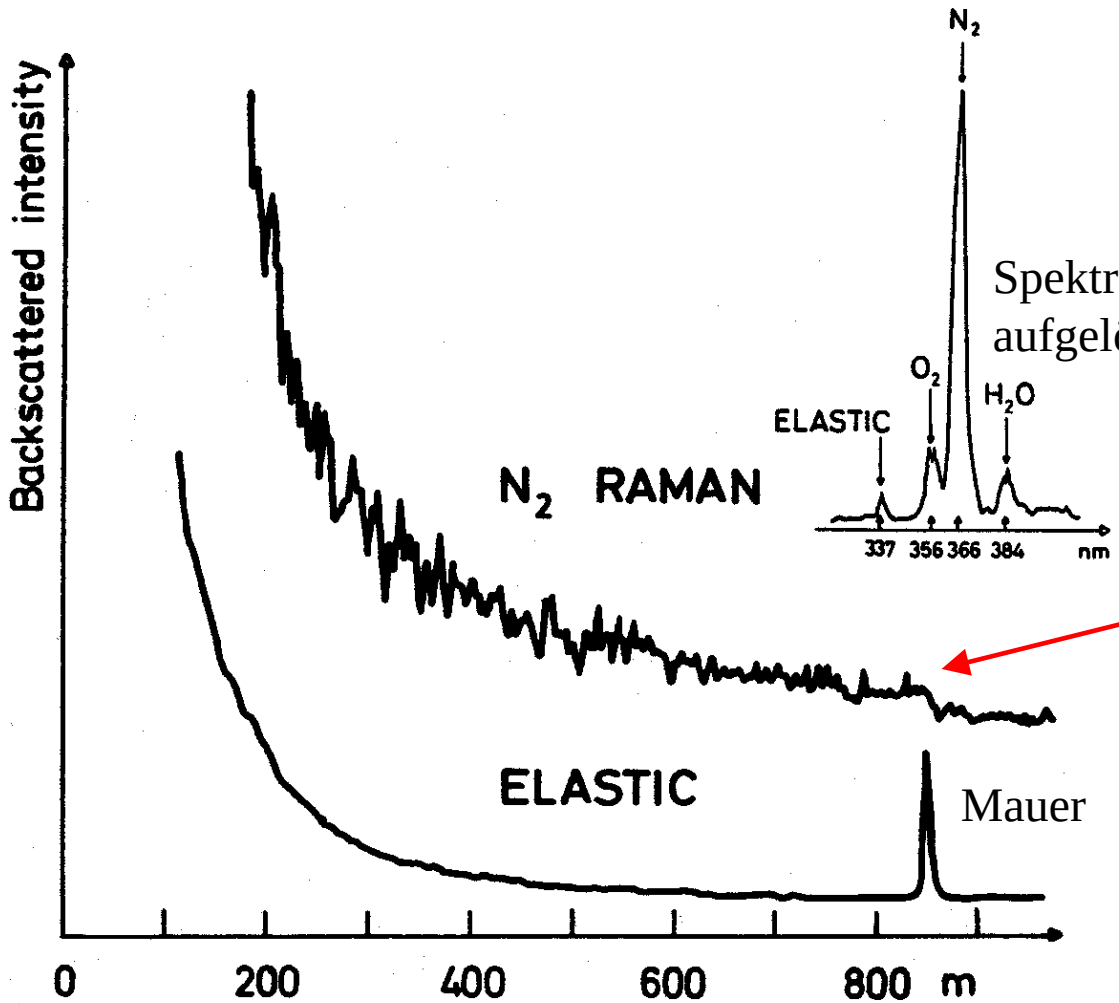

The reflection peak from the wall is missing in the Raman signal

Figure 3.11. Elastic backscattering and N_2 Raman scattering recordings against a solid target at an 850-m distance. The measurements were performed with a nitrogen laser operating at 337 nm. Inset: a spectrally resolved recording of atmospheric backscattering is shown, featuring peaks due to oxygen, nitrogen, and water vapor. From Fredriksson et al. (1977).

UV Raman Lidar System Details

Parameters of the LIDAR system:

Transmitter:	**Receiver:**
Wavelength 354.7 nm	**Wavelengths 353.0 nm**
Max. power 0.35 J per pulse	**353.9 nm**
Average Power 17.5W	**354.7 nm**
Pulse width 7 ns	**386.7nm**
Repetition rate 50 Hz	**407.8 nm**
Beam diameter 0.1 m	**Range resolution 6 m**
Beam divergence 0.1 mr	**Field-of-view 0.3 mr** **Mirror diameter 0.45 m**

http://www.chilbolton.rl.ac.uk/lidarsystem.htm

Analysis of the Raman signal

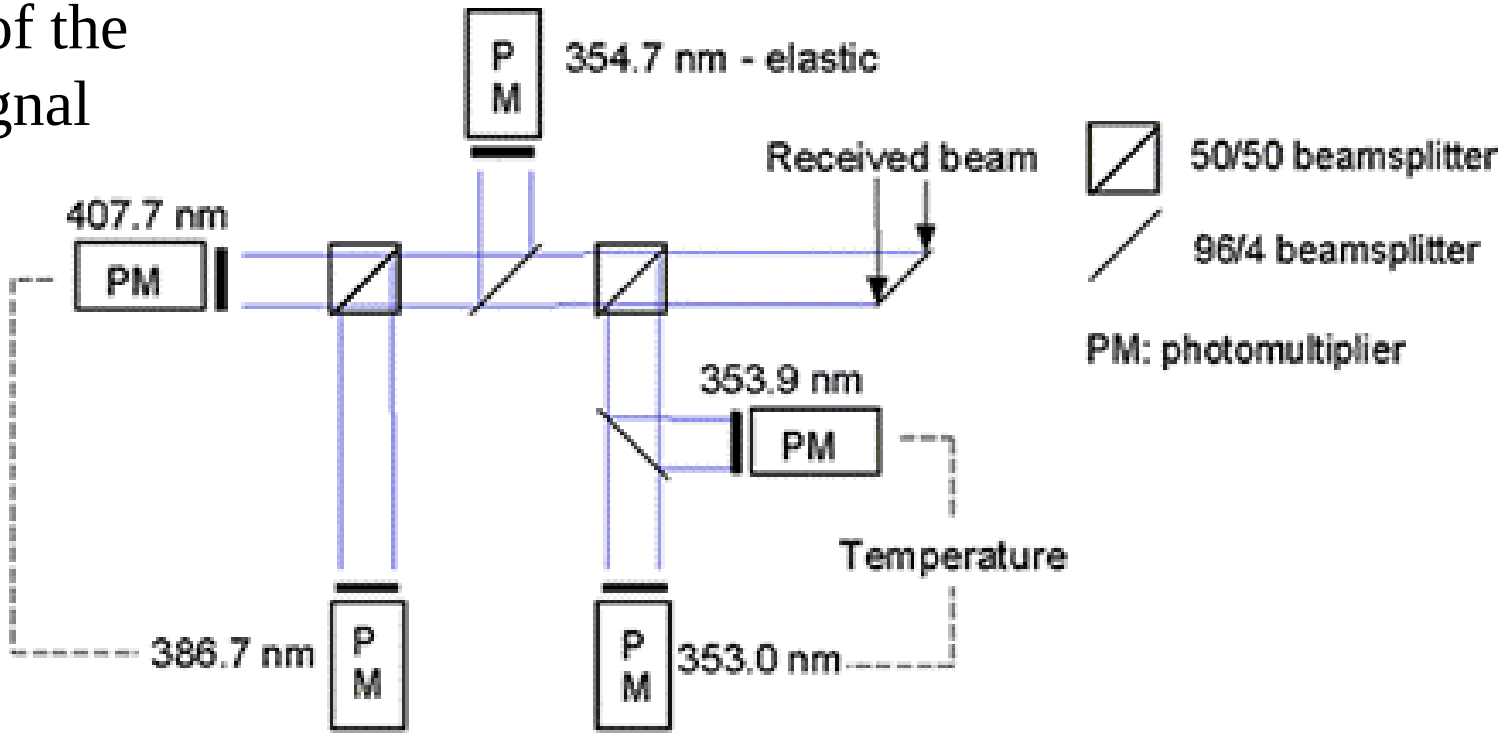

Messung von Temperaturprofilen:

-Extrem kleine Wellenlängenänderungen durch Rotationsübergänge

-Besetzungswahrscheinlichkeit der Rotationszustände ist temperaturabhängig:

-Messung an N_2, O_2

Bis hierher

http://www.chilbolton.rl.ac.uk/lidarsystem.htm

Raman-LIDAR for H_2O

In contrast to N2 or O2, the H2O concentration is highly variable

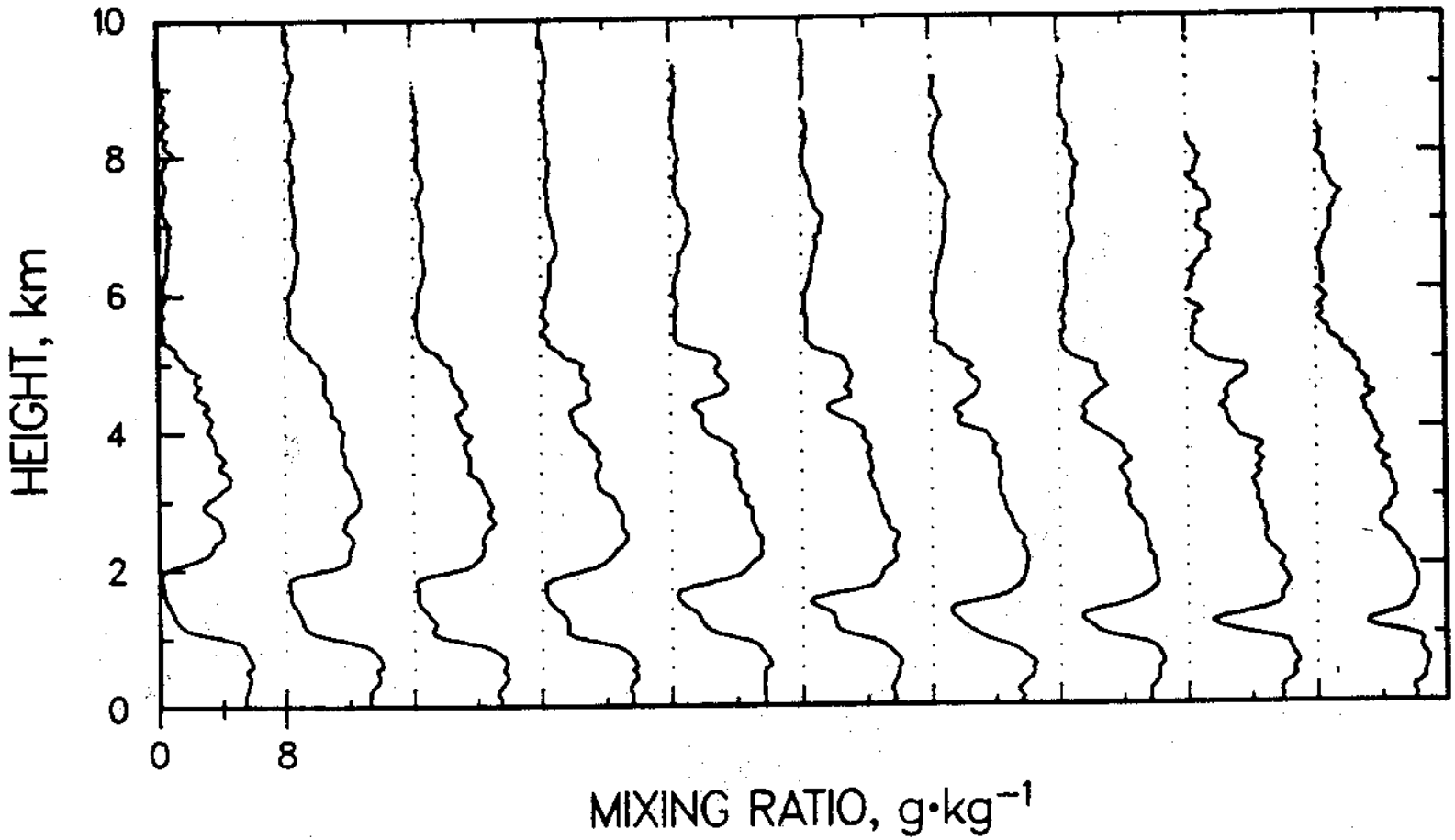

Figure 3.12. Water vapor Raman lidar curves, plotted as mixing ratios (water vapor to dry air). From Ansmann et al. (1992).

DIfferential Absorption Lidar
DIAL

Zur Bestimmung von Spurenstoffkonzentrationen werden im Gegensatz zum “gewöhnlichen” (= Aerosol-) LIDAR wenigstens zwei verschiedene Wellenlängen verwandt:

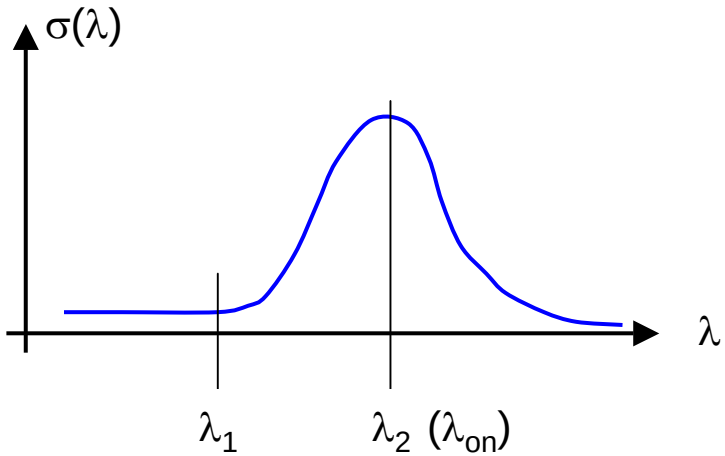

Ähnliche Streuquerschnitte (Mie, Rayleigh)
aber unterschiedliche Absorption

Die DIAL – Gleichung erhält man durch Division zweier LIDAR – Gl. für λ_1 bzw. λ_2:

$$\frac{E(\lambda_2, R)}{E(\lambda_1, R)} = \exp\left(-2(\sigma_2 - \sigma_1) \cdot \int_0^R n_A(r)\,dr \right)$$

Annahme: σ_{SR} und σ_S für λ_1 bzw. λ_2 gleich sind.
Gerechtfertigt solange $\lambda = \lambda_2 - \lambda_1$ hinreichend klein ist (wenige nm)

DIAL NO_2 on-off resonance

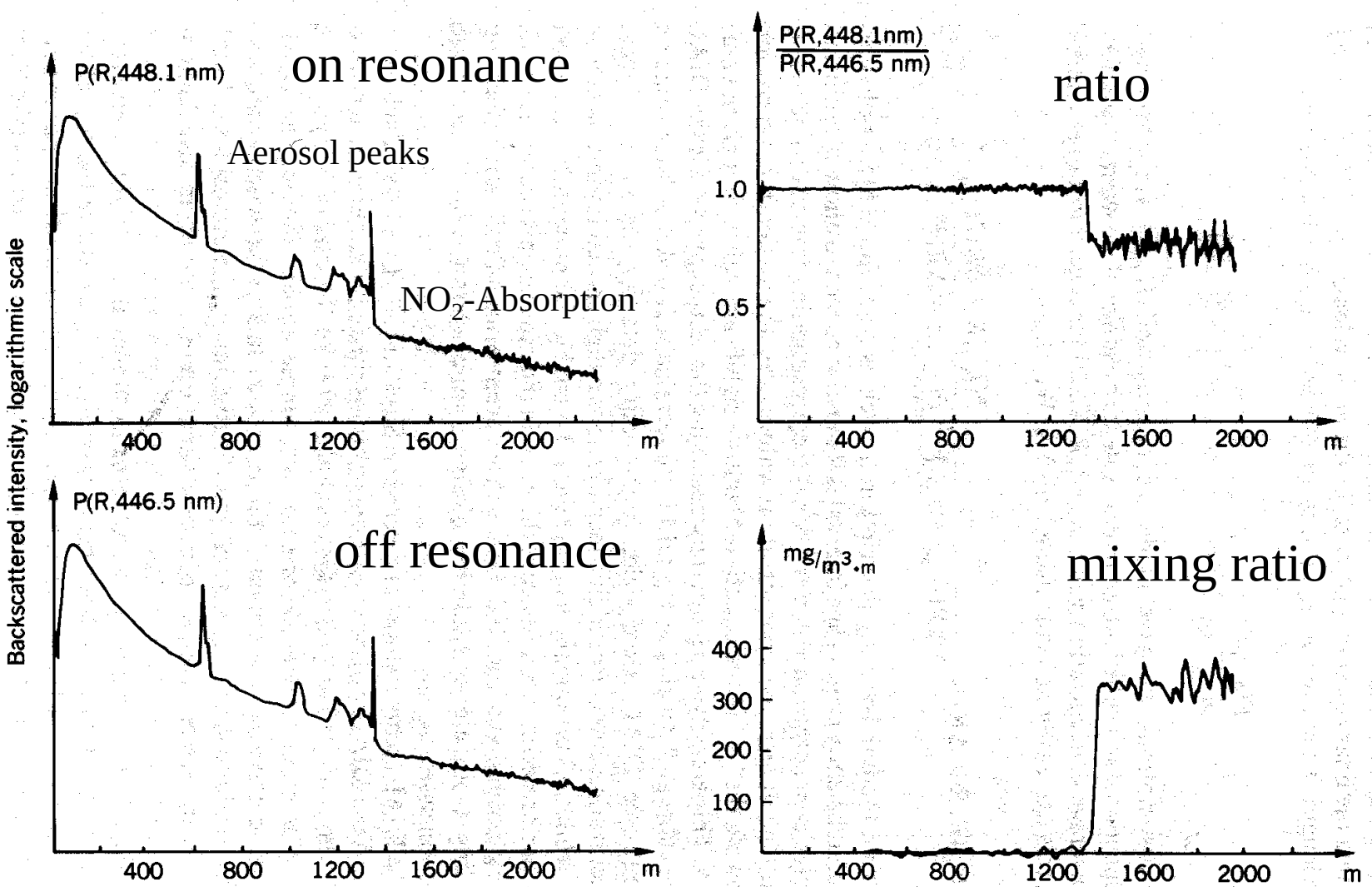

Figure 3.17. Nitrogen dioxide DIAL measurement of a plume from a saltpeter plant. On- and off-resonance lidar curves are shown together with the divided (DIAL) curve and the integrated NO_2 contents as a function of range. From Fredriksson et al. (1981).

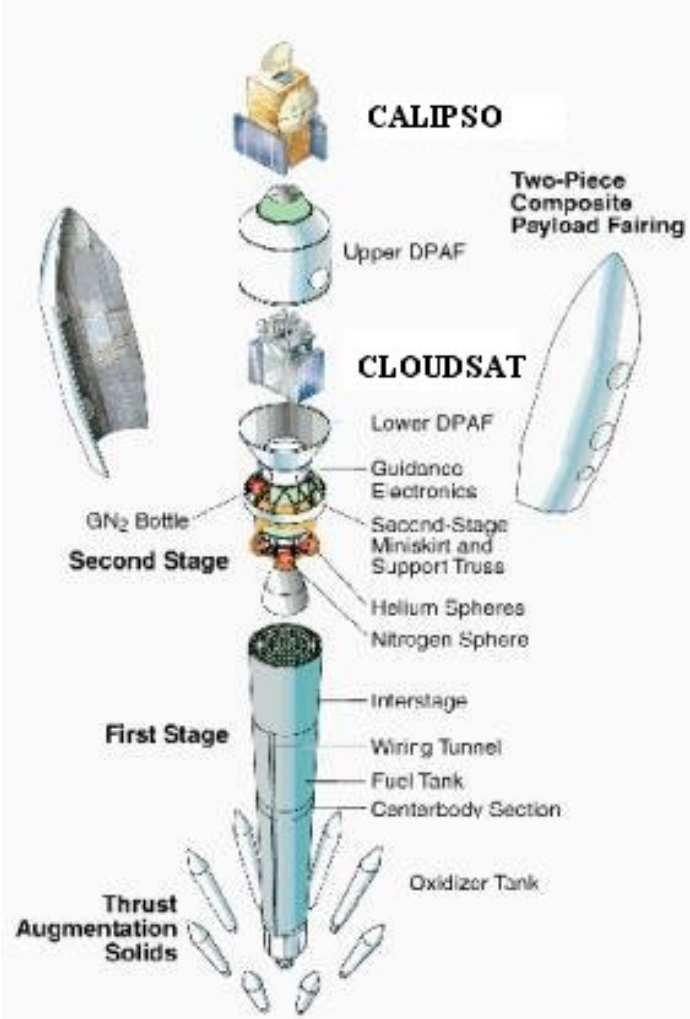

Launch: April 28, 2006

CALIPSO: **Cloud LIDAR**

CloudSat: **Cloud Profiling Radar (CPR)**

CALIPSO and CloudSat fly in formation with three other satellites in the ‘A-train constellation’

CloudSat and CALIPSO were launched together from Space Launch Complex 2W at Vandenberg Air Force Base, California, on a two-stage Delta 7420-10C launch vehicle

http://cloudsat.atmos.colostate.edu/mission

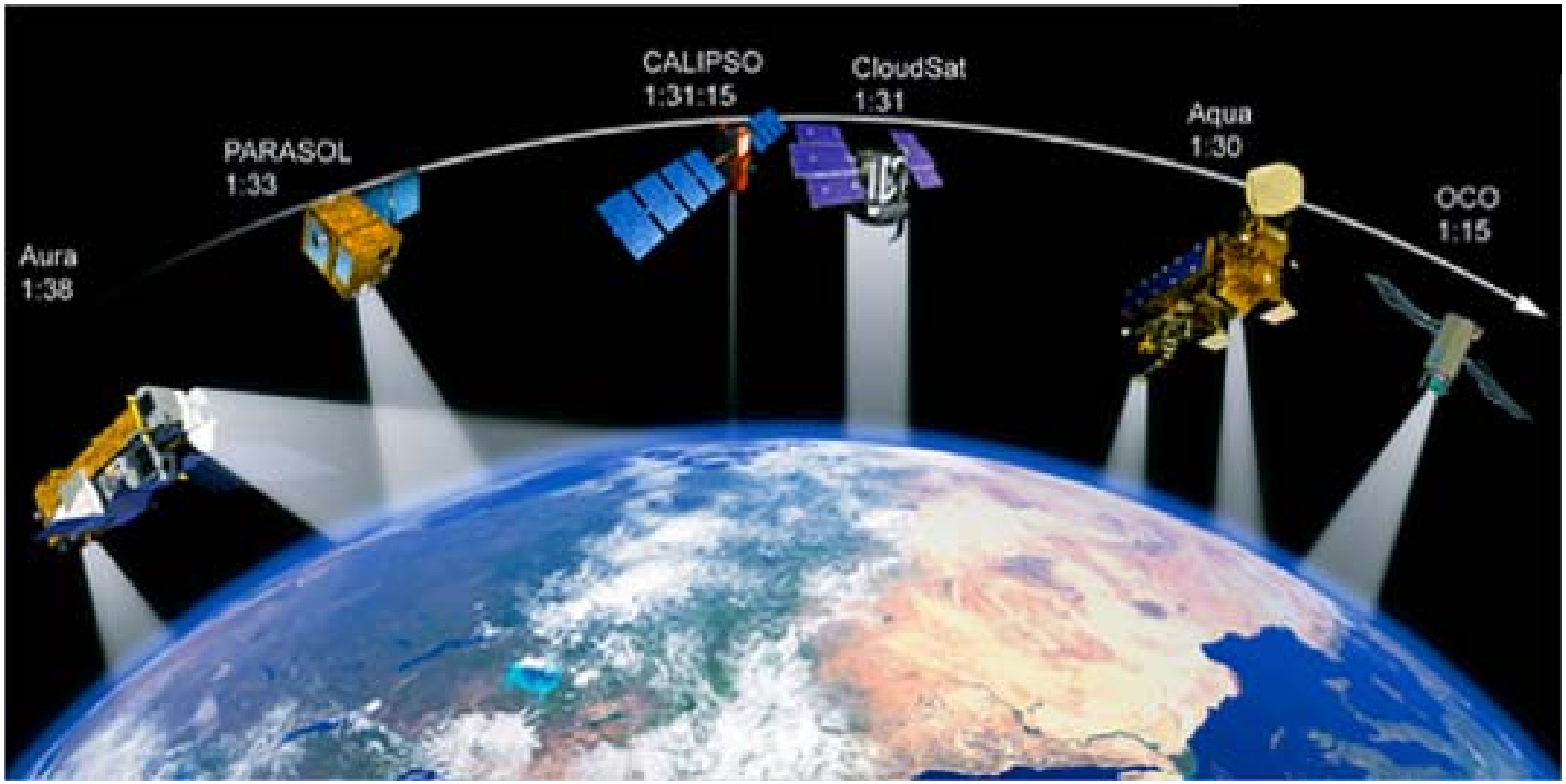

A-TRAIN CONSTELLATION

The Afternoon or "A-Train" satellite constellation presently consists of three satellites flying in formation around the globe (NASA's Aqua and Aura satellites and CNES' PARASOL satellite). The CALIPSO and CloudSat satellite missions were inserted in orbit behind Aqua in April 2006. A sixth spacecraft, OCO, is planned for launch in 2008 and will be placed ahead of Aqua.

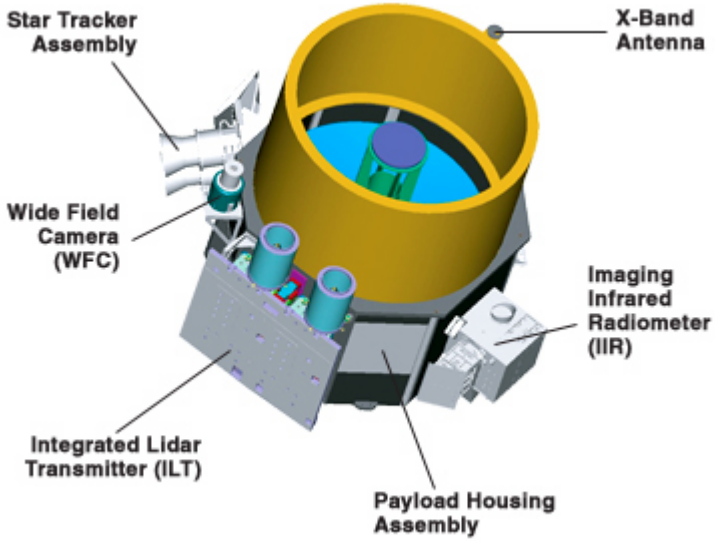

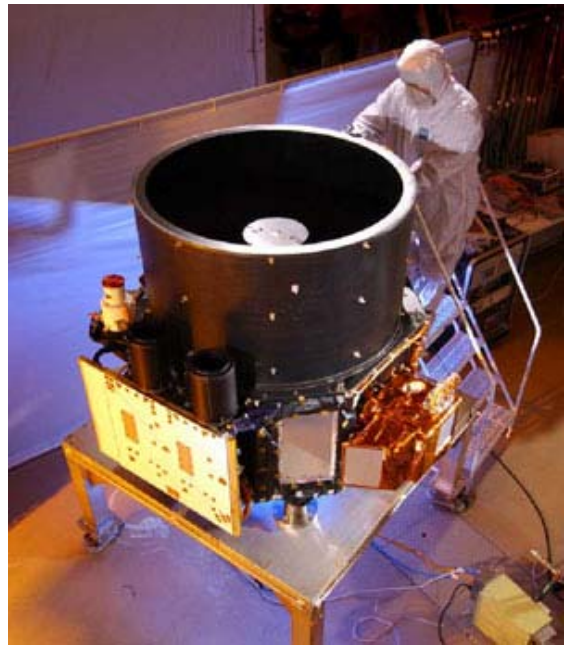

Characteristics CALIOP laser: Nd: YAG, diode-pumped, Q-switched, frequency doubled wavelengths: 532 nm, 1064 nm pulse energy: 110 mJoule/channel repetition rate: 20.25 Hz receiver telescope: 1.0 m diameter polarization: 532 nm footprint/FOV: 100 m/ 130 µrad vertical resolution: 30-60 m horizontal resolution: 333 m linear dynamic range: 22 bits data rate: 316 kbps

CALIPSO PAYLOAD

The CALIPSO payload consists of three co-aligned nadir-viewing instruments:

- the Cloud-Aerosol Lidar with Orthogonal Polarization (CALIOP)
- the Imaging Infrared Radiometer (IIR)
- the Wide Field Camera (WFC)

Attenuated backscatter 532nm

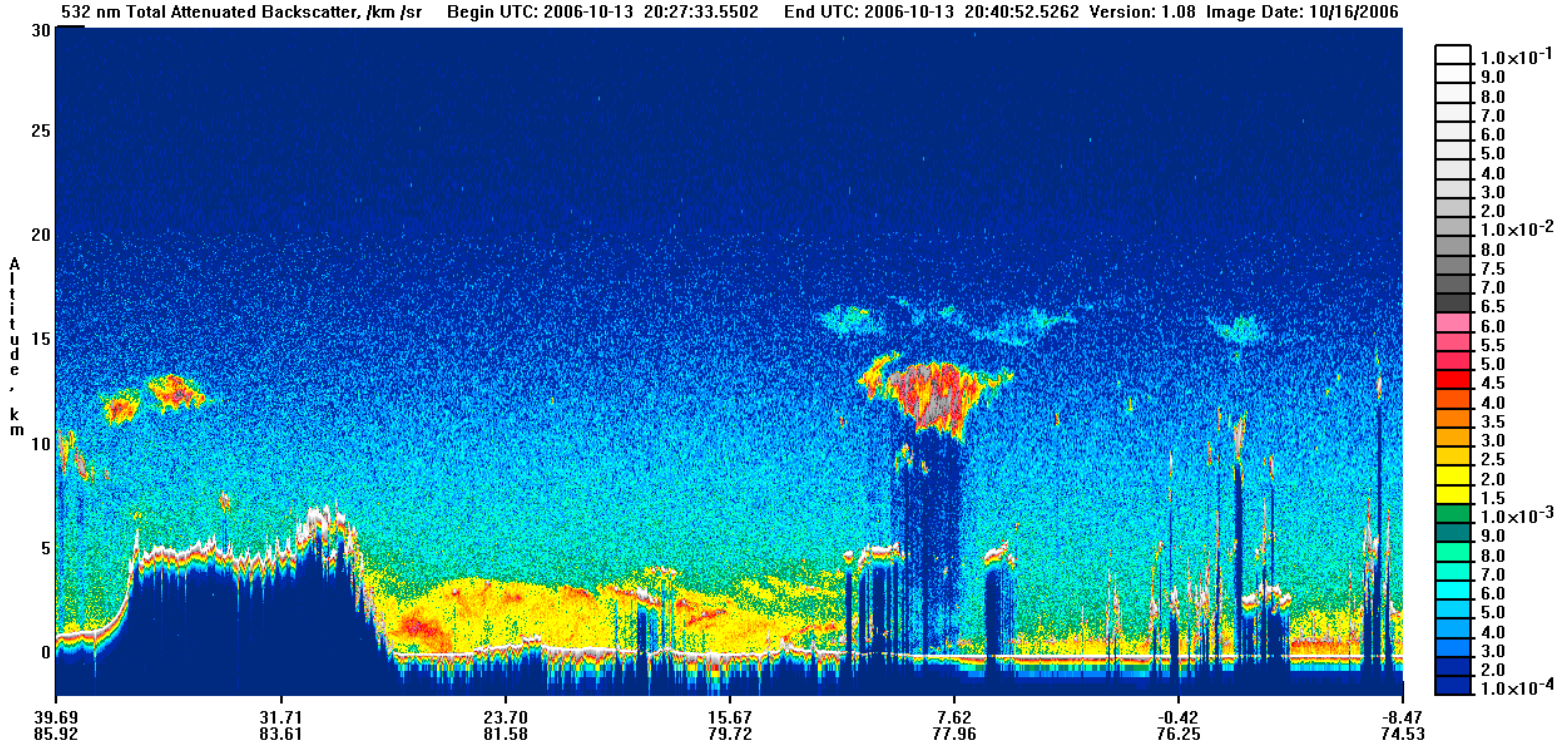

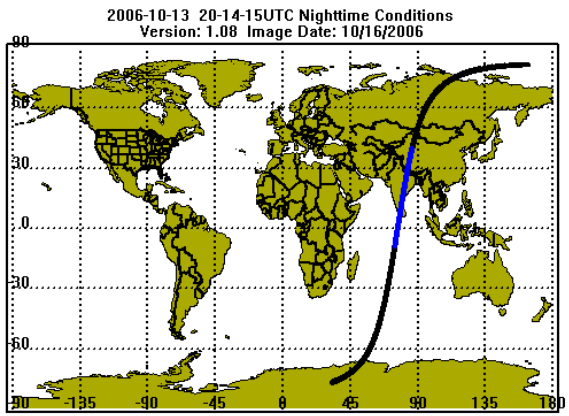

http://www-calipso.larc.nasa.gov/products/lidar/

Attenuated backscatter 532nm

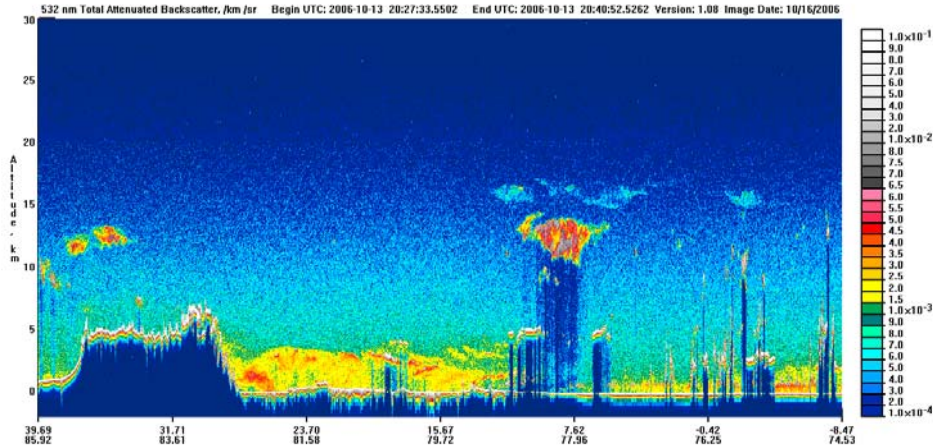

Perpendicular attenuated backscatter 532nm

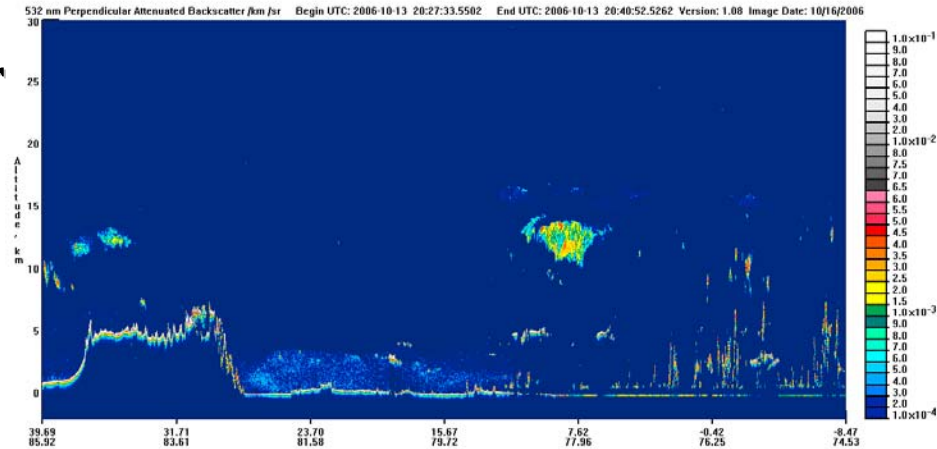

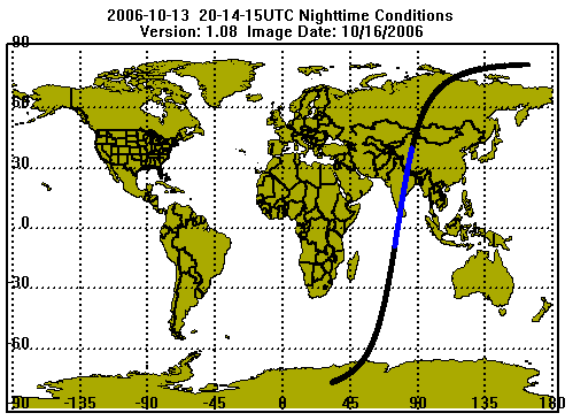

Attenuated backscatter 1064nm

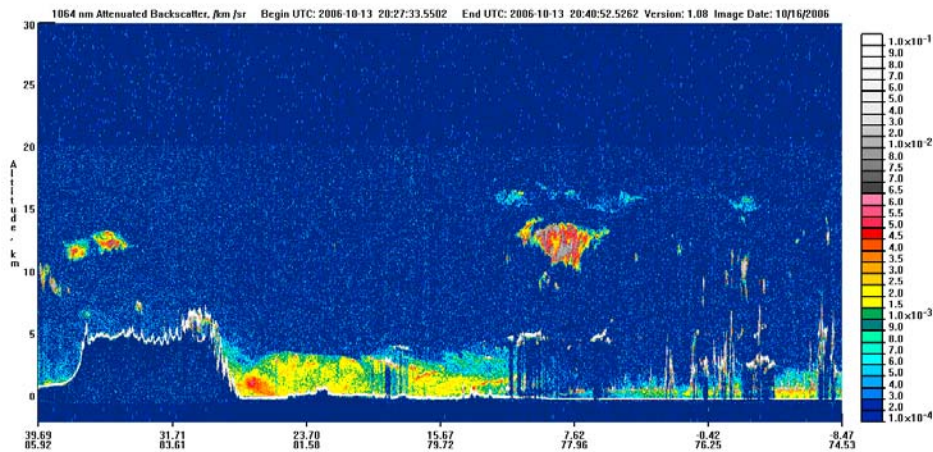

http://www-calipso.larc.nasa.gov/products/lidar/

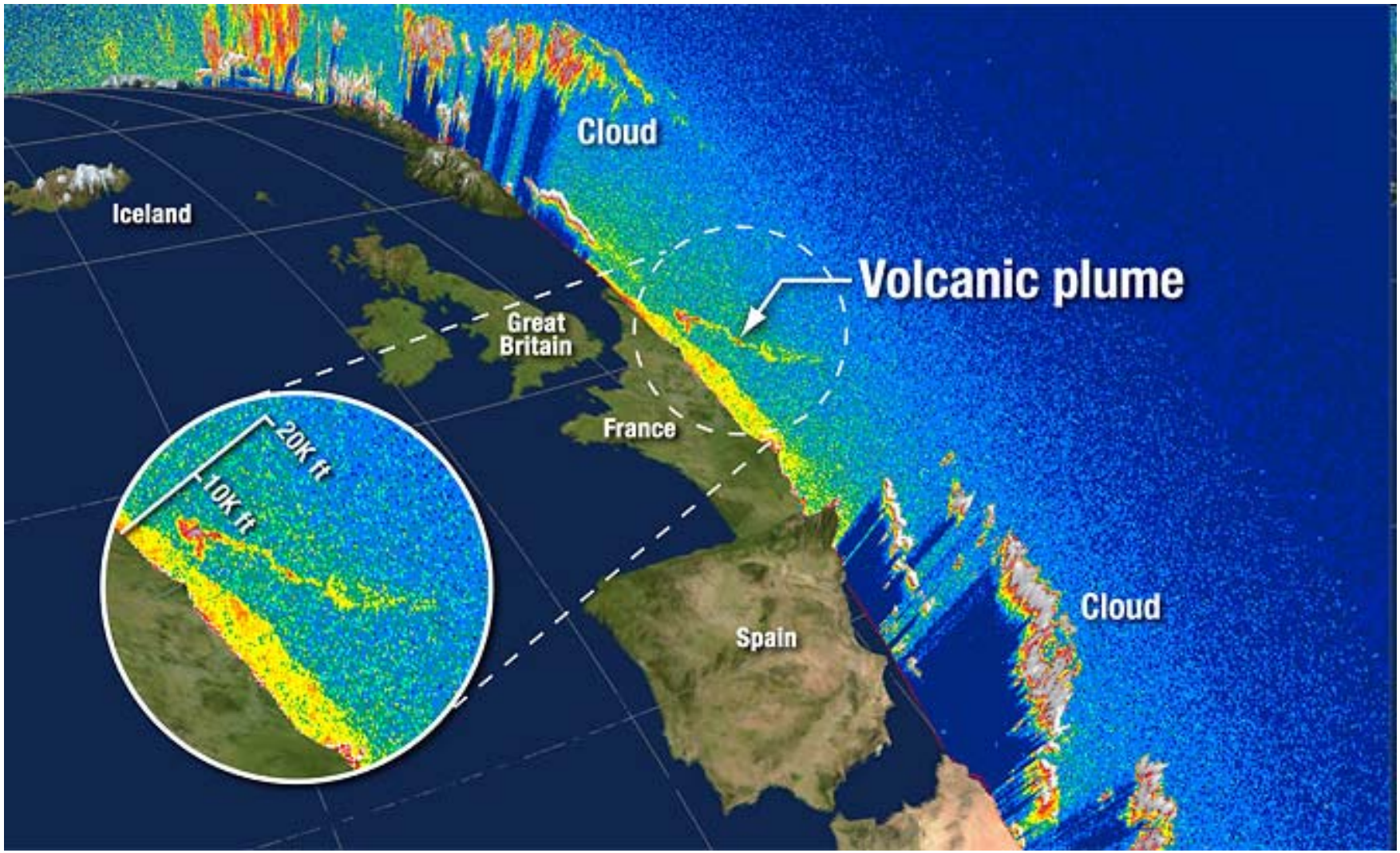

CALIPSO, 20.04.2010

http://www.nasa.gov/topics/earth/features/iceland-volcano-plume-archive1.html

Active methods with focus on time information

-LIDAR Light detection and ranging

-RADAR Radio detection and ranging

-SODAR Sound detection and ranging

RADAR

Scattering of electromagnetic radiation is caused by different ‘objects’:

-aerosols
-cloud drops
-raindrops
-snow flakes, hail

-insects, birds, airplanes…

-turbulence elements

Remote sensing in different parts of the EM spectrum

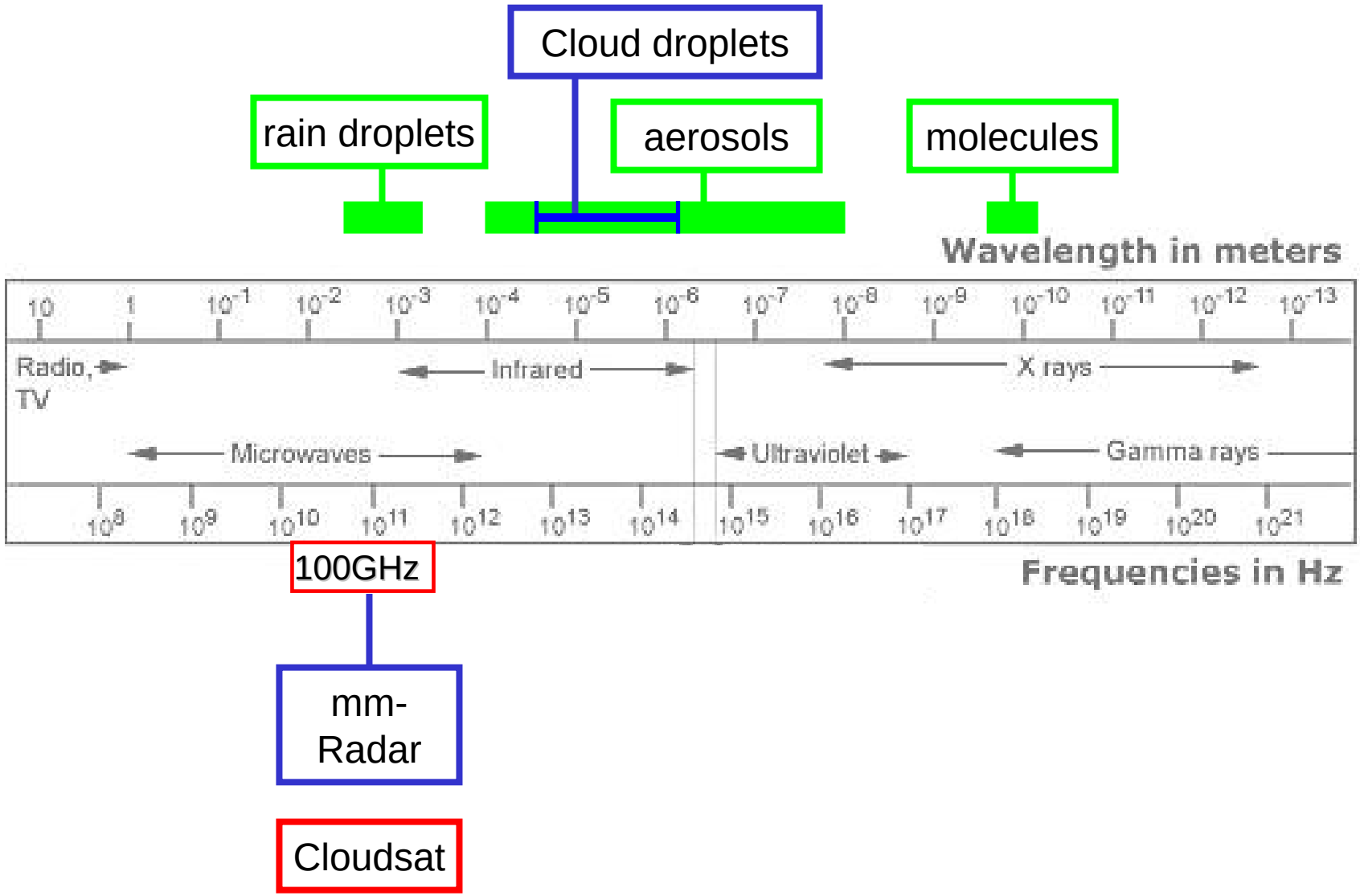

RADAR

Scattering of electromagnetic radiation is caused by different 'objects':

-aerosols
-cloud drops
-raindrops
-snow flakes, hail

~100 GHz (~2mm)

-turbulence elements

irregularities in the radio refractive index of the atmosphere; most sensitive to scattering by turbulent eddies whose spatial scale is ½ the wavelength of the radar Bragg scattering

~1 GHz (~20cm)
to
50 MHz (~5m)

-insects, birds, airplanes…

95 GHz Doppler Polarimetric Cloud Radar

http://radar.kharkov.com/radar36.html

VHF-Radar: Emitter und Empfänger (Kühlungsborn)

Technische Parameter
Frequenz 53,5 MHz
Spitzenleistung 90 kW
Mittlere Leistung 4,5 kW (bei 5% Duty Cycle)
3dB-Öffnungswinkel 6°
Impulslänge 1 ... 32 µs
Pulswiederholfrequenz < 50 kHz
Höhenbereiche (0,4) 1 ... 18 km (65...95 km)
Höhenauflösung 150 m, 300 m, 600 m, 1000 m
Zeitauflösung ~ 1 min
Sendesignal Einzelimpuls, Komplementärkodes
Impulsformen Rechteck, modifizierter Gauß (für max. Leistung)

RADAR

Basic RADAR equation (for single scattering points)

$$P_r = \left[P_t \frac{G^2 \lambda^2 \sigma^0}{(4\pi)^3 R^4} \right] \propto \frac{\sigma^0}{R^4}$$

P_r is received power, P_t is transmitted power,
G_t is the gain of the transmitting antenna, λ is radar wavelength,
σ is the radar cross section of the target
R is the distance from transmitter to target.

Modified RADAR equation (for volume scatterers)

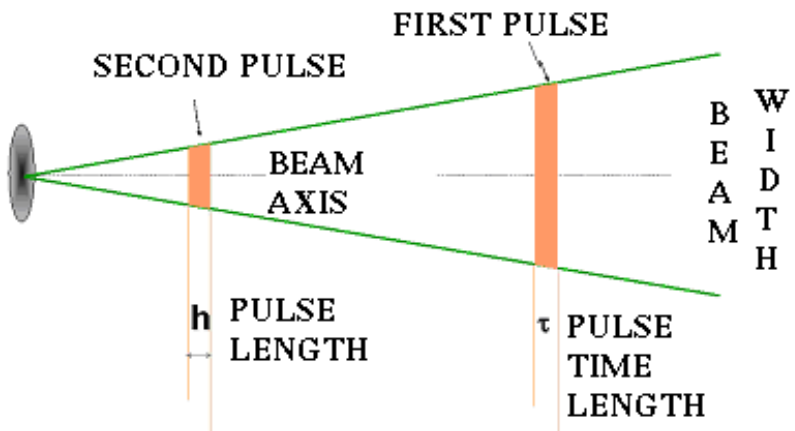

Beam path and scanned volume

$$P_r \propto \frac{\eta}{R^2}$$

0.5 bis 16 km Troposphärenwindprofiler

0.2 bis 3 km Grenzschichtwindprofiler

Meteorologisches Observatorium Lindenberg

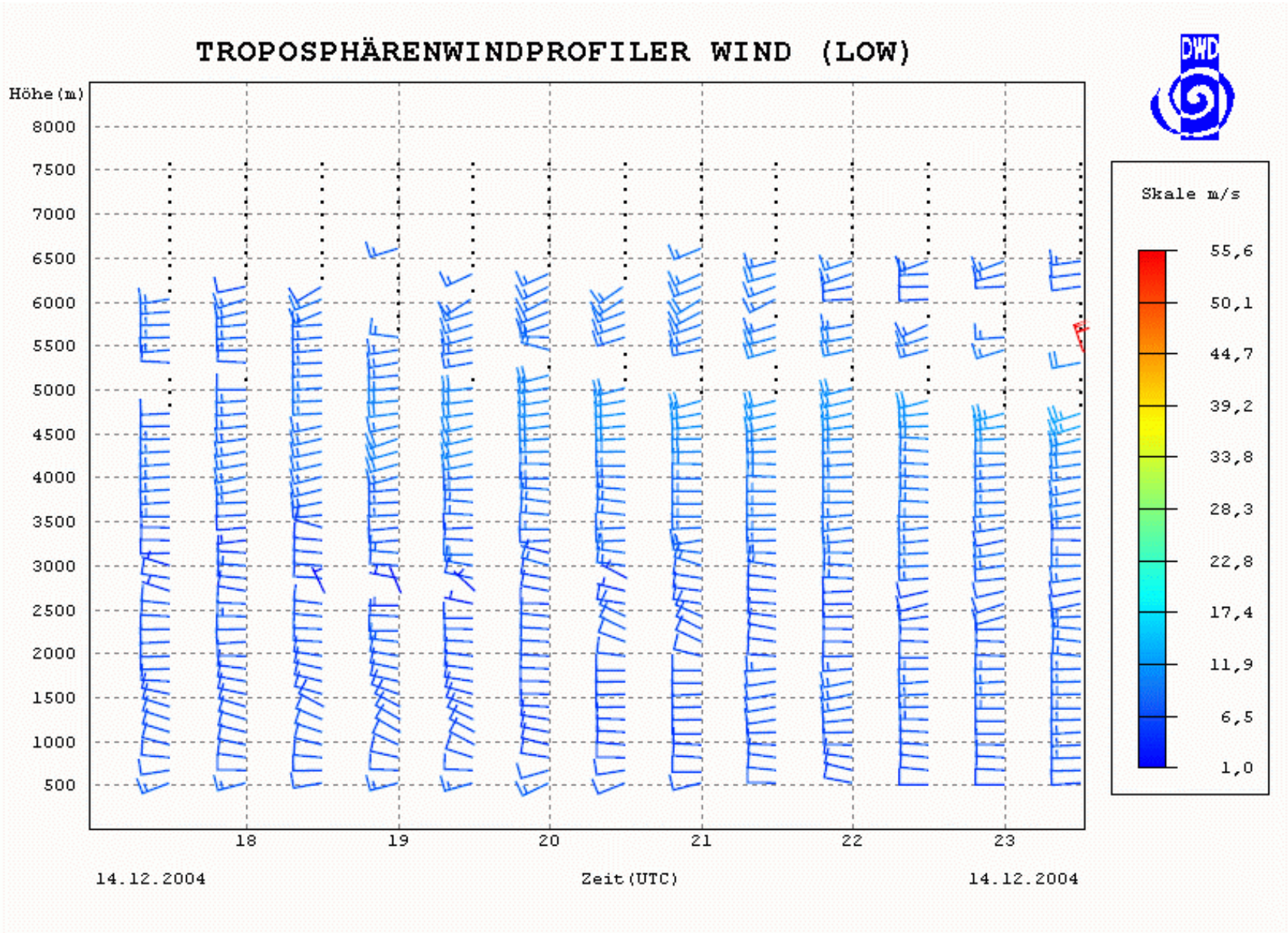

Meteorologisches Observatorium Lindenberg

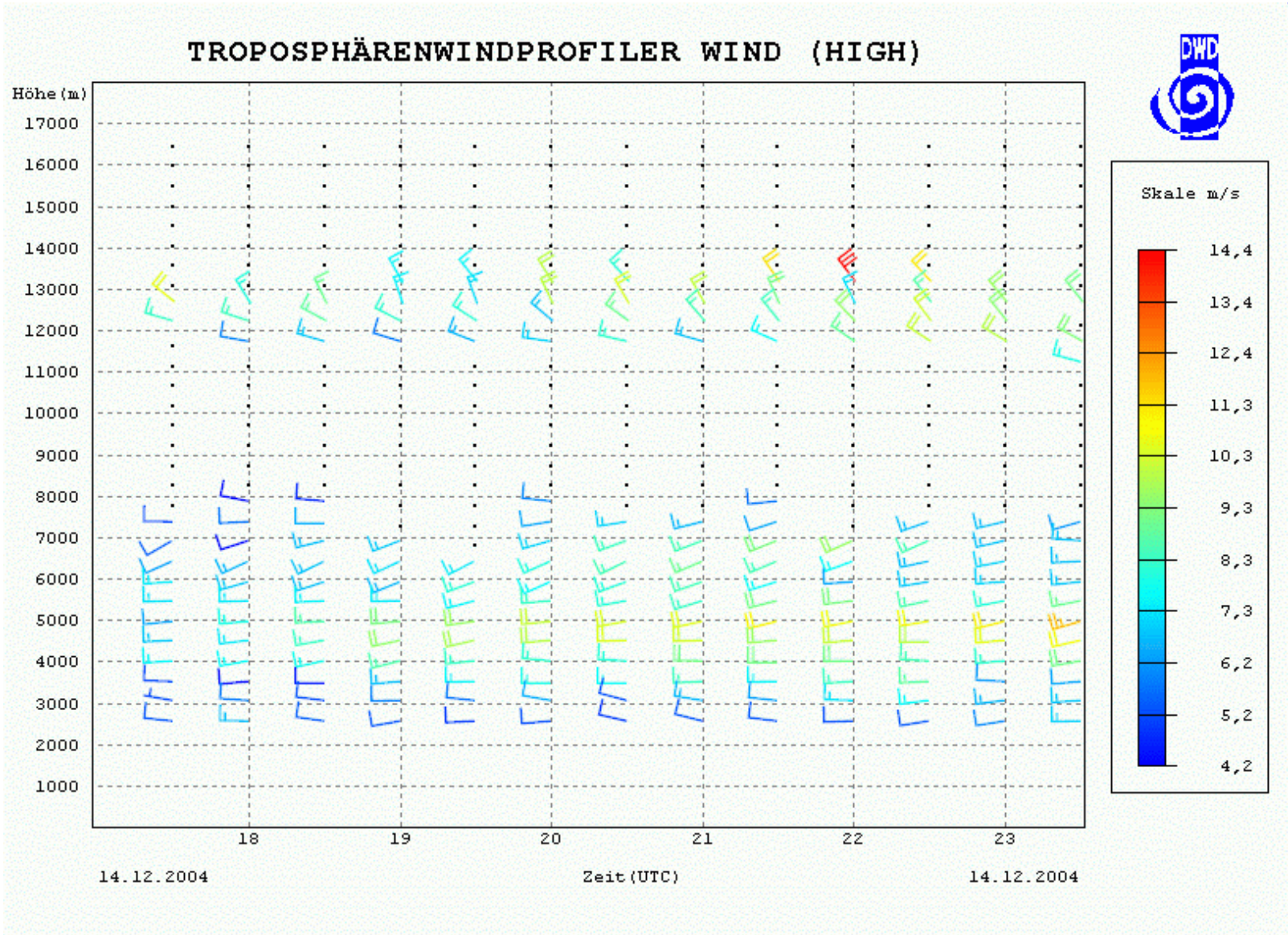

Meteorologisches Observatorium Lindenberg

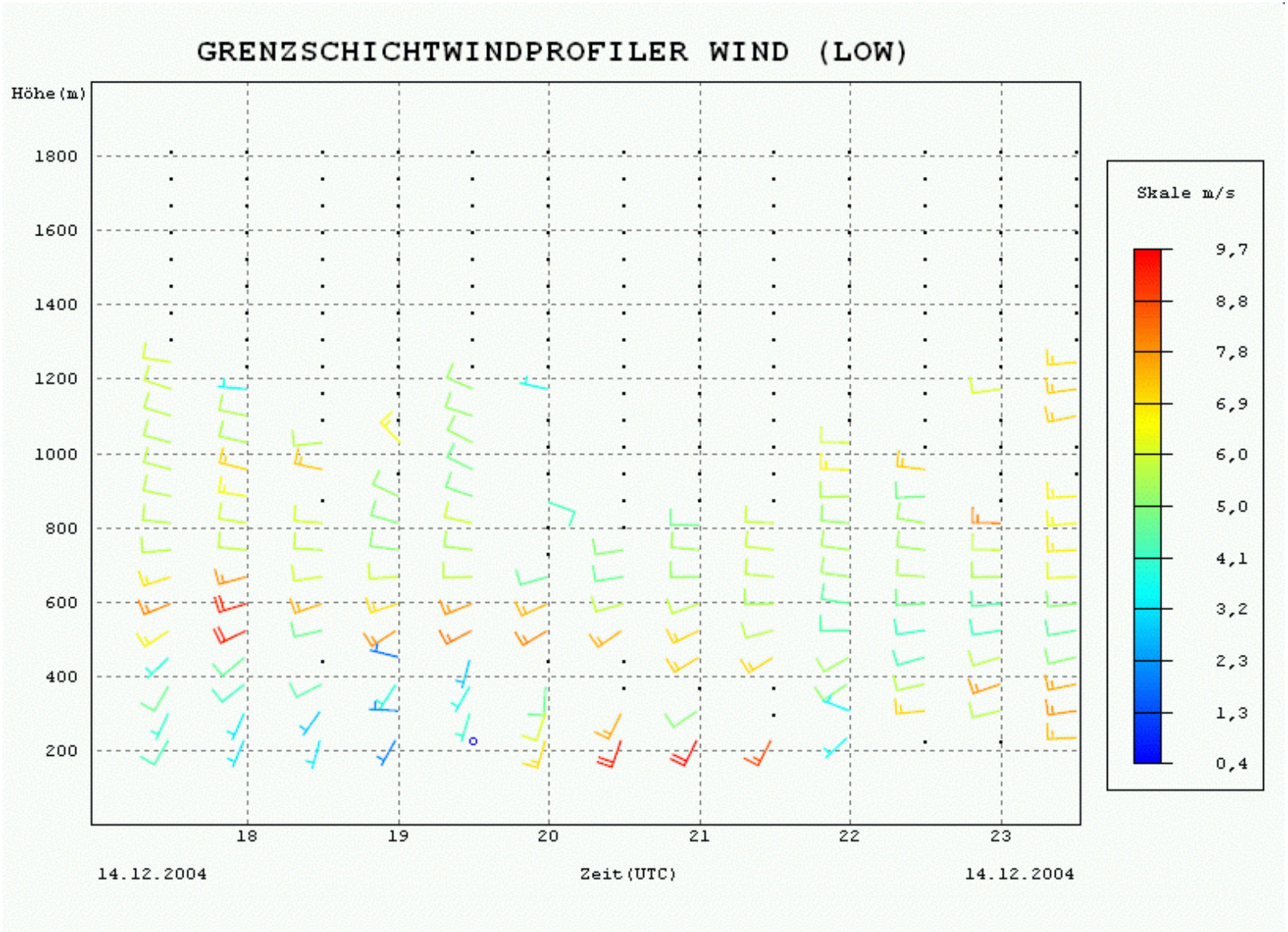

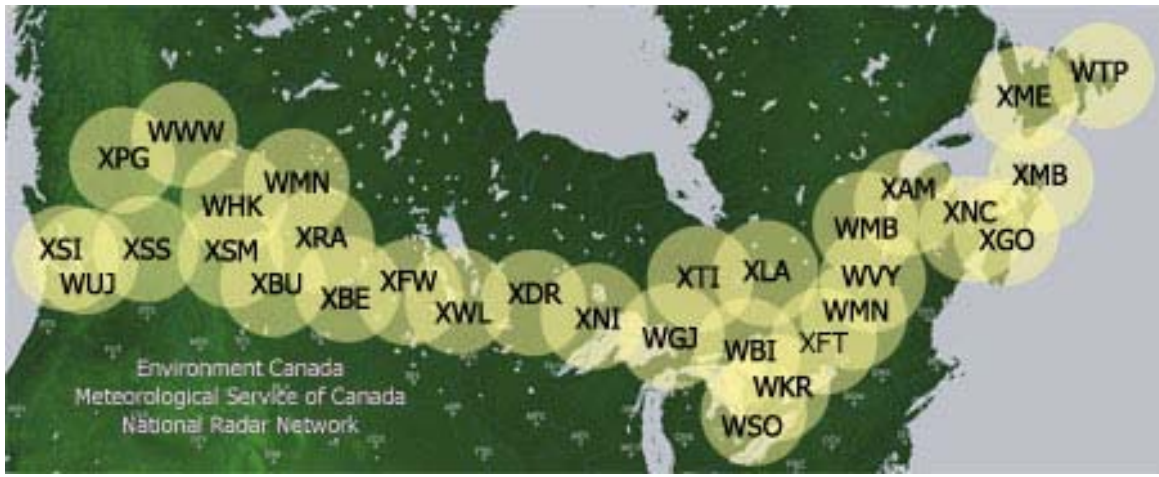

The CWKR Environment Canada Weather Radar Station located in King City, Ontario.

Elevation: 341 meters ASL.
Latitude: 43° 58' 0" N (deg min sec), 43.9667° (decimal), 4358.00N (LORAN)
Longitude: 79° 34' 0" W (deg min sec), -79.5667° (decimal), 07934.00W (LORAN)

Reflectivity

Return echoes from targets are analyzed for their intensities in order to establish the precipitations rate in the scanned volume. The wavelength used (1 to 10 cm) ensure that this return is proportional to the precipitations rate because they are within the validity of Rayleigh scattering which states that the targets must be much smaller than the wavelength of the scanning wave (by a factor of 10).

Velocity

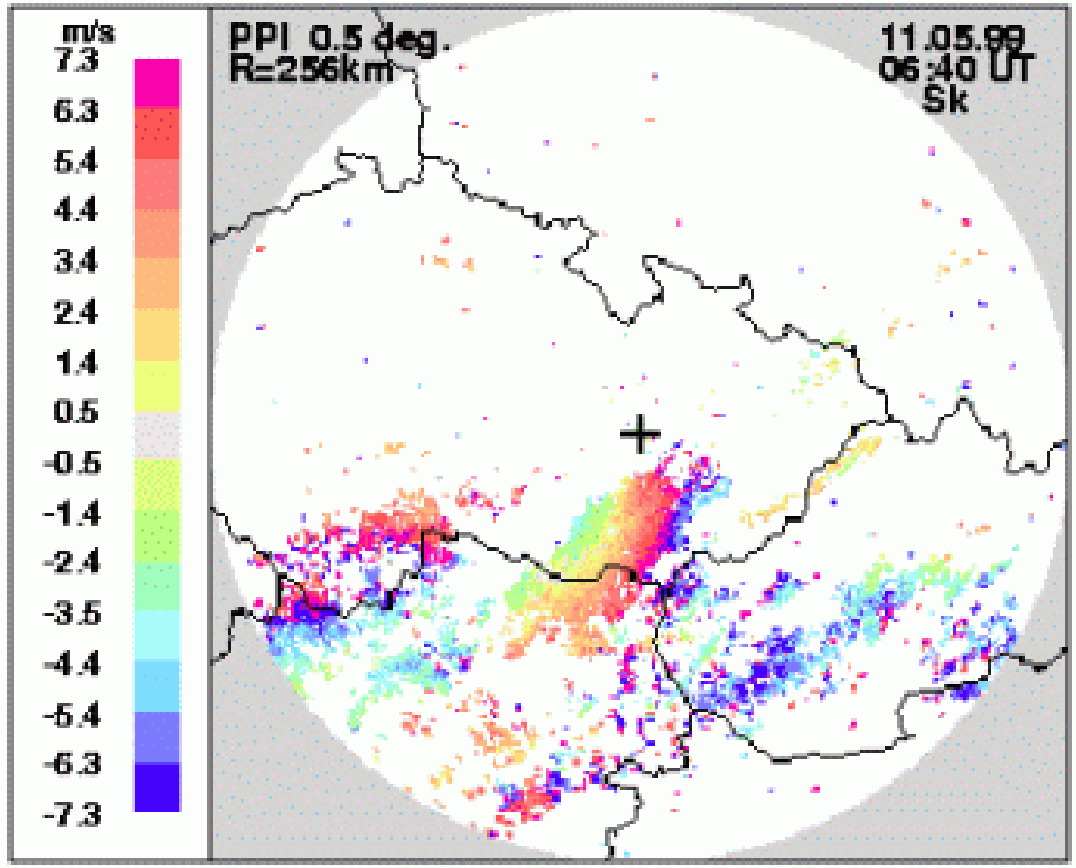

Petr Novák
(petr_novak@chmi.cz)

Idialized example of Doppler output. Approaching velocities are in blue and receeding one in red in the usual convention. Notice the sinuosidal variation of speed when going around the display along a particular ring. (Source: Environment Canada).

Polarization

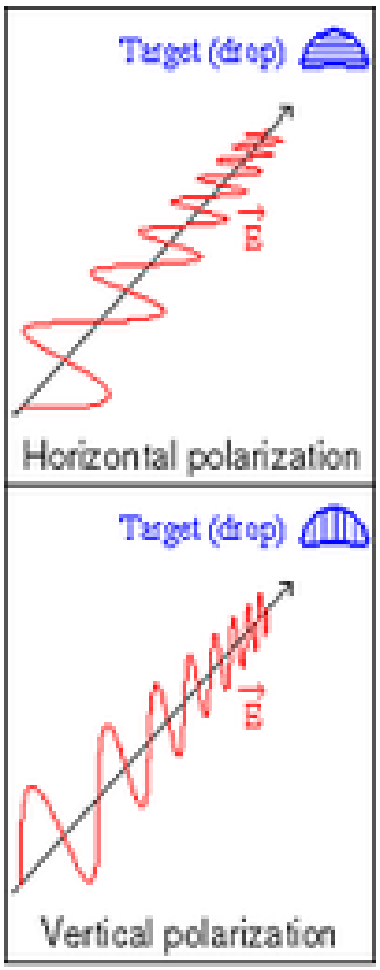

Most liquid hydrometeors have a larger horizontal axis due to the drag coefficient of air while falling (water droplets). This causes the water molecule dipole to be oriented in that direction so radar beams are generally polarized horizontally to receive the maximal return.

If we decide to send simultaneously two pulses with orthogonal polarization: vertical and horizontal, we receive two sets of data proportional to the two axis of the droplets that are independent

Targeting with dual-polarization will reveal the form of the droplet

Niederschlagsradar (gelb/blau), projiziert auf das Satellitenbild der Wolkenbedeckung. Das Regengebiet am Rhein entsprach der Realität, das Radarecho im Norden beruht auf einer Täuschung.

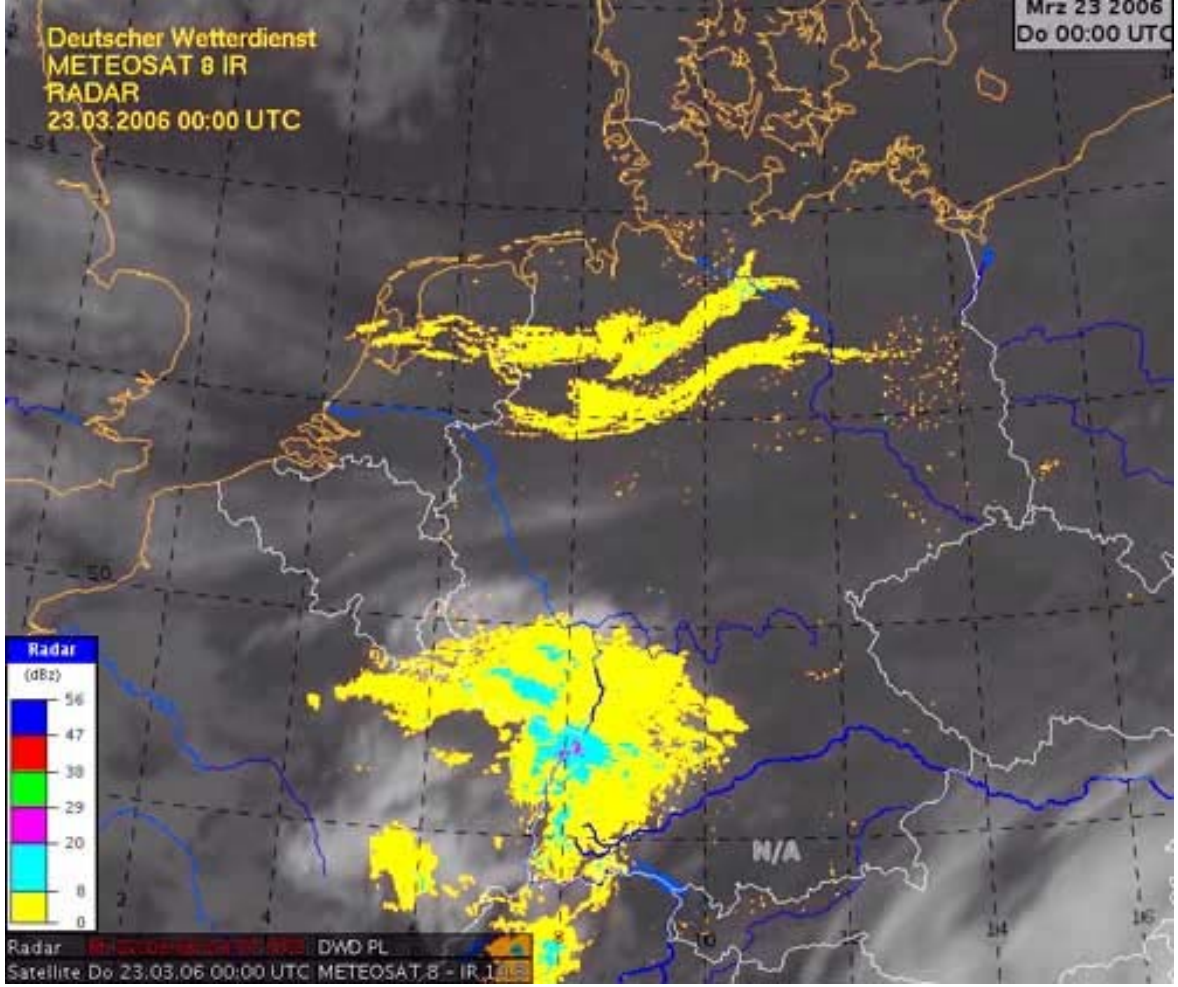

…es ist bekannt, dass die Briten und Deutschen im Zweiten Weltkrieg Stanniolfäden vom Himmel fallen ließen, um das gegnerische Radar zu stören. Heute werden dafür hauchdünne metallüberzogene Kunststofffäden genutzt, die Düppel. Sie sind wenige Zentimeter lang und werden in der Atmosphäre ausgestreut. So bildet sich eine Art unsichtbare Mauer, die Radarstrahlen reflektiert.
(http://service.spiegel.de/digas/find?DID=46421554)

Niederschlagsbild: Baden-Württemberg So, 09.05. 00:00 - 09:00

http://www.wetteronline.de

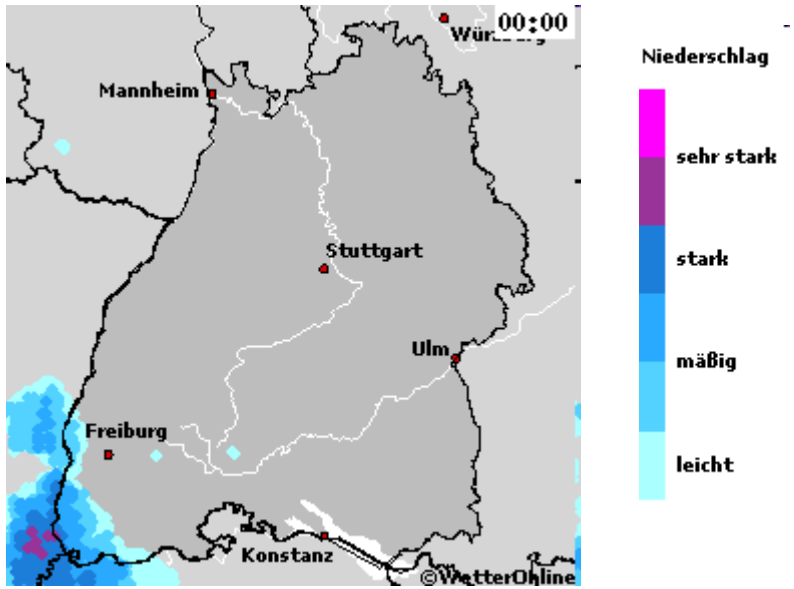

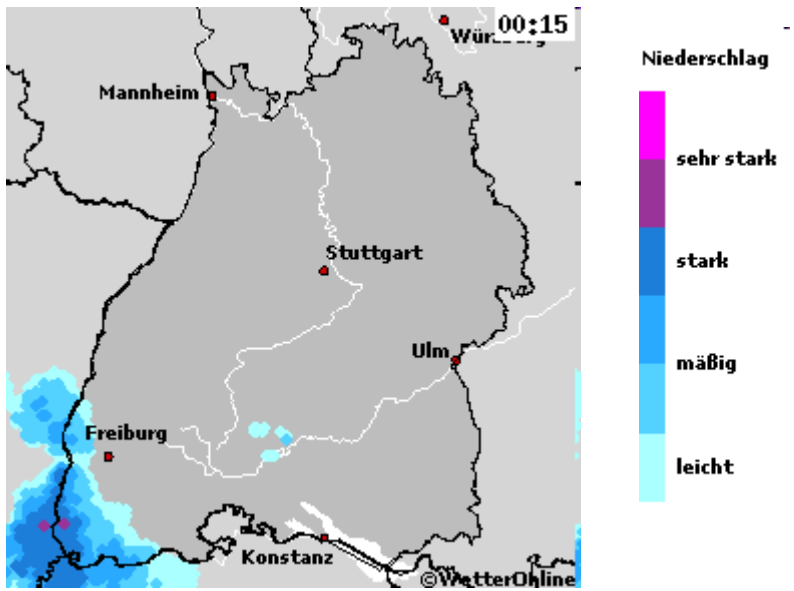
00:15
Mannheim
Stuttgart
Ulm
Freiburg
Konstanz
©WetterOnline
Niederschlag
sehr stark
stark
mäßig
leicht

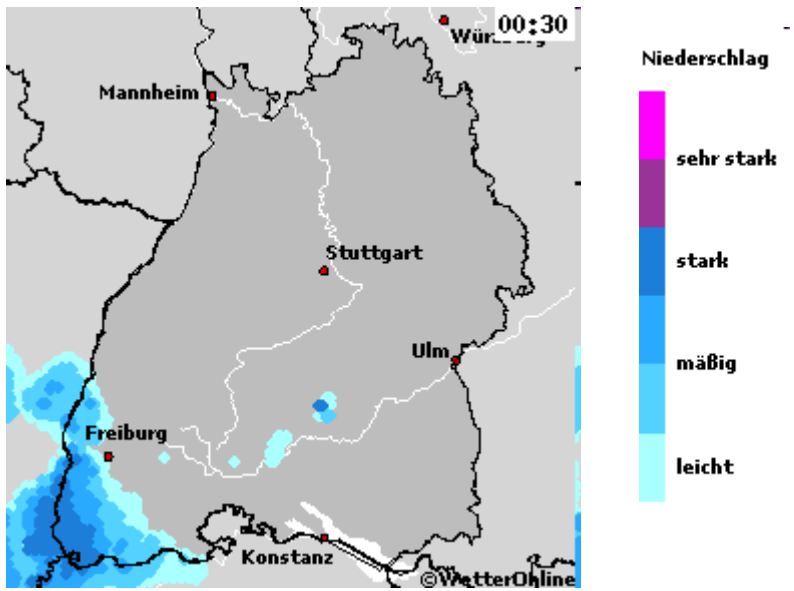
00:30
Mannheim
Stuttgart
Ulm
Freiburg
Konstanz
©WetterOnline
Niederschlag
sehr stark
stark
mäßig
leicht

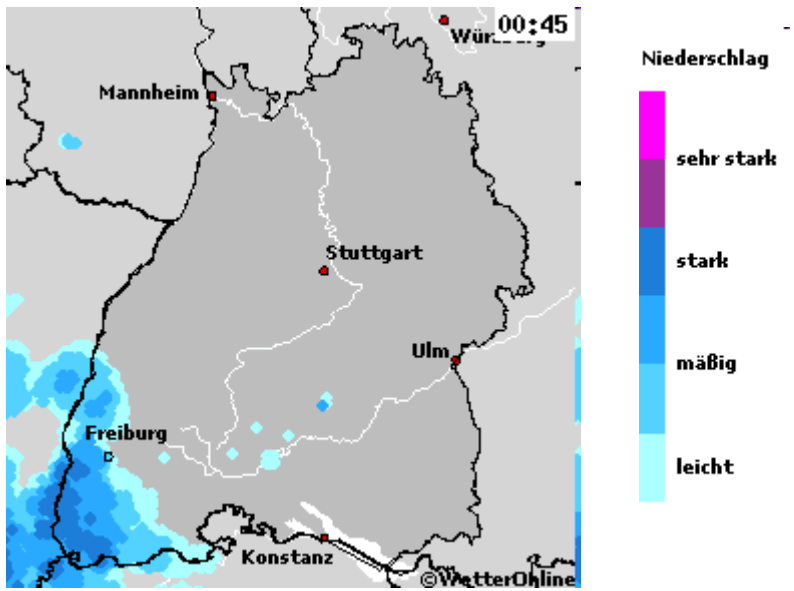
00:45
Mannheim
Stuttgart
Ulm
Freiburg
Konstanz
©WetterOnline
Niederschlag
sehr stark
stark
mäßig
leicht

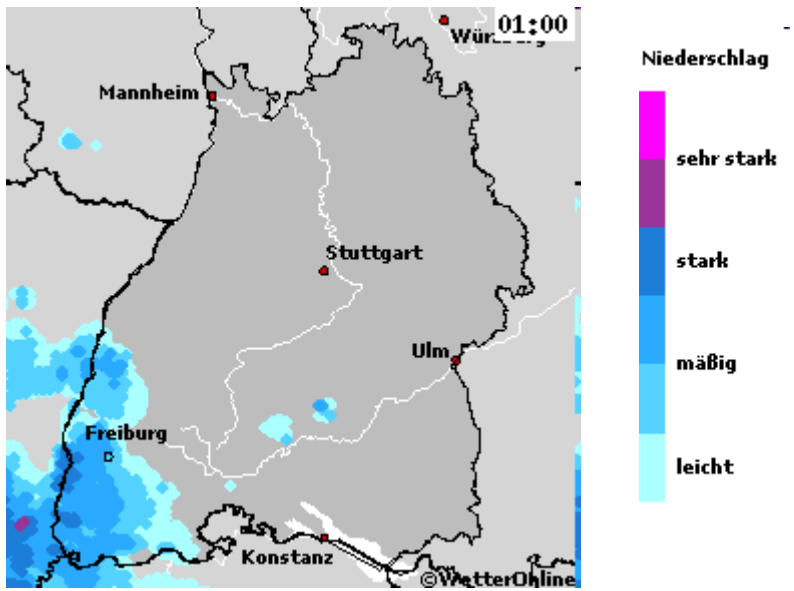
01:00
Mannheim
Stuttgart
Ulm
Freiburg
Konstanz
©WetterOnline
Niederschlag
sehr stark
stark
mäßig
leicht

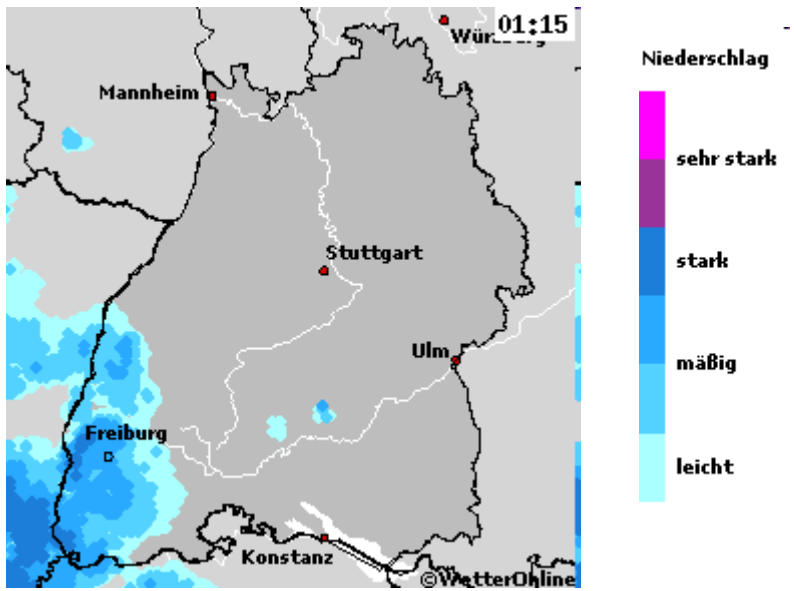
01:15
Mannheim
Stuttgart
Ulm
Freiburg
Konstanz
©WetterOnline
Niederschlag
sehr stark
stark
mäßig
leicht

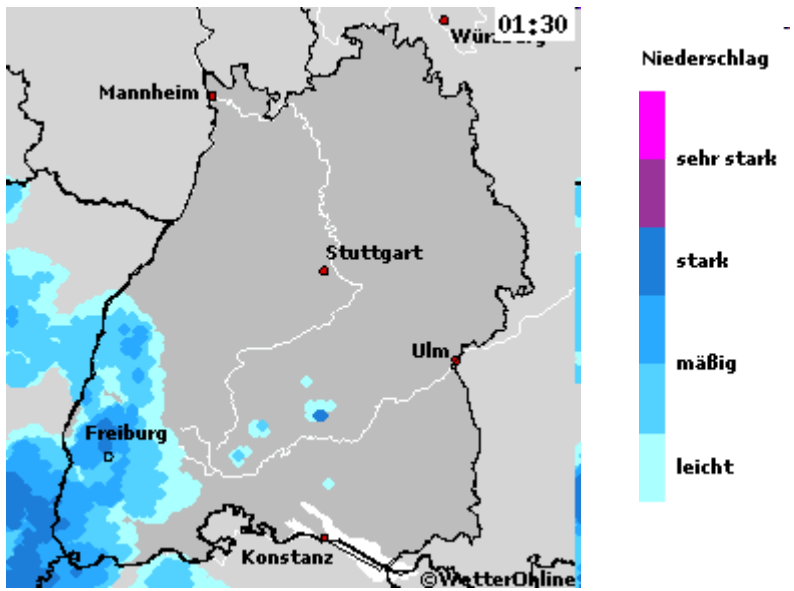
01:30
Mannheim
Stuttgart
Ulm
Freiburg
Konstanz
©WetterOnline
Niederschlag
sehr stark
stark
mäßig
leicht

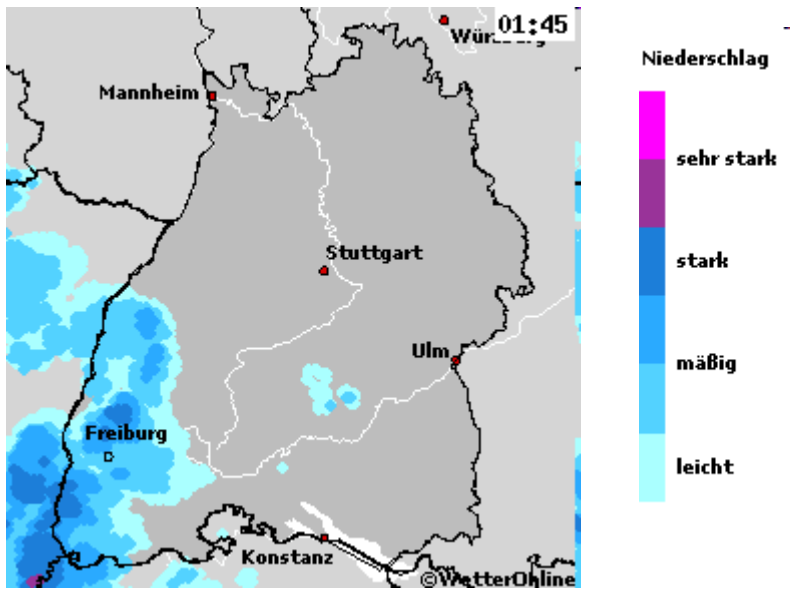
01:45
Mannheim
Stuttgart
Ulm
Freiburg
Konstanz
©WetterOnline
Niederschlag
sehr stark
stark
mäßig
leicht

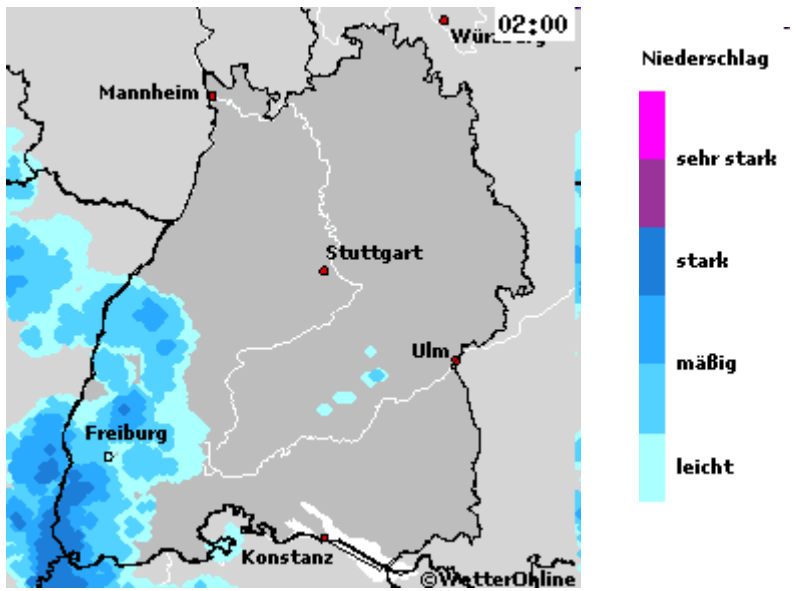
02:00
Mannheim
Stuttgart
Ulm
Freiburg
D
Konstanz
©WetterOnline
Niederschlag
sehr stark
stark
mäßig
leicht

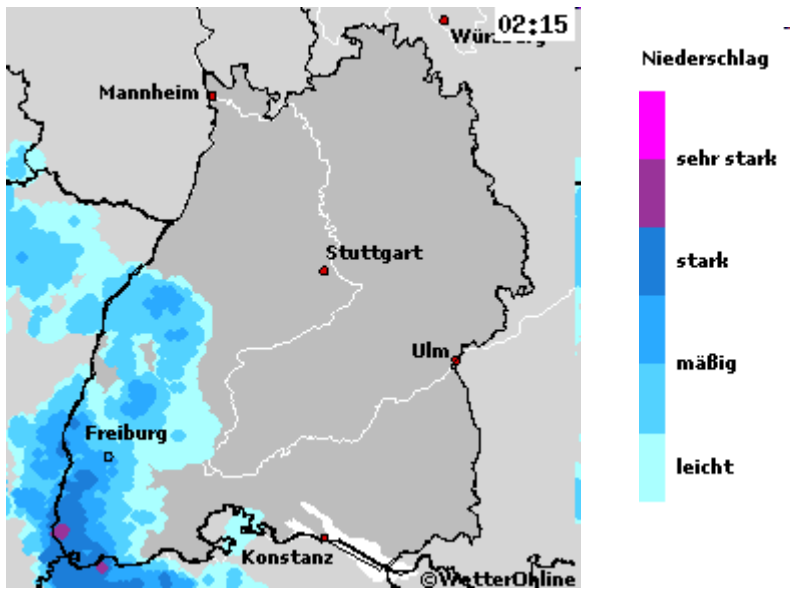
02:15
Mannheim
Stuttgart
Ulm
Freiburg
Konstanz
©WetterOnline
Niederschlag
sehr stark
stark
mäßig
leicht

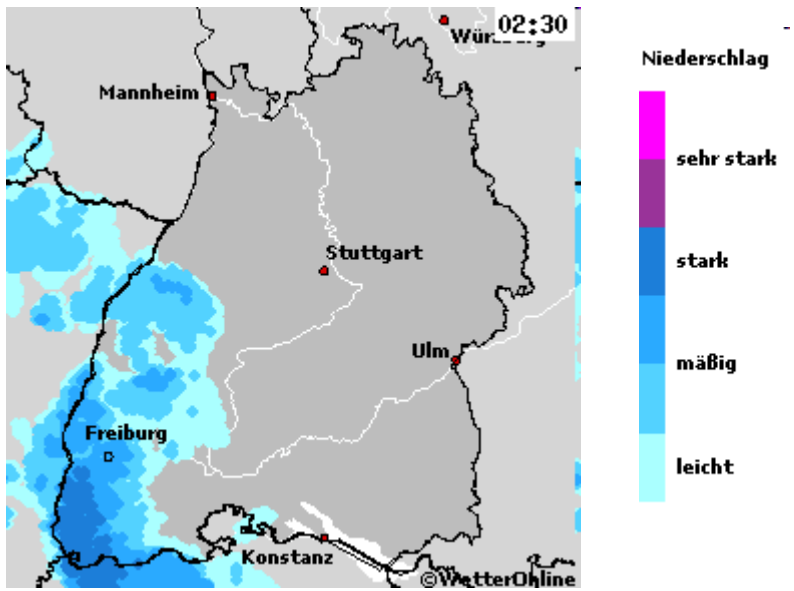
02:30
Mannheim
Stuttgart
Ulm
Freiburg
Konstanz
©WetterOnline
Niederschlag
sehr stark
stark
mäßig
leicht

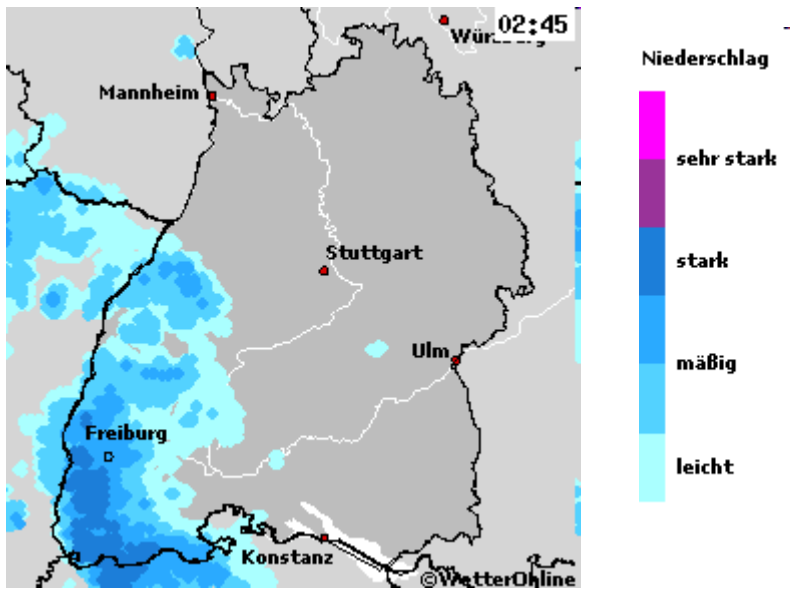
02:45
Mannheim
Stuttgart
Ulm
Freiburg
Konstanz
©WetterOnline
Niederschlag
sehr stark
stark
mäßig
leicht

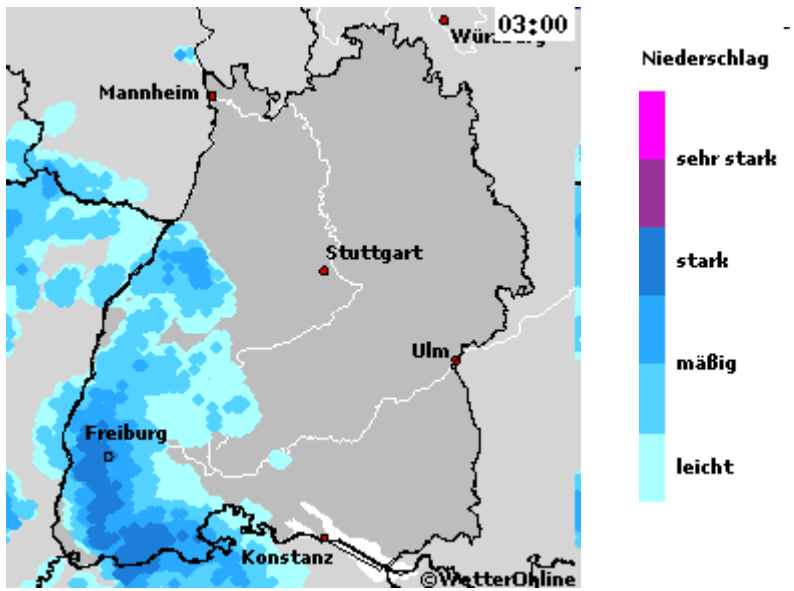
03:00
Mannheim
Stuttgart
Ulm
Freiburg
Konstanz
©WetterOnline
Niederschlag
sehr stark
stark
mäßig
leicht

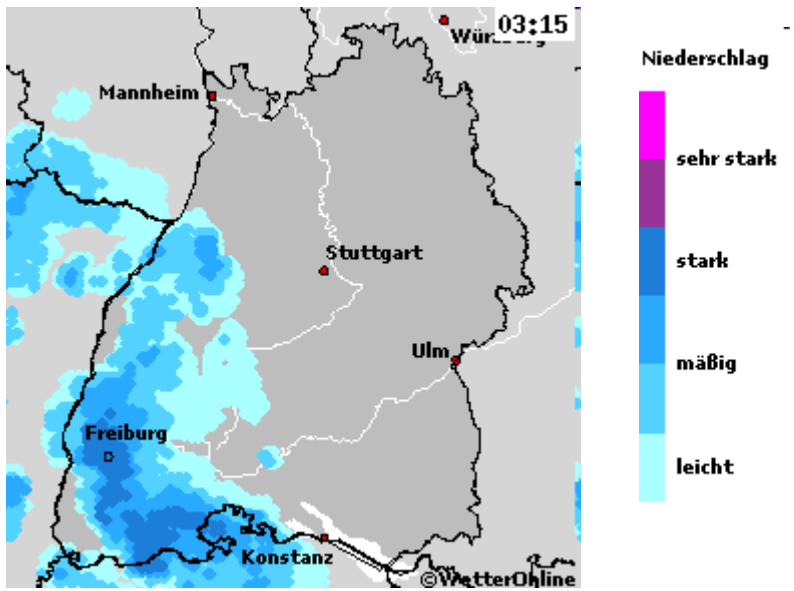
03:15
Mannheim
Stuttgart
Ulm
Freiburg
Konstanz
©WetterOnline
Niederschlag
sehr stark
stark
mäßig
leicht

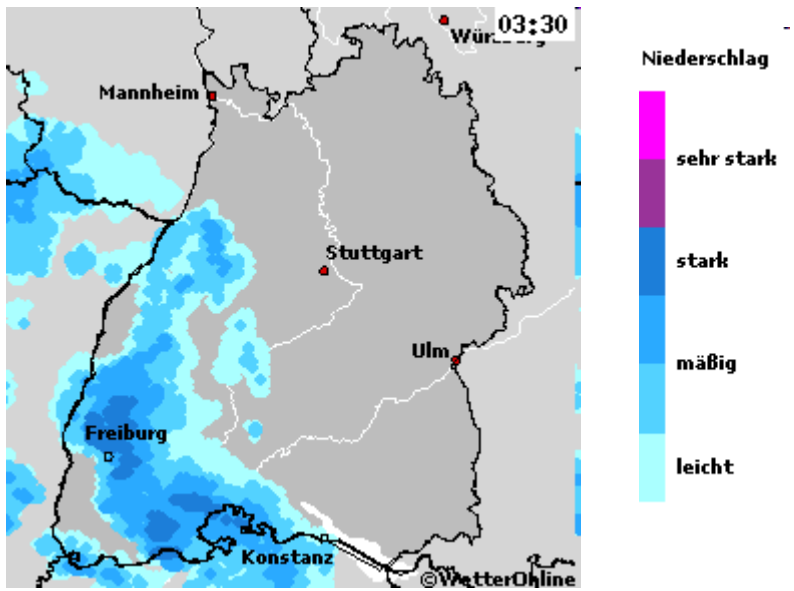
03:30
Mannheim
Stuttgart
Ulm
Freiburg
Konstanz
©WetterOnline
Niederschlag
sehr stark
stark
mäßig
leicht

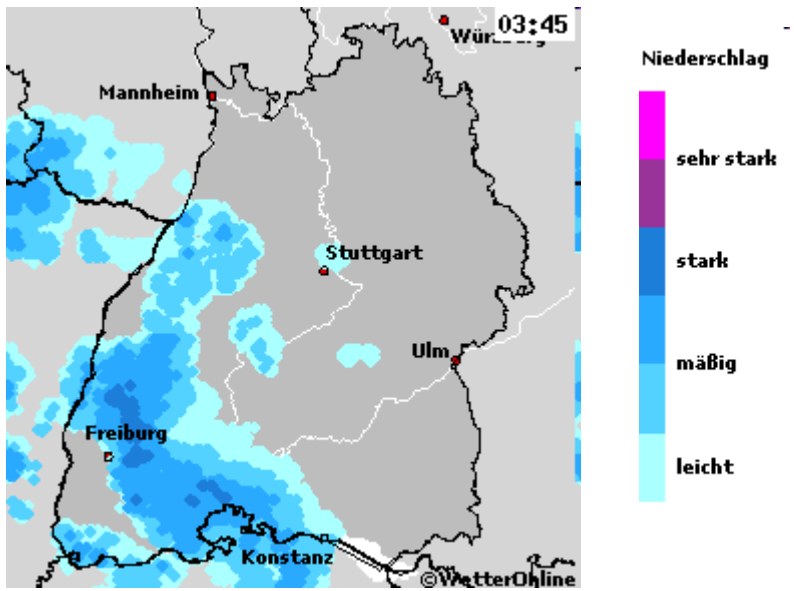
03:45
Mannheim
Stuttgart
Ulm
Freiburg
Konstanz
©WetterOnline
Niederschlag
sehr stark
stark
mäßig
leicht

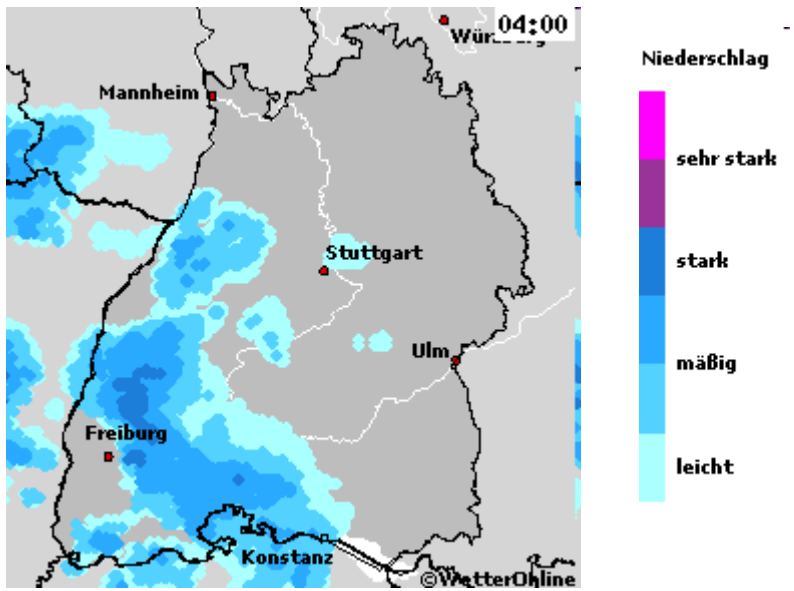
04:00
Mannheim
Stuttgart
Ulm
Freiburg
Konstanz
©WetterOnline
Niederschlag
sehr stark
stark
mäßig
leicht

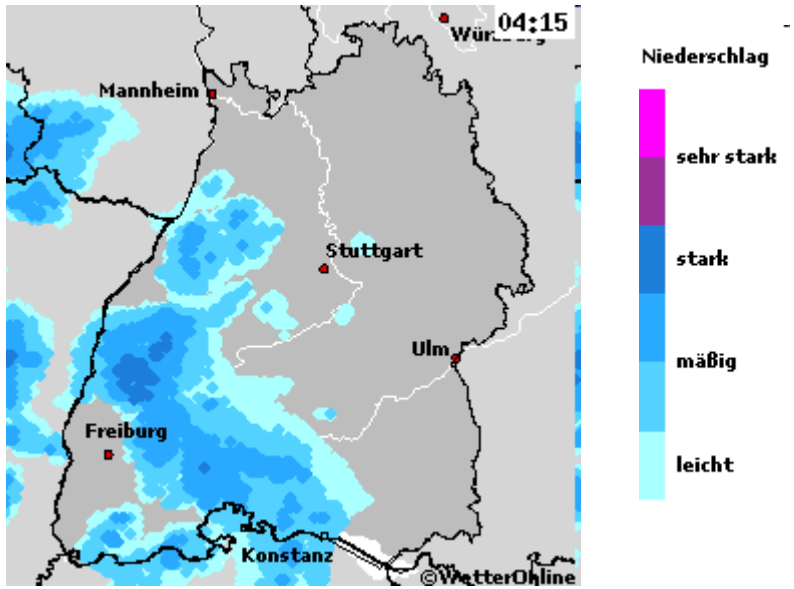
04:15
Mannheim
Stuttgart
Ulm
Freiburg
Konstanz
©WetterOnline
Niederschlag
sehr stark
stark
mäßig
leicht

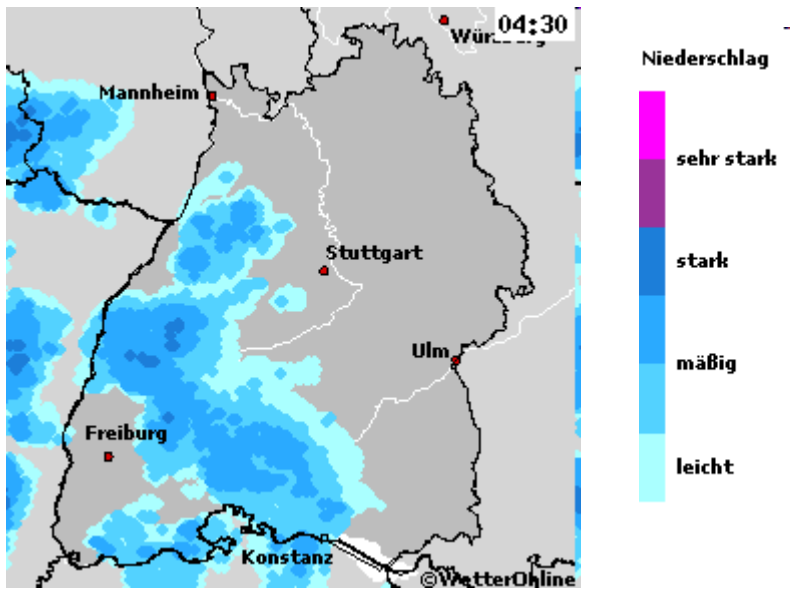
04:30
Mannheim
Stuttgart
Ulm
Freiburg
Konstanz
©WetterOnline
Niederschlag
sehr stark
stark
mäßig
leicht

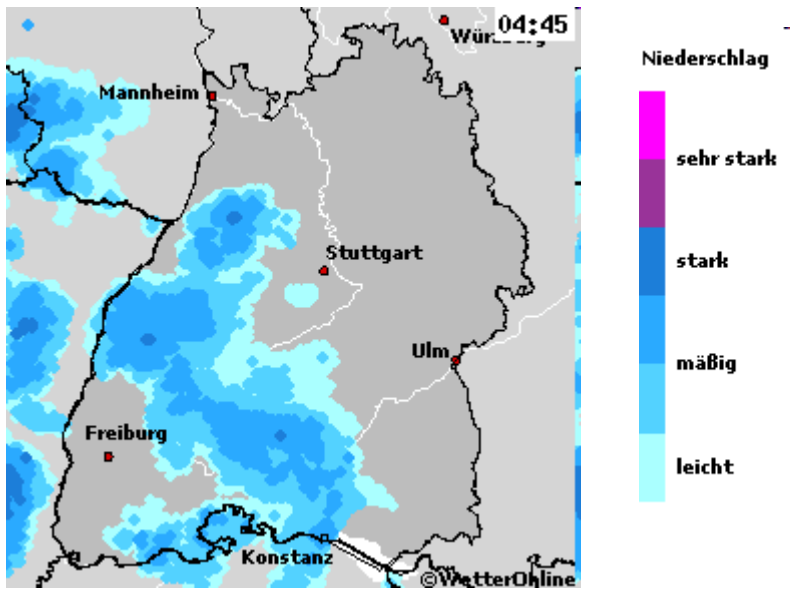
04:45
Mannheim
Stuttgart
Ulm
Freiburg
Konstanz
©WetterOnline
Niederschlag
sehr stark
stark
mäßig
leicht

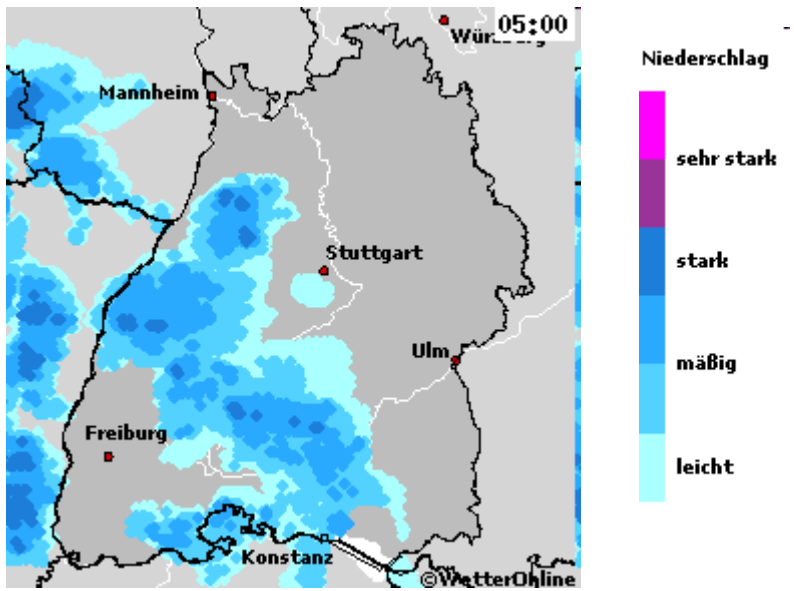
05:00
Mannheim
Stuttgart
Ulm
Freiburg
Konstanz
©WetterOnline
Niederschlag
sehr stark
stark
mäßig
leicht

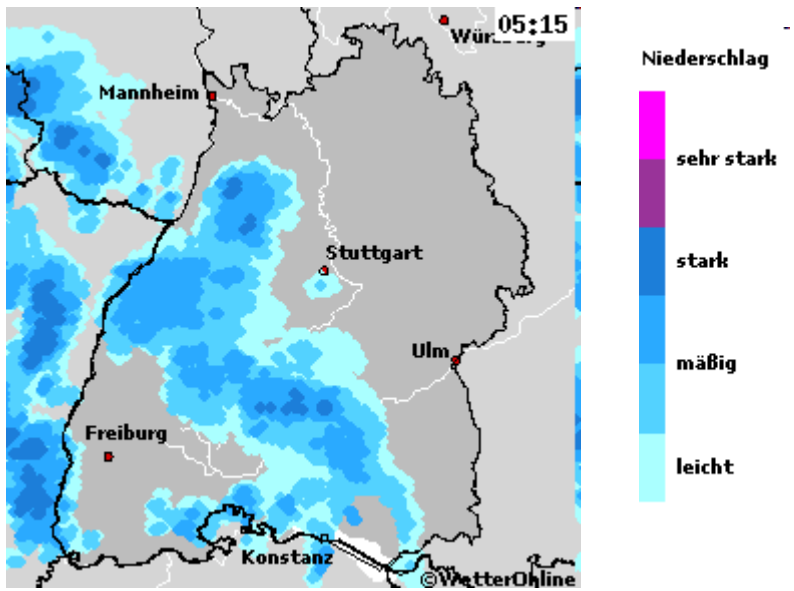
05:15
Mannheim
Stuttgart
Ulm
Freiburg
Konstanz
©WetterOnline
Niederschlag
sehr stark
stark
mäßig
leicht

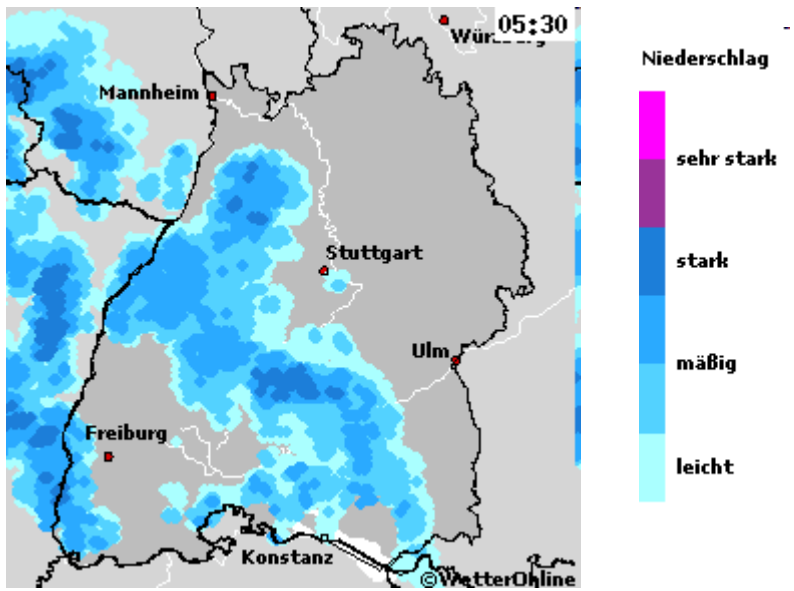
05:30
Mannheim
Stuttgart
Ulm
Freiburg
Konstanz
©WetterOnline
Niederschlag
sehr stark
stark
mäßig
leicht

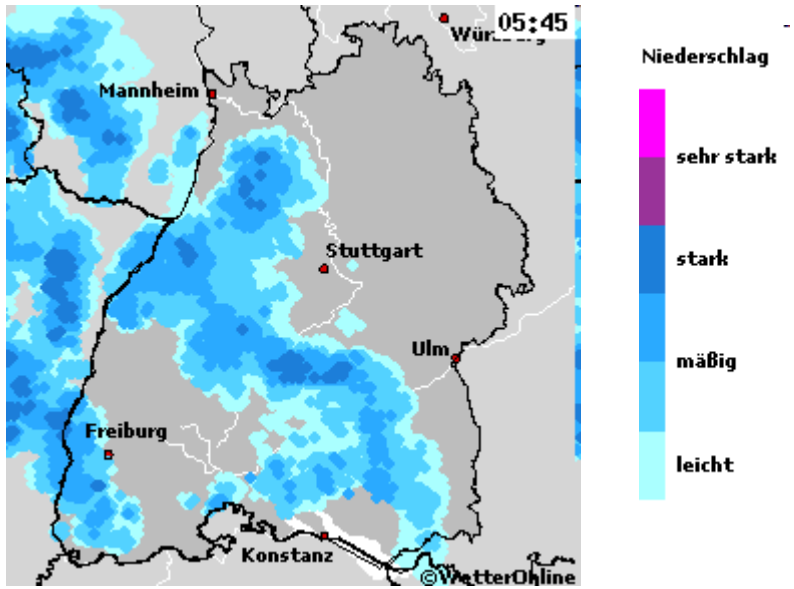
05:45
Mannheim
Stuttgart
Ulm
Freiburg
Konstanz
©WetterOnline
Niederschlag
sehr stark
stark
mäßig
leicht

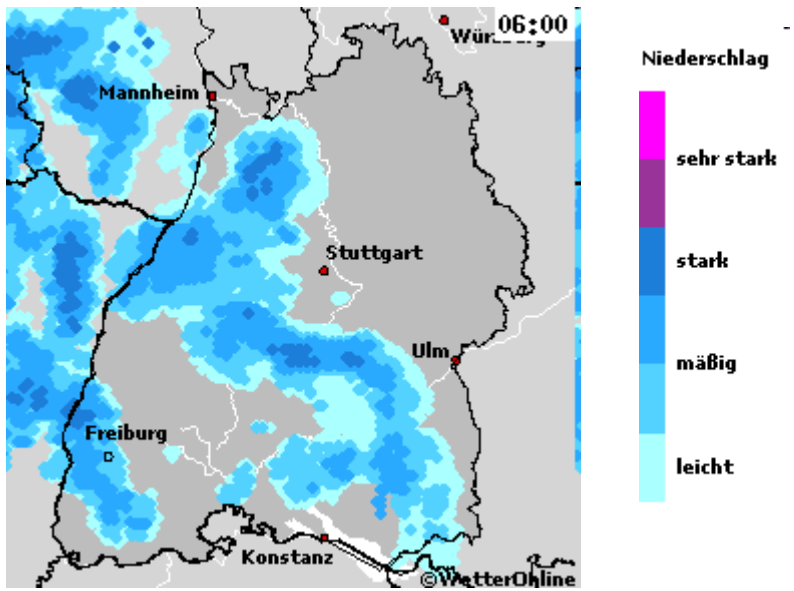
06:00
Mannheim
Stuttgart
Ulm
Freiburg
Konstanz
©WetterOnline
Niederschlag
sehr stark
stark
mäßig
leicht

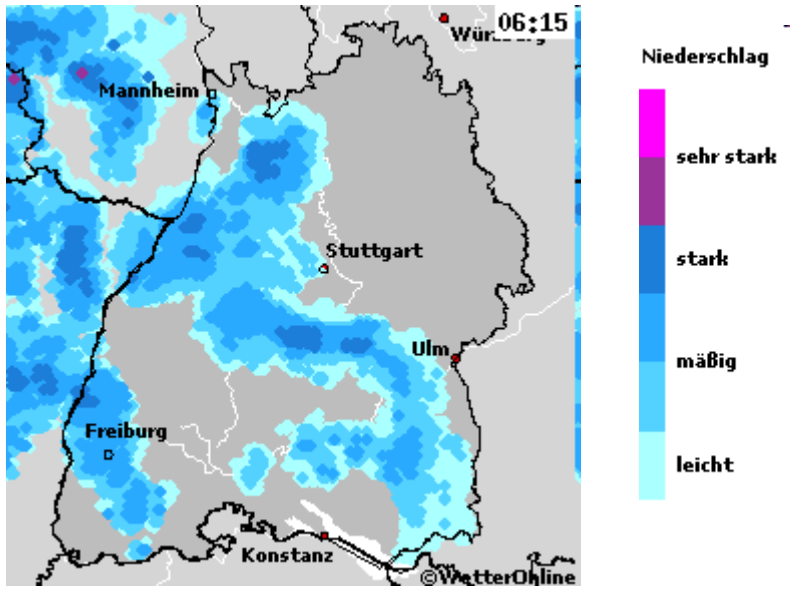
06:15
Mannheim
Stuttgart
Ulm
Freiburg
Konstanz
©WetterOnline
Niederschlag
sehr stark
stark
mäßig
leicht

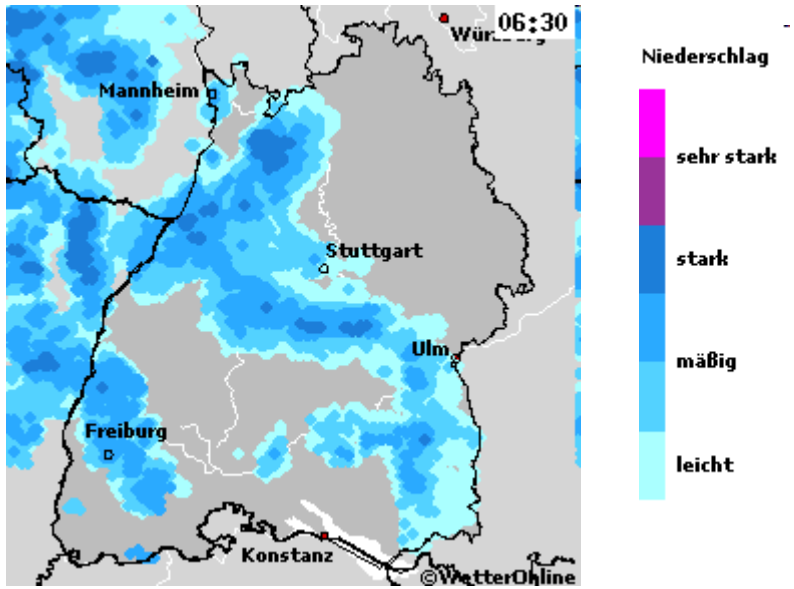
06:30
Mannheim
Stuttgart
Ulm
Freiburg
Konstanz
©WetterOnline
Niederschlag
sehr stark
stark
mäßig
leicht

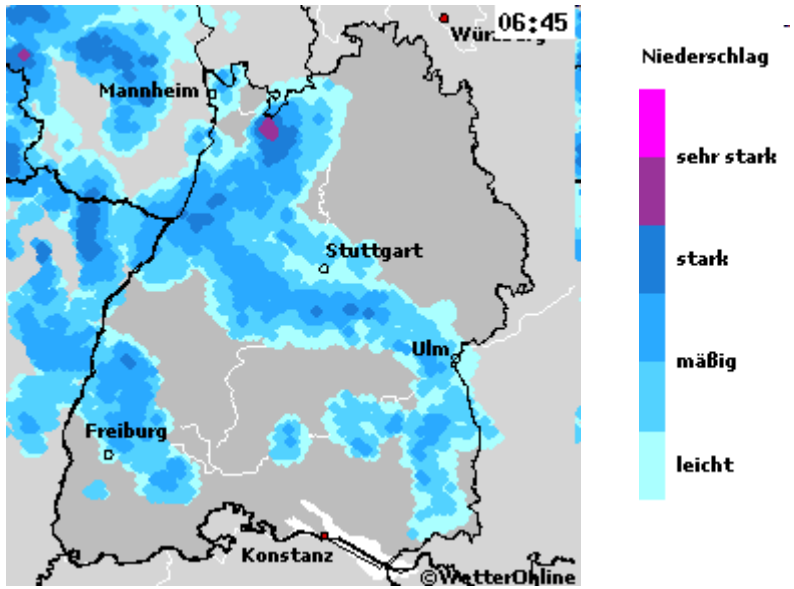
06:45
Mannheim
Stuttgart
Ulm
Freiburg
Konstanz
©WetterOnline
Niederschlag
sehr stark
stark
mäßig
leicht

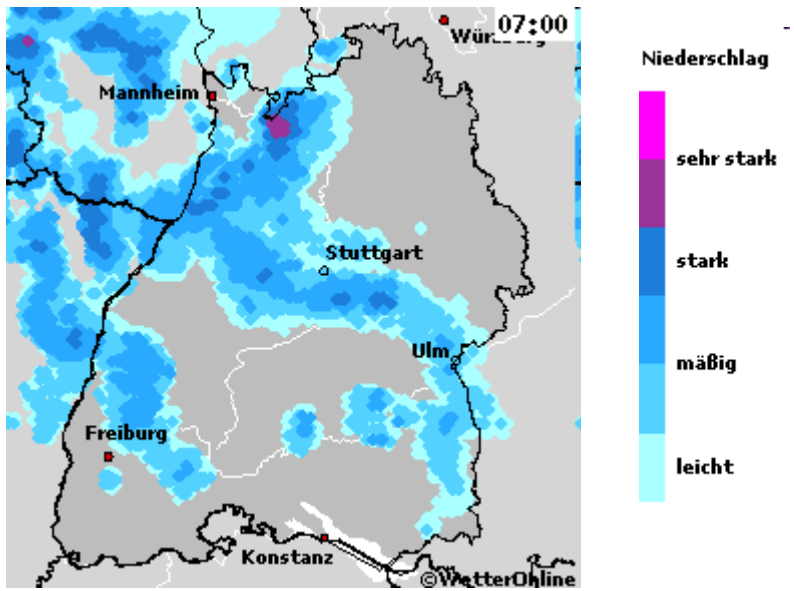
07:00
Mannheim
Stuttgart
Ulm
Freiburg
Konstanz
©WetterOnline
Niederschlag
sehr stark
stark
mäßig
leicht

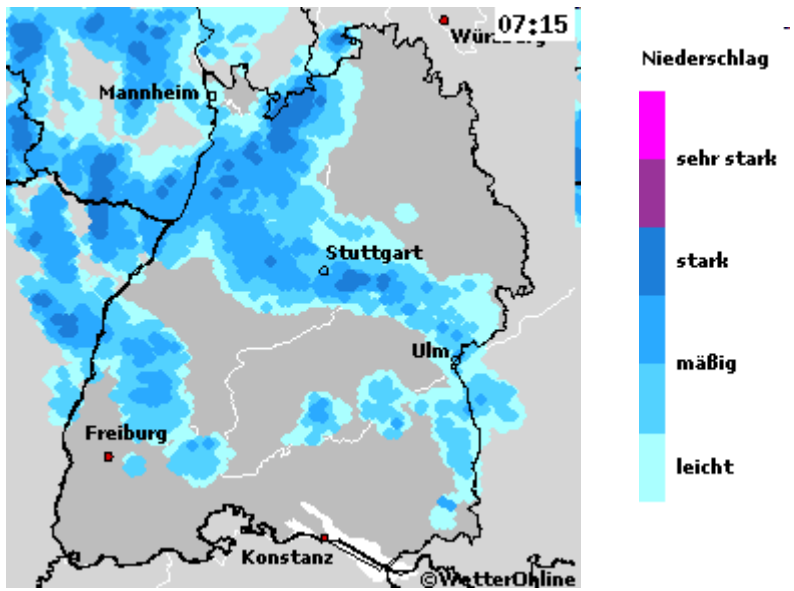
07:15
Mannheim
Stuttgart
Ulm
Freiburg
Konstanz
©WetterOnline
Niederschlag
sehr stark
stark
mäßig
leicht

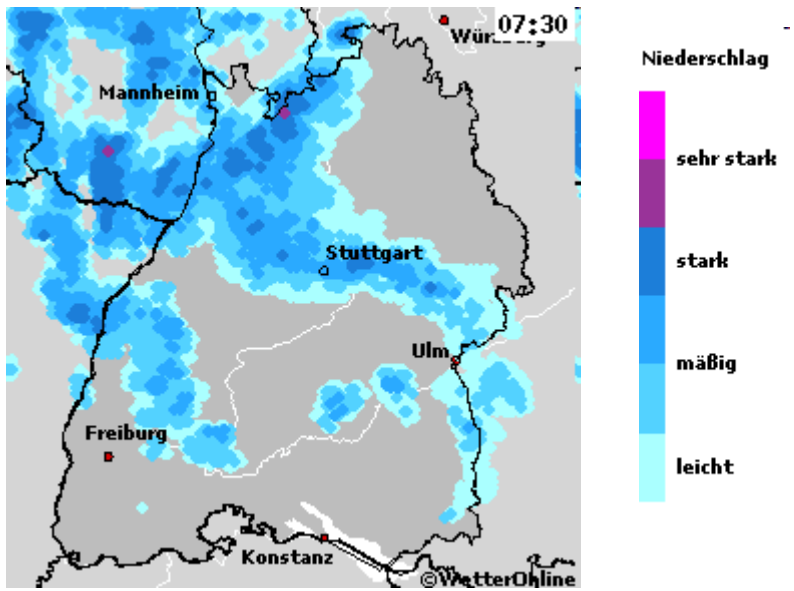
07:30
Mannheim
Stuttgart
Ulm
Freiburg
Konstanz
©WetterOnline
Niederschlag
sehr stark
stark
mäßig
leicht

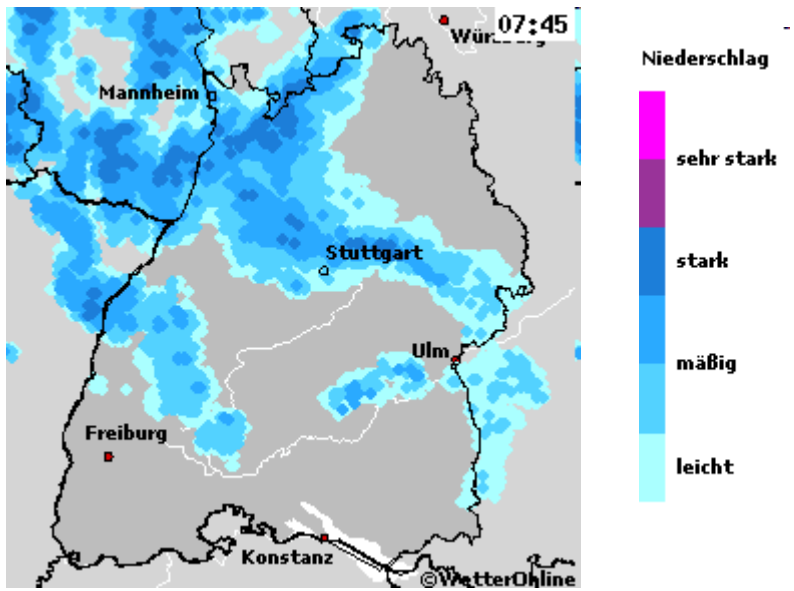
07:45
Mannheim
Stuttgart
Ulm
Freiburg
Konstanz
©WetterOnline
Niederschlag
sehr stark
stark
mäßig
leicht

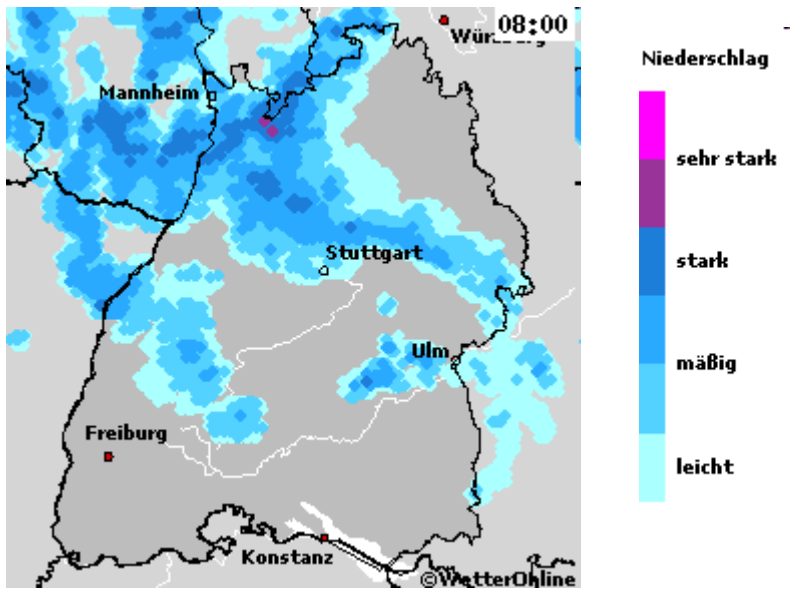
08:00
Mannheim
Stuttgart
Ulm
Freiburg
Konstanz
©WetterOnline
Niederschlag
sehr stark
stark
mäßig
leicht

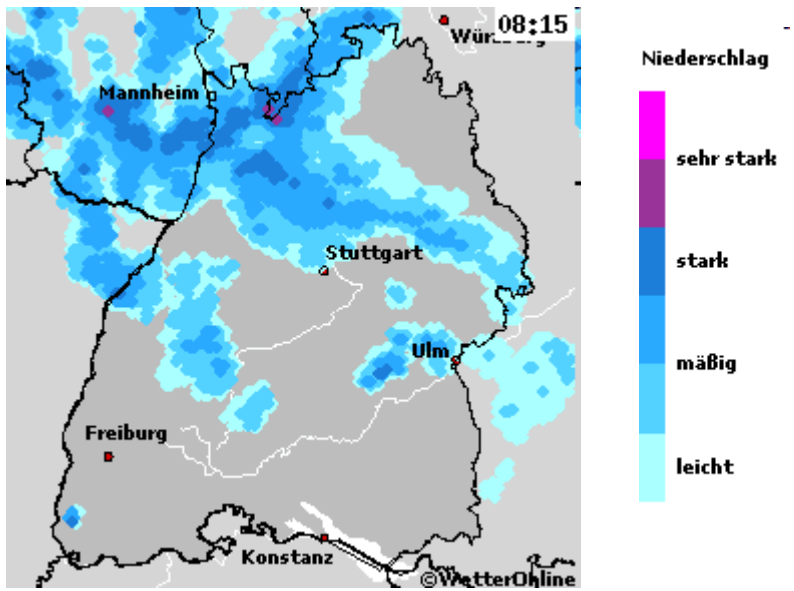
08:15
Mannheim
Stuttgart
Ulm
Freiburg
Konstanz
©WetterOnline
Niederschlag
sehr stark
stark
mäßig
leicht

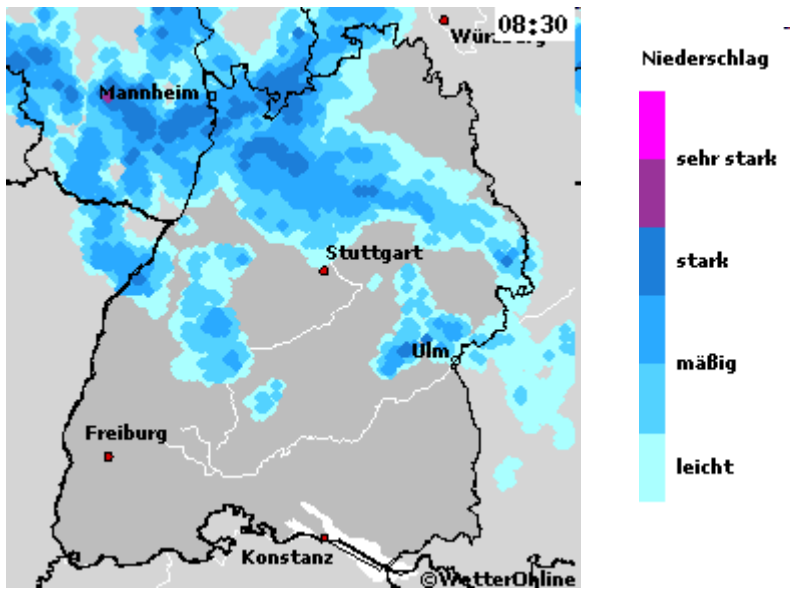
08:30
Mannheim
Stuttgart
Ulm
Freiburg
Konstanz
©WetterOnline
Niederschlag
sehr stark
stark
mäßig
leicht

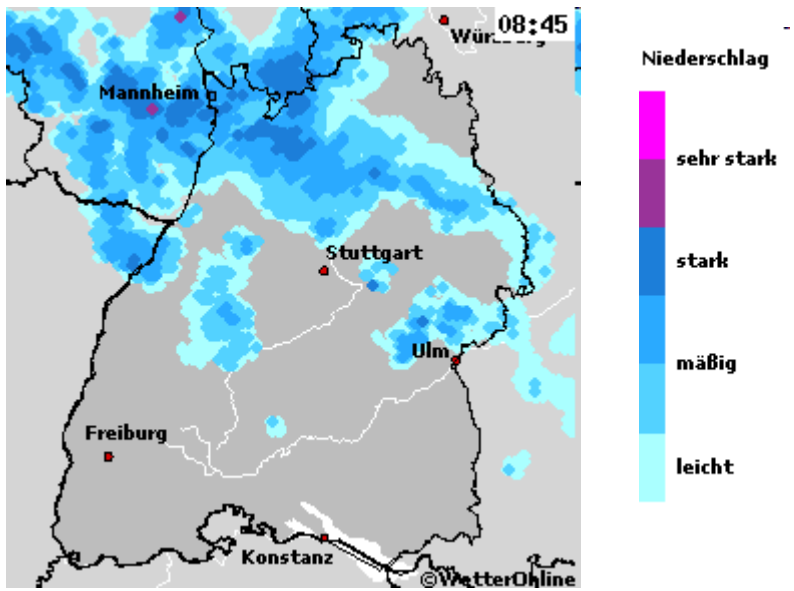
08:45
Mannheim
Stuttgart
Ulm
Freiburg
Konstanz
©WetterOnline
Niederschlag
sehr stark
stark
mäßig
leicht

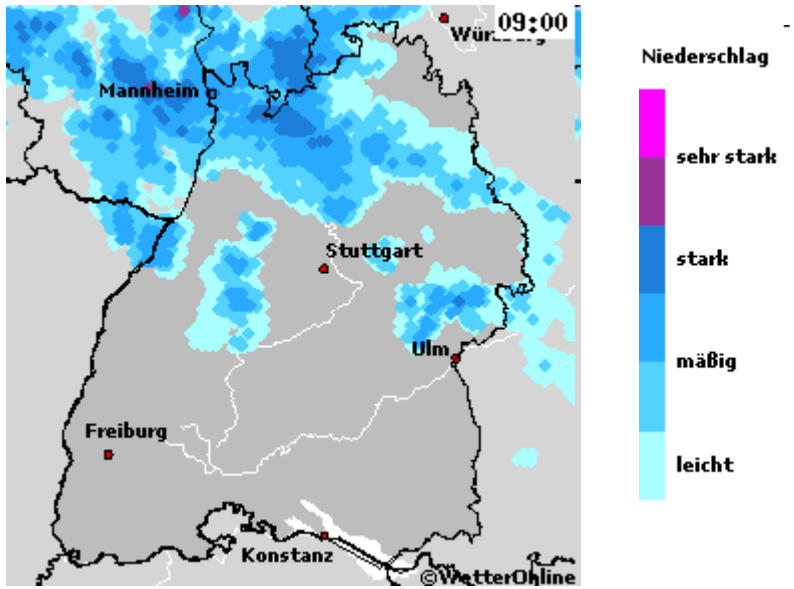
09:00
Mannheim
Stuttgart
Ulm
Freiburg
Konstanz
©WetterOnline
Niederschlag
sehr stark
stark
mäßig
leicht

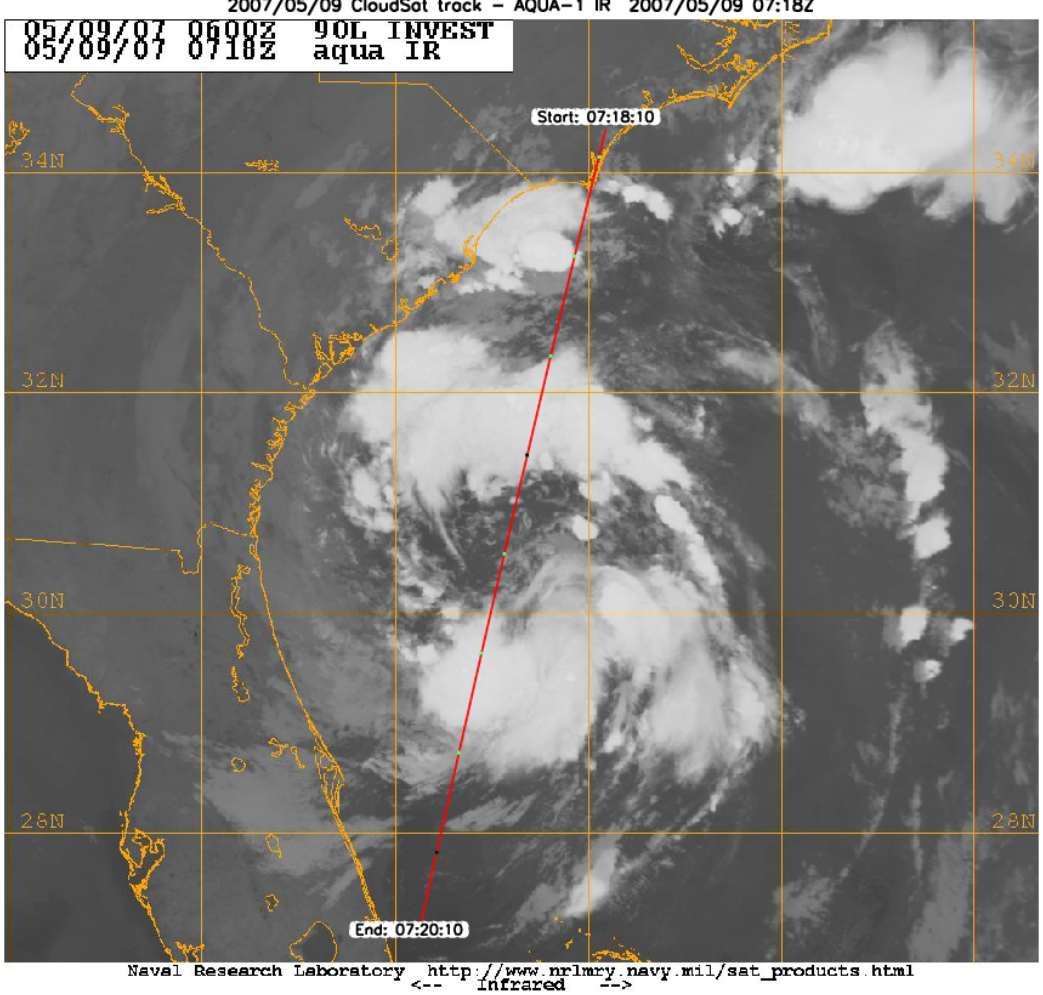

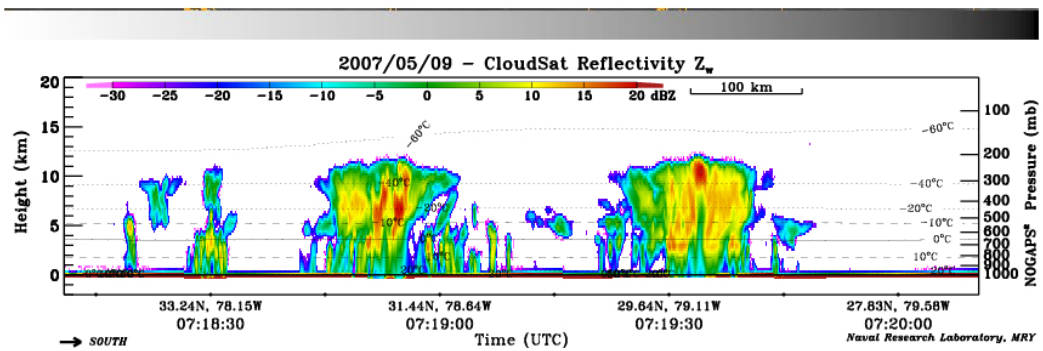

CloudSat's **Cloud Profiling Radar** captured a profile across Tropical Storm Andrea on Wednesday, 9 May 2007 near the SC/GA/FL Atlantic coast. The upper image shows an infrared view of TS Andrea from the MODIS instrument on the Aqua satellite, with CloudSat's ground track from 0718-0720 UTC (3:18-3:20 EDT) shown as a red line. The lower image is the vertical cross section of radar reflectivity along this path, where the colors indicate the intensity of the reflected radar energy. CloudSat orbits approximately one minute behind Aqua in a satellite formation known as the A-Train. [Images courtesy of the Naval Research Laboratory-Monterey]

http://cloudsat.atmos.colostate.edu/

CloudSat

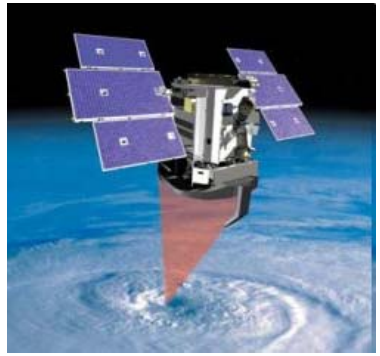

Nominal Frequency	94 GHz
Pulse Width	3.3 µsec
PRF	4300 Hz
Minimum Detectable Z*	< -29 dBZ
Data Window	0-25 km
Antenna Size	1.85 m
Dynamic Range	70 dB
Integration Time	0.16 sec
Nadir Angle (since 15 Aug 2006***)	0.16°
Vertical Resolution	500 m
Cross-track Resolution	1.4 km
Along-track Resolution**	1.7 km
Data Rate	20 kbps

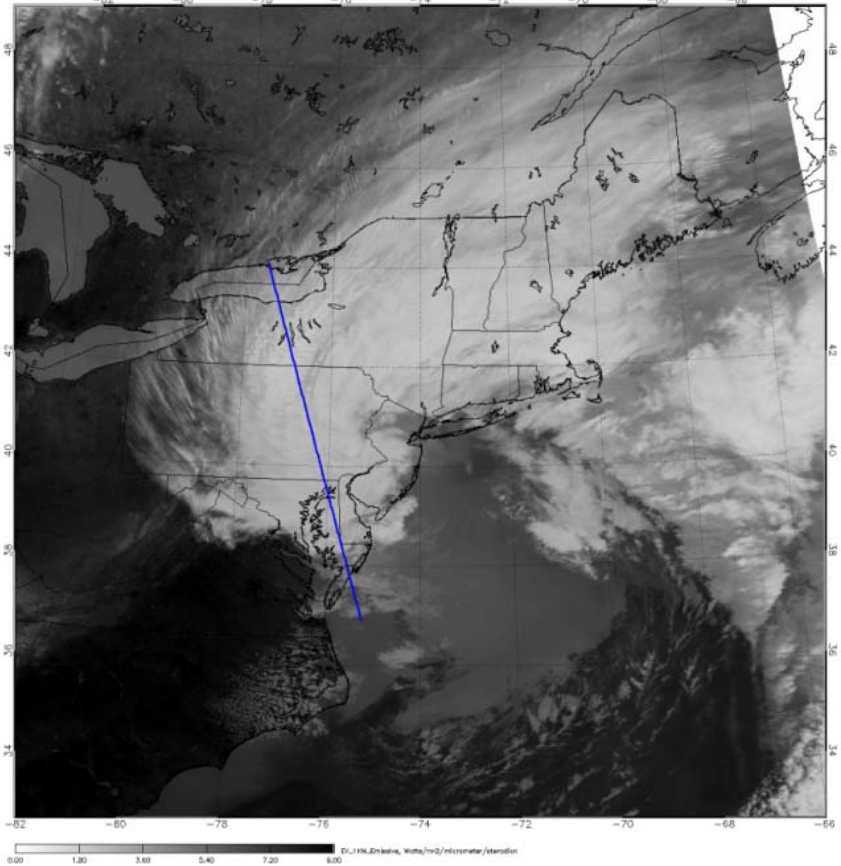

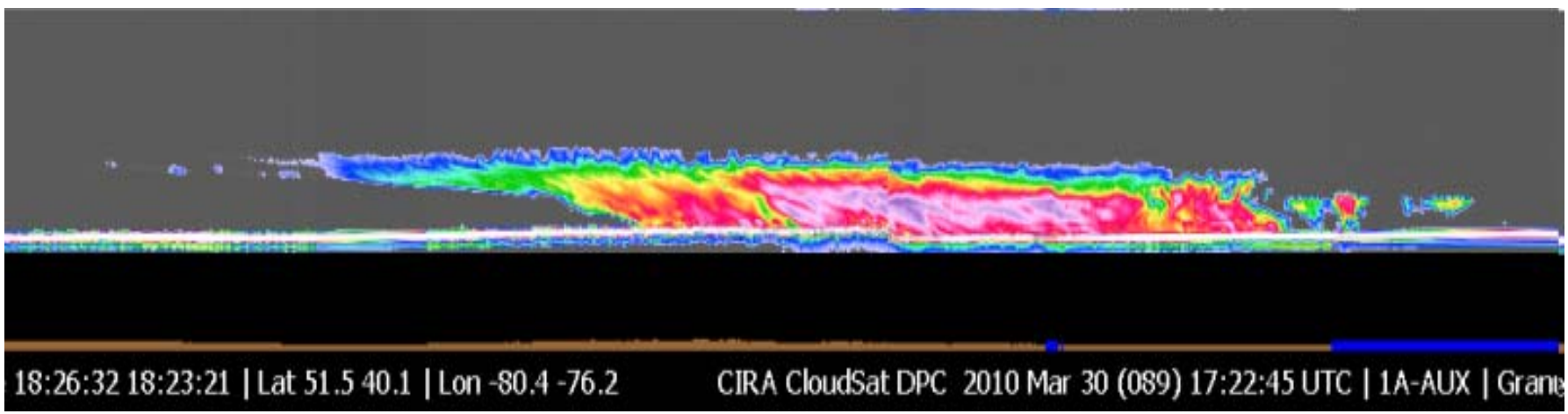

http://cloudsat.atmos.colostate.edu/

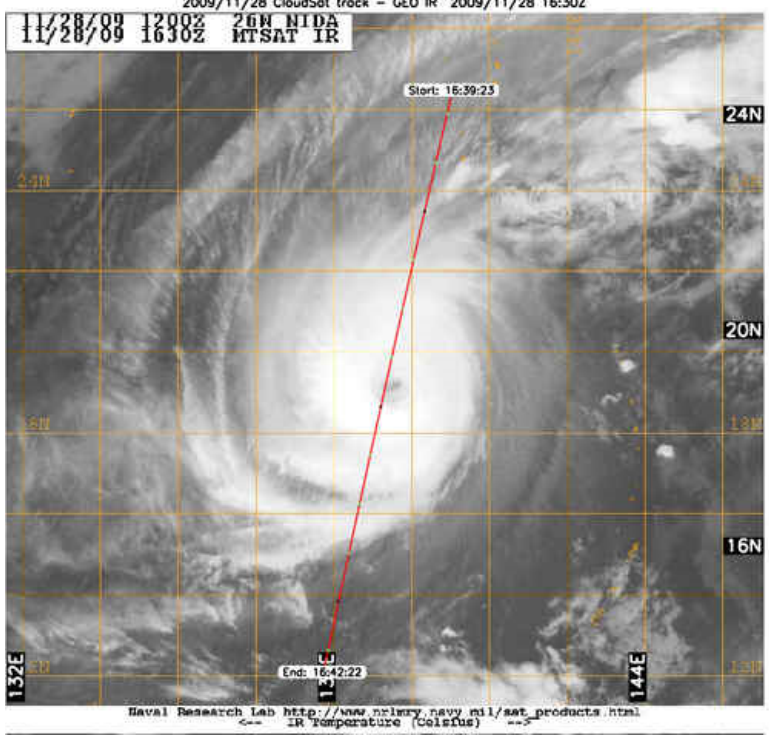

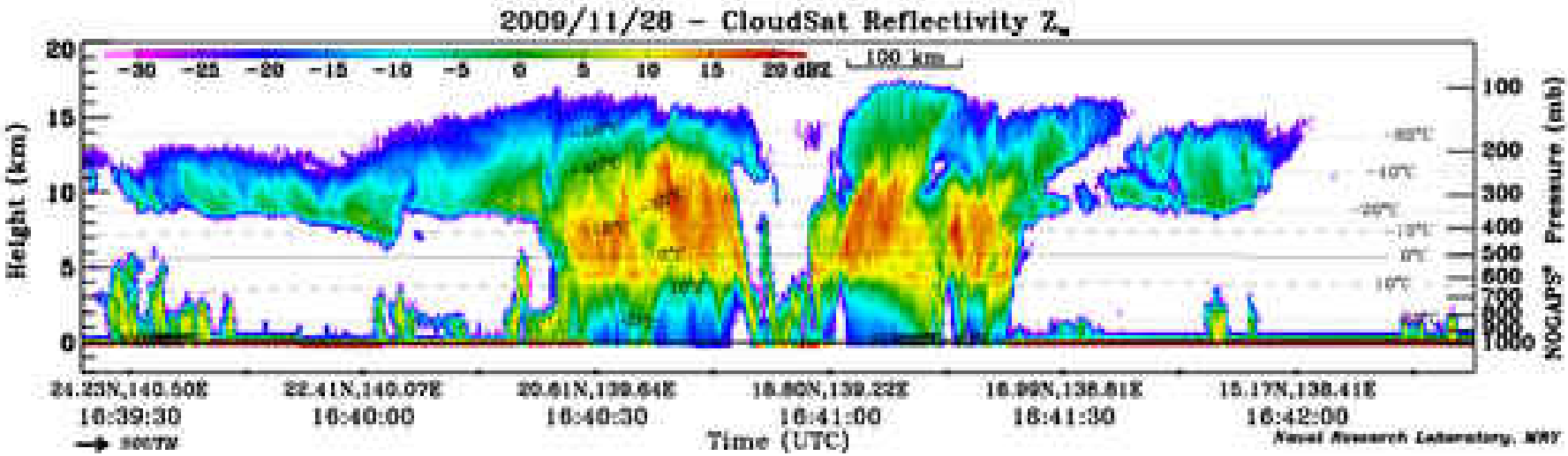

http://cloudsat.atmos.colostate.edu/

Synergy between Cloudsat and Calipso

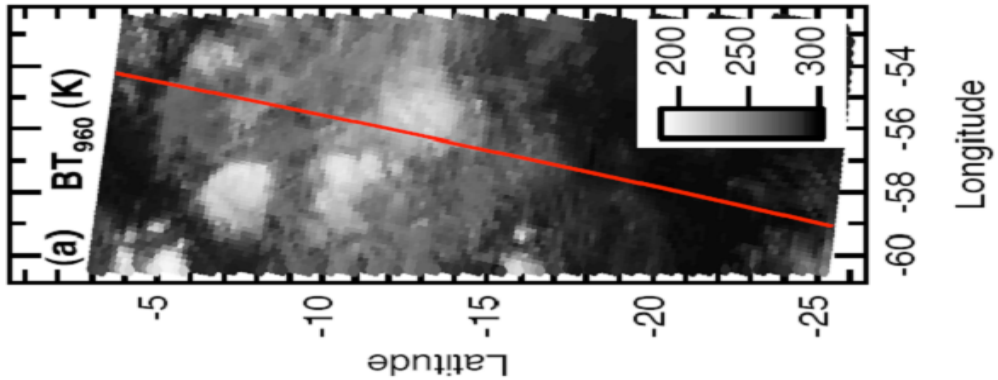

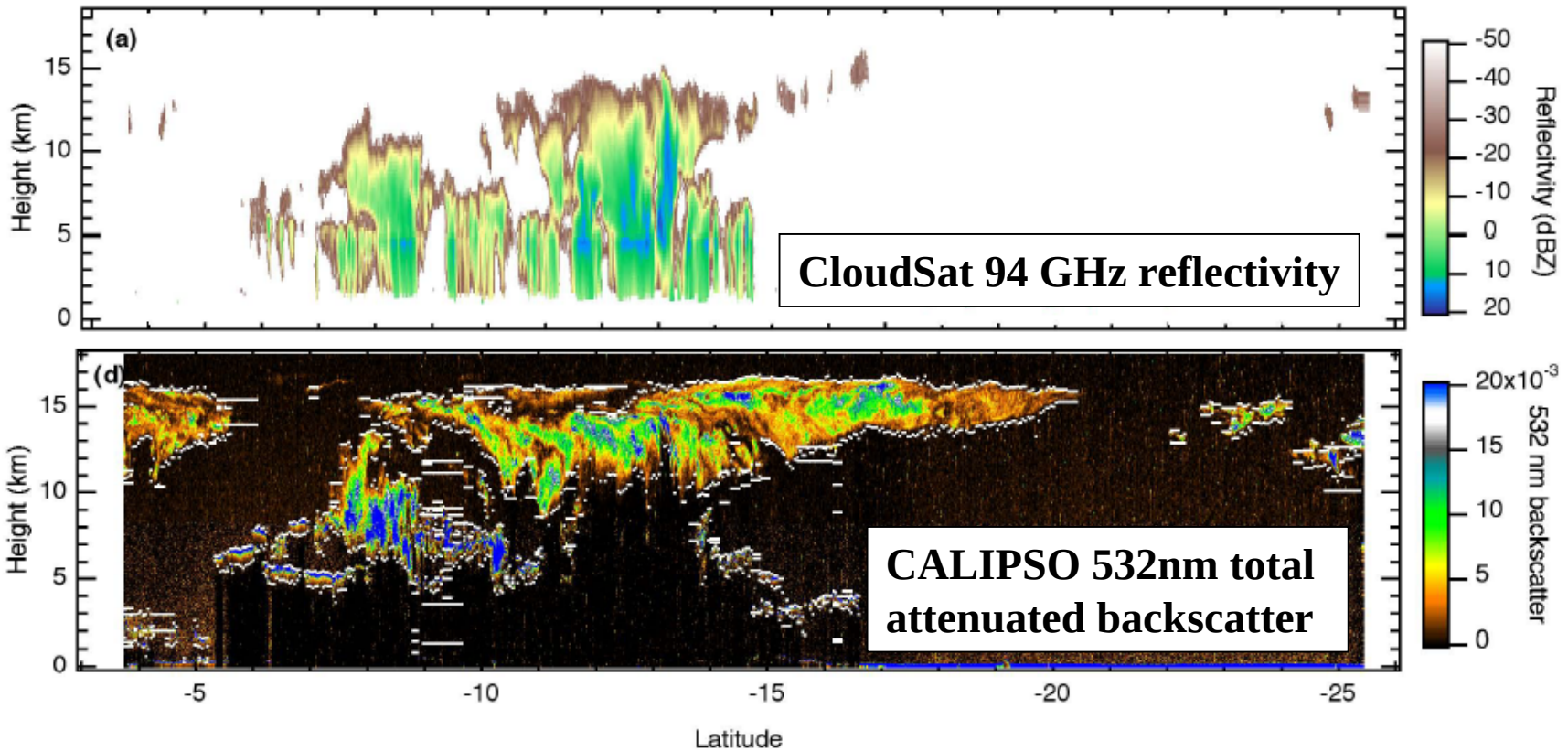

Kahn, B. H., Chahine, M. T., Stephens, G. L., Mace, G. G., Marchand, R. T., Wang, Z., Barnet, C. D., Eldering, A., Holz, R. E., Kuehn, R. E., and Vane, D. G.: Cloud type comparisons of AIRS, CloudSat, and CALIPSO cloud height and amount, Atmos. Chem. Phys. Discuss., 7, 13915-13958, doi:10.5194/acpd-7-13915-2007, 2007.

Active methods with focus on time information

-LIDAR Light detection and ranging

-RADAR Radio detection and ranging

-**SODAR** **Sound detection and ranging**

SODAR Sound Detecting And RAnging

Sound (as acoustic pulses) is emitted into the atmosphere and the echos are recieved and analysed

-the echo intensity varies according to thermal turbulence and structure

-the frequency shift of the echo varies according to the wind speed (DOPPLER effect)

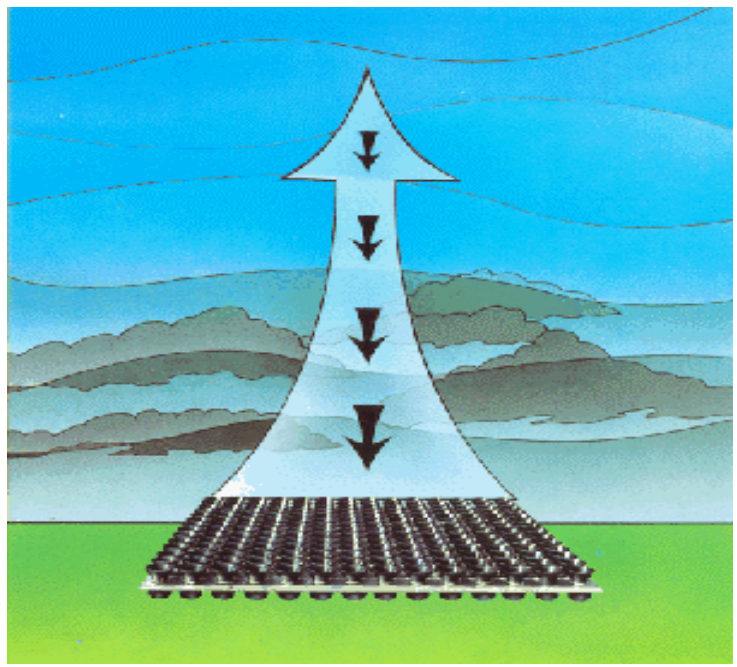

SODAR Sound Detecting And RAnging

Mono-static systems are usually operated in three directions

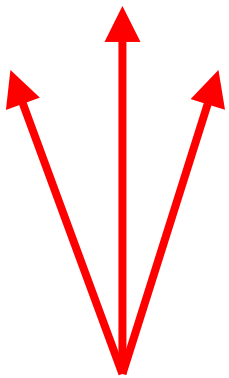

Zenith angles
typically 15°
to 30 °

two categories:
a) individual antennas at multiple axis
single transducer focused into a parabolic dish

b) single phased-array antenna
array of speaker drivers and horns (transducers), the beams are electronically steered by phasing the transducers appropriately.

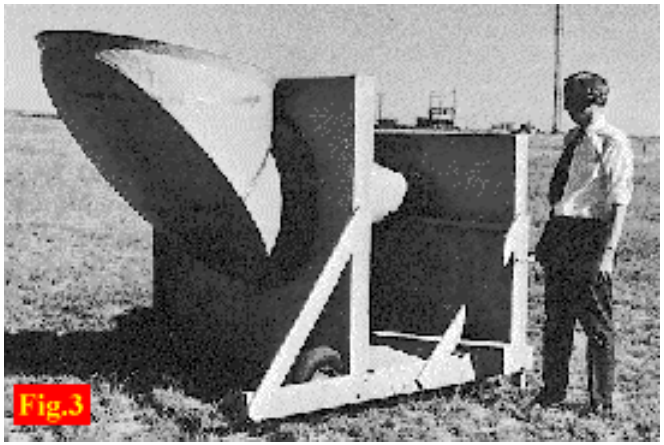

An example of an old monostatic system is presented in Figure 3. The antenna is constructed from an electrodynamic transducer in the focal point of a parabolic dish reflector. It is clear that the system is heavy and it is difficult to move it in hard to reach places.

phased-array antenna

SODAR Sound Detecting And RAnging

-The horizontal components of the wind velocity are calculated from the radially measured Doppler shifts and the specified tilt angle from the vertical.

-A correction for the vertical velocity should be applied in systems with zenith angles less than 20° (or when the expected vertical velocities are greater than about 0.2 ms^{-1})

- The vertical range of sodars is approximately 0.2 to 2 kilometers (km) depending on frequency, power output, atmospheric stability, turbulence, and, most importantly, the noise environment in which a sodar is operated.

-Operating frequencies range from less than 1000 Hz to over 4000 Hz, with power levels up to several hundred watts.

SODAR Sound Detecting And RAnging

Meteorologisches Observatorium Lindenberg

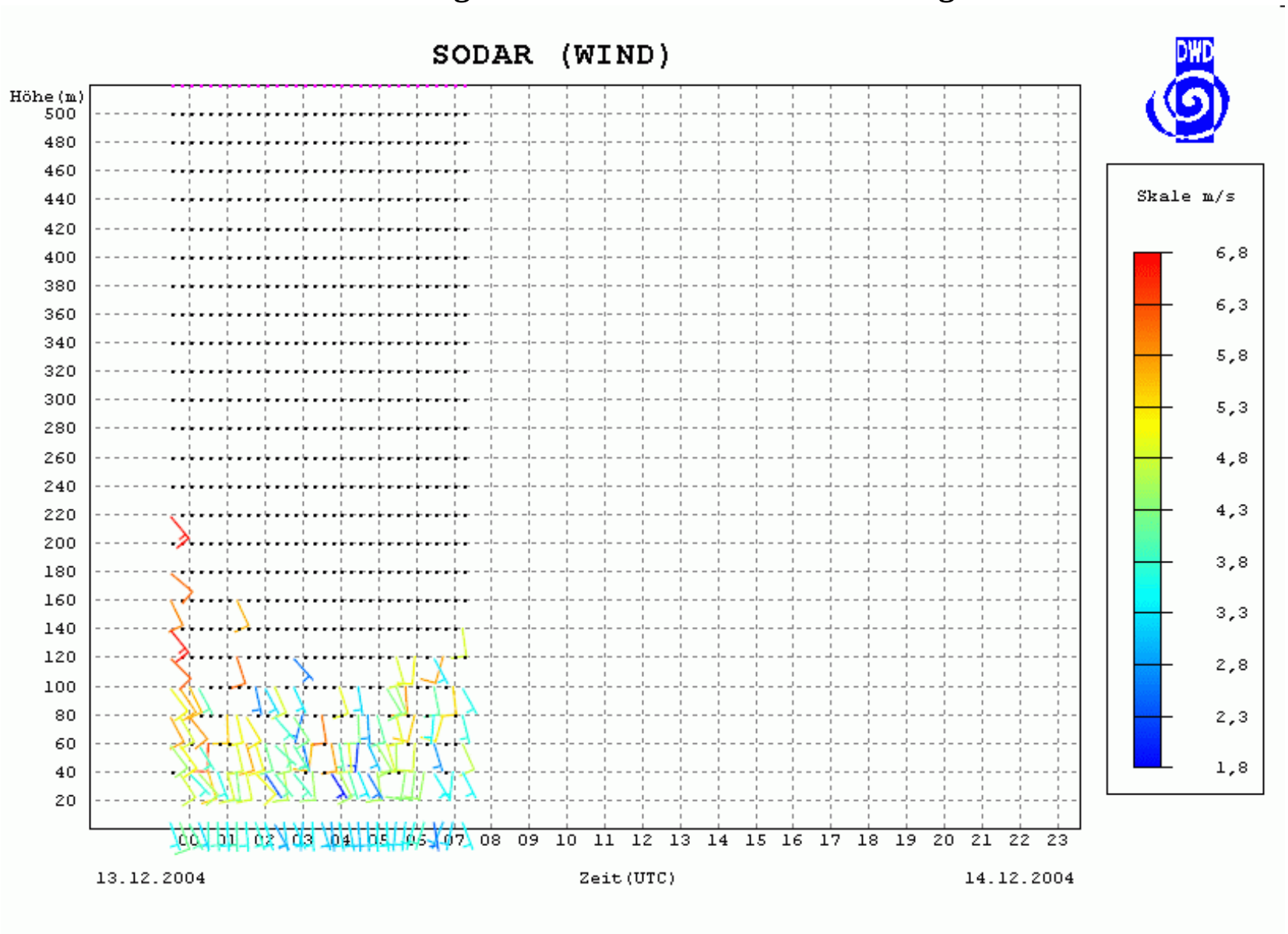

Radio Acoustic Sounding System (RASS)

- Bragg scattering occurs when the wavelength of the acoustic signal matches the half-wavelength of the radar

-As the frequency of the acoustic signal is varied, strongly enhanced scattering of the radar signal occurs when the Bragg match takes place.

-When this occurs, the Doppler shift of the radar signal produced by the Bragg scattering can be determined, => vertical velocity.

-the speed of sound as a function of altitude can be measured, from which virtual temperature (T_v) profiles can be calculated (The virtual temperature of an air parcel is the temperature that dry air would have if its pressure and density were equal to those of a sample of moist air)

-three or four vertically pointing acoustic sources (equivalent to high quality stereo loud speakers) are placed around the radar wind profiler's antenna,

-The acoustic sources are used only to transmit sound into the vertical beam of the radar

-The vertical resolution of RASS data is determined by the pulse length(s) used by the radar. RASS sampling is usually performed with a 60- to 100-m pulse length.

-the altitude range is usually 0.1 to 1.5 km, depending on atmospheric conditions (e.g., high wind velocities tend to limit RASS altitude coverage to a few hundred meters because the acoustic signals are blown out of the radar beam).

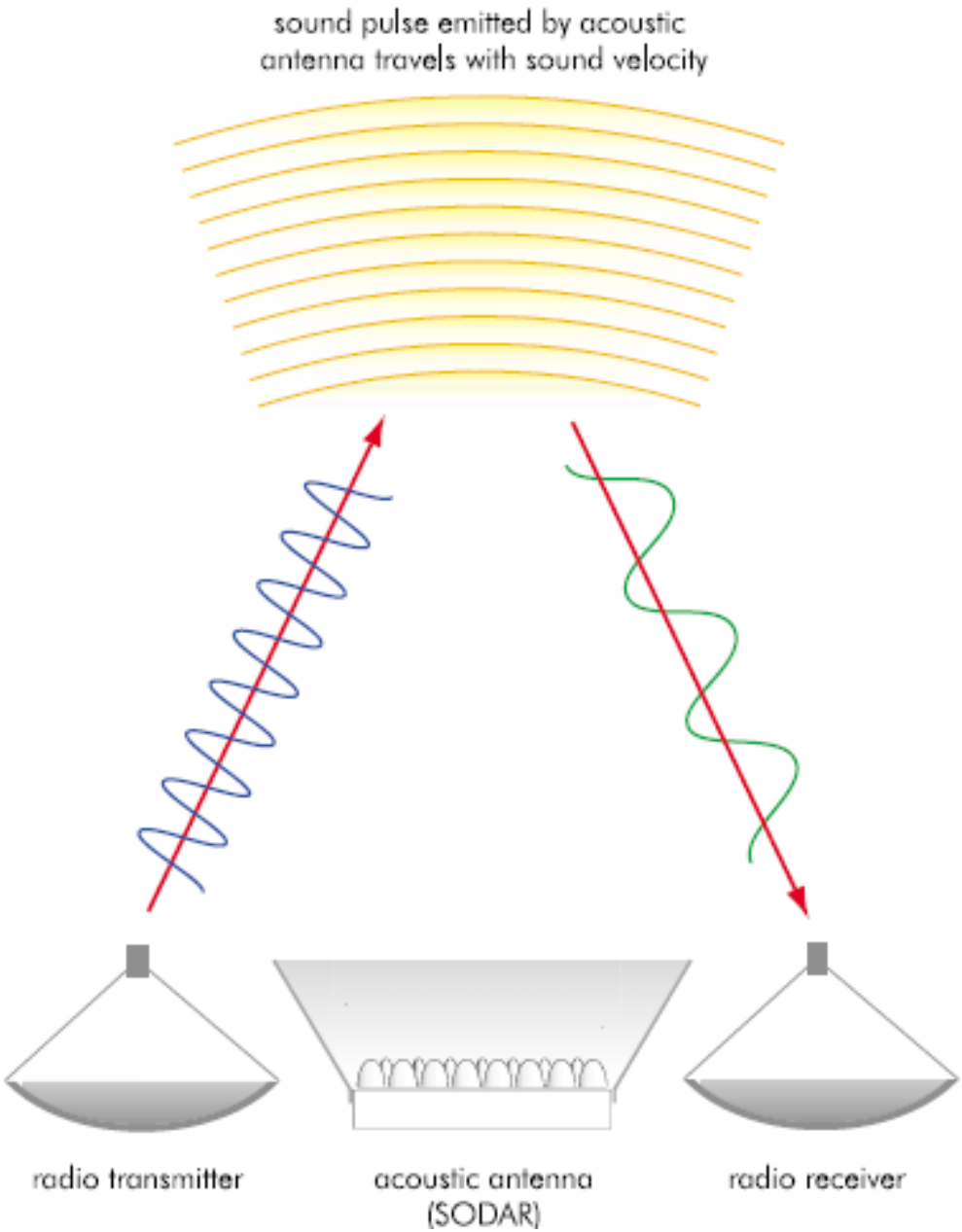
sound pulse emitted by acoustic
antenna travels with sound velocity
radio transmitter
acoustic antenna
(SODAR)
radio receiver

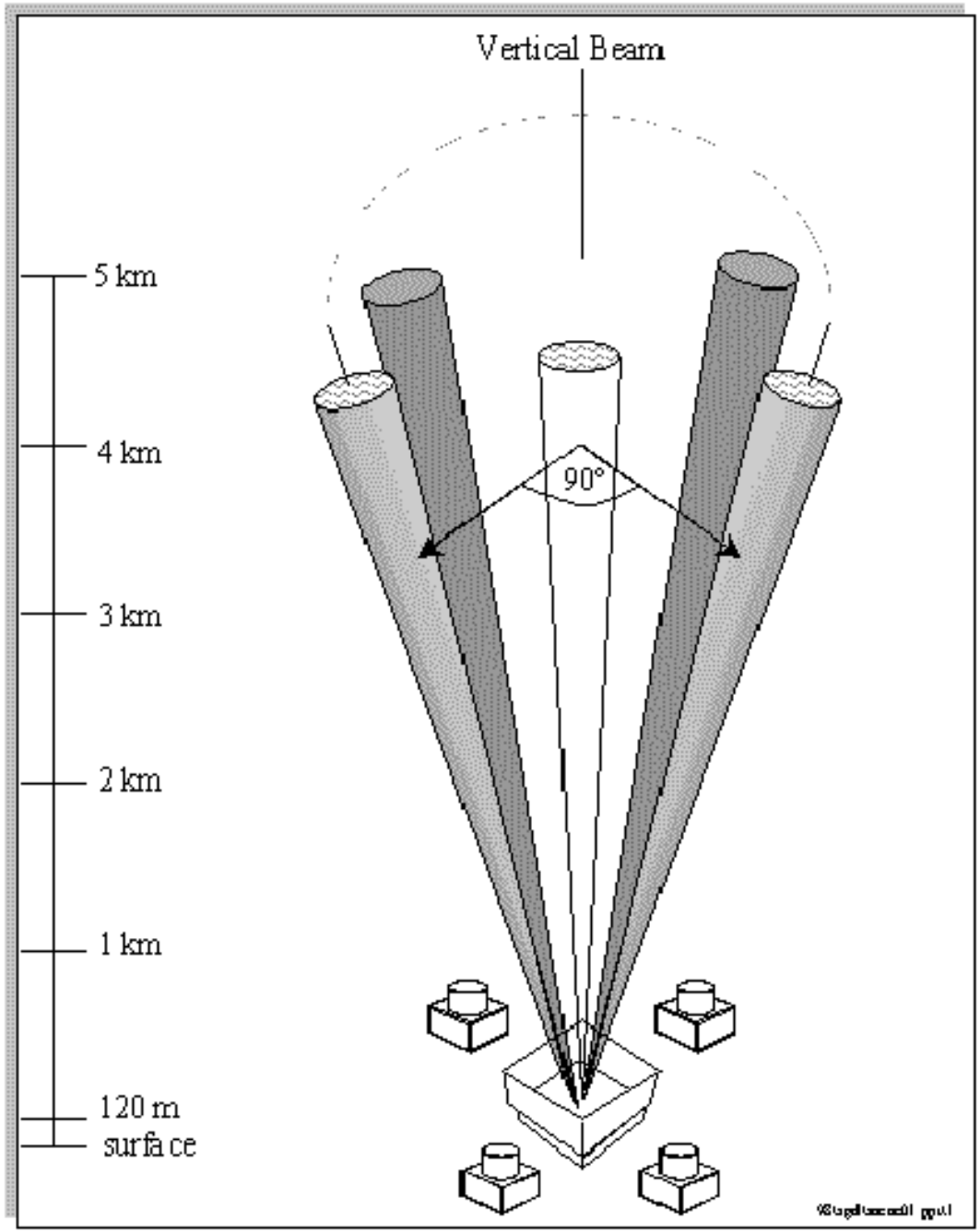

Schematic of sampling geometry for a radar wind profiler with RASS

The 915 MHz Radar Wind Profiler (915RWP) and radio acoustic sounding system (RASS) at the North Slope of Alaska site in Barrow, Alaska.

Meteorologisches Observatorium Lindenberg

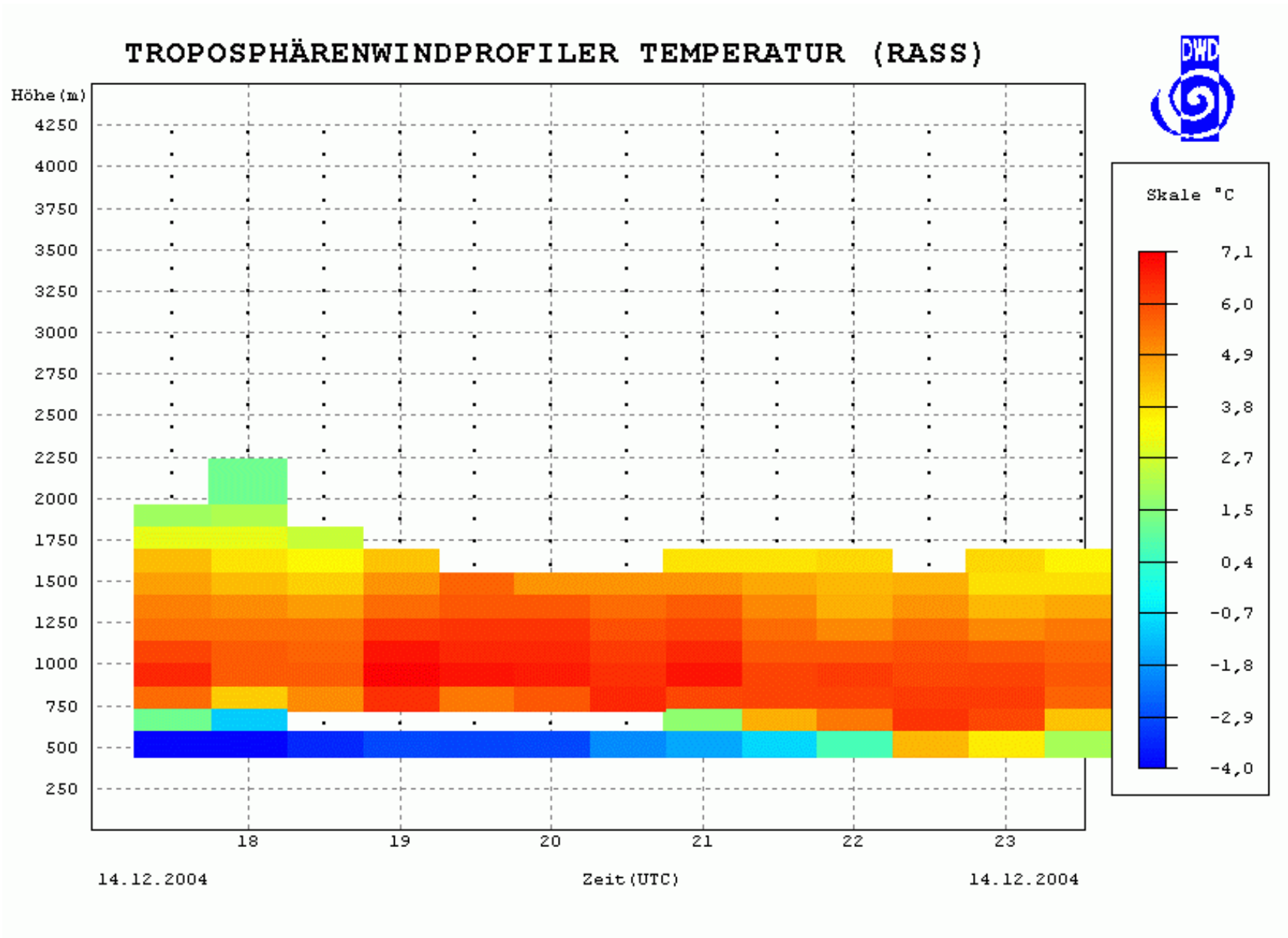

Summary active (time resolved) methods:

-active methods:
    -mainly optical and microwave range
    -also sound is used

Advantages:
-highly resolved spatial information
-measurement conditions can be freely chosen

Disadvantages:
-high instrumental effort
-only small temporal and spatial coverage
-often qualitative (not quantitative) information is retrieved